UC Riverside

UC Riverside Electronic Theses and Dissertations

Title

Environmental Chamber Studies of Reduced Nitrogen Compounds Observed in Anthropogenic Emissions

Permalink

https://escholarship.org/uc/item/0kf6q8q2

Author

Price, Derek Jason

Publication Date

2015

Peer reviewed|Thesis/dissertation

eScholarship.org Powered by the California Digital Library
University of California

UNIVERSITY OF CALIFORNIA
RIVERSIDE

Environmental Chamber Studies of Reduced Nitrogen Compounds Observed in Anthropogenic Emissions

A Dissertation submitted in partial satisfaction
of the requirements for the degree of

Doctor of Philosophy

in

Chemical and Environmental Engineering

by

Derek Jason Price

August 2015

Dissertation Committee
Dr. David R. Cocker III, Chairperson
Dr. Akua Asa-Awuku
Dr. Kathleen L. Purvis-Roberts

Copyright by
Derek Jason Price
2015

The Dissertation of Derek Jason Price is approved:

_____

_____

_____

Committee Chairperson

University of California, Riverside

Acknowledgements

As my graduate studies at UCR come to a close, there are many people that I would like to acknowledge for helping me along my journey. First and foremost, I would not be where I am now without the support and encouragement of my family and friends. I would especially like to thank my parents, Delwin and Suzanne Price. They taught me that work, prayer, and perseverance are the keys to reaching any goal. I must also acknowledge my siblings, Greg, Yeala and Travis for their emotional support. I'm also grateful for the support of great friends Bob and Kaydee McMahon, Karl and Crystal Lowry, Reed and Emilie Bickmore, Craig and Sara Wallace, Mark Farrell (a man of character), Daniel Johnson, Courtney Bradshaw, Ashleigh Lutes, and many others.

I have had the privilege of working with three wonderful advisors. Dr. Phil Silva started me on this research path as an undergraduate at USU. I learned much from my masters advisor, Dr. Robert Brown, also at USU. I cannot overstate how wonderful it has been to work with my current advisor, Dr. David Cocker. Despite his extremely demanding schedule, he always had time to help me in the lab. He always trusted in my research abilities, even before I knew I had them. Thank you, David, for not only being a great advisor, but also a good friend. Thank you for inviting me to your home for Thanksgiving and potlucks. Your lighthearted nature and sage wisdom were greatly appreciated. I would also like to acknowledge my other committee members, Dr. Akua Asa-Awuku and Dr. Kathleen Purvis-Roberts for your guidance and direction with this dissertation and other research endeavors.

Over the years, I had the opportunity to work with many wonderful graduate students. I would like to acknowledge the former Cocker group members. Thank you, Dr. Quentin Malloy, Dr. Shunsuke Nakao, Dr. Christopher Clark, Dr. Ping (Annie) Tang, and Dr. Xiaochen (Esther) Tang for teaching me how to run atmospheric chamber experiments and for training me on all of the instrumentation in the lab. I'm also grateful for all of the helpful insights and advice you gave me. Thank you, Dr. Poornima Dixit for allowing me to hide out in the Analytical lab when I needed a break. I enjoyed our many conversations. I would also like to acknowledge the current Cocker group members. Nick Gysel and Chia-li (Candice) Chen, you came to UCR with me and I have enjoyed working with you. Candice, you are the most genuinely kind person that I know. I'm grateful for my office mates, Candice, Lijie (Sara) Li, and Weihua Li. Thank you for providing a clean, quiet environment to work. I didn't understand most of the conversations in that office, but I just assumed you were saying nice things about me. I would especially like to acknowledge the assistance of my friend and co-worker, Mary Kacarab. I could not have asked for a better colleague than I found in you. I always knew that, together, we could accomplish any task; whether that was troubleshooting instrumentation, managing undergraduate students, constructing new atmospheric chambers, or just keeping the lab running. You were the Kirk to my Spock, the Bad Cop to my Good, the Leia to my Luke, the Kenneth to my Dirk. Thank you, Mary, for your friendship. I would also like to thank Paul Van Rooy for assisting with those last few experiments. I wish you luck as you take over the amine research projects.

There are several students from the Asa-Awuku group that I would like to acknowledge. Thank you, Dr. Shaokai Gao, for your help with the Syft instrument and for being so kind. I'm grateful for the friendship of Dr. Daniel Short and Diep Vu. Thank you, Dan, for the helpful insights and advice you offered at the lab. Thank you, Diep, for your help with experiments and instrumentation. I'm grateful for the many lunch breaks and pleasant conversations I had with you and Mary.

I have also worked with many great undergraduate students here at UCR. Thank you, Thomas and Sarah Kwan, Daisy Jimenez, Carlton Nguyen, Danah Alkurdi, Melanie Zecca, Kyle Schaefer, and Shannon Lopez for your assistance on a variety of projects over the years. I knew that I could trust you with any assignment, and that was of great service to me.

I would like to acknowledge the administrative staff; the unsung heroes of CE-CERT. Thank you, Nicole Davis and Kathy Vang for taking time out of your demanding schedules to chat and lift my spirits during those long days at the lab. Thank you, Valerie Thomas for dealing with all of my purchase requests. Thanks go to Cindy Howard, Angelique Butler, and Berenice Murillo-Quintana for keeping all of the financial and academic requirements in order for us graduate students. Thanks also to Ed Sponsler for the technical assistance and keeping my antiquated computer running. I cannot fail to acknowledge the assistance of Mr. Kurt Bumiller with technical troubleshooting, chamber repair, and general laboratory advice.

Finally, I would like to acknowledge the funding from the University of California Transportation Center, W. M. Keck Foundation, National Science Foundation (ATM-0449778), California Air Resources Board, and stipend funding from the GAANN fellowship and the University of California, Riverside, Department of Chemical and Environmental Engineering. Chapter 2 of this dissertation was previously published in Atmospheric Environment, 2014, 96, pgs. 135-144.

Dedicated to my parents
Delwin and Suzanne Price

ABSTRACT OF THE DISSERTATION

Environmental Chamber Studies of Reduced Nitrogen Compounds
Observed in Anthropogenic Emissions

by

Derek Jason Price

Doctor of Philosophy, Graduate Program in Chemical and Environmental Engineering
University of California, Riverside, August 2015
Dr. David R. Cocker III, Chairperson

Secondary organic aerosol (SOA) pollution has negative impacts on human health and well-being. While efforts have been made to characterize the chemical reactions leading to SOA formation, reduced nitrogen compounds remain a poorly studied class of chemicals contributing to air pollution. Sources of reduced nitrogen compounds include agricultural emissions, biomass burning, carbon capture sequestration and selective catalytic reduction control devices, low vapor pressure volatile organic compounds (LVP-VOC) found in many consumer products, and charbroiled meats. Understanding the atmospheric chemical mechanisms of reduced nitrogen compounds is important for comprehensive design of effective air pollution strategies. Therefore, this study seeks to determine the impact of reduced nitrogen compound chemistry on SOA formation. Experiments were conducted at the UCR College of Engineering – Center for Environmental Research and Technology (CE-CERT) Atmospheric Processes Laboratory. This facility houses several well characterized indoor environmental chambers, which allow for the study of atmospheric processes under controlled conditions. Chamber experiments consisted of a reduced nitrogen compound being

reacted with atmospheric oxidants including hydroxyl radical (OH) and nitrate radical (NO_3). The chemical composition of the gas and aerosol species were determined through mass spectrometry techniques. The physical properties of the aerosol, including density, volatility, and hygroscopicity, as well as particle concentration and size distribution were measured with a variety of house built particle mobility analyzers. A suite of gas analyzers were used to measure Ozone, NO_x, and CO concentrations. Experiments with primary, secondary, and tertiary aliphatic amines have provided insights into previously undiscovered reaction mechanisms. Aqueous phase acid catalyzed aldol addition/condensation reactions were observed in secondary amine experiments under humid conditions. Carcinogenic nitramines were observed in secondary amine reactions with nitrate radical. Longer chain secondary amines formed less dense aerosol, suggesting the formation of fractal shaped particles. The discovery of oligomer formation in the reaction of amines with methyl functional groups (dimethylamine, trimethylamine, 2-dimethylaminoethanol) with atmospheric radicals has important implications for SOA formation in areas with high concentrations of amine emissions. Meteorological factors including humidity and temperature played an important role in the reaction chemistry of reduced nitrogen compounds. Humidity provided additional, aqueous phase, reaction pathways. Temperature had an effect on gas to particle partitioning, particularly with the amine salts. The concentration of aerosol formed during radical oxidation of amino alcohols has implications on the use of these compounds in carbon capture sequestration control devices.

Table of Contents

List of Tables

List of Figures

Chapter 1: Introduction

1.1. Introduction of Dissertation

Atmospheric aerosols are known to cause negative effects on human health, visibility, and the environment (Dockery, 2009; IPCC, 2007; Pope et al., 1995; Watson, 2002). Among these atmospheric pollutants, the formation of secondary organic aerosol (SOA) from alkyl amines has been gaining more attention. There are both anthropogenic and biogenic sources of these amines, including agricultural emissions, by-products of selective catalytic reduction control technologies, and biomass burning (Cadle and Mulawa, 1980; Mosier et al., 1973; Westerholm et al., 1993).

Previous studies have suggested that secondary organic aerosol formation from amines is dominated by the production of salt through acid/base reactions with nitric and sulfuric acids (Ge et al., 2011; Murphy et al., 2007). These acid/base reactions alone, however, are insufficient to explain the total secondary organic aerosol observed from atmospheric aliphatic amine oxidation (Silva et al., 2008; Tang et al., 2013). There has been little attention in the scientific literature given to the importance of peroxy radical chemistry in the formation of secondary organic aerosol from amines. Therefore, a series of environmental chamber experiments were conducted to ascertain the impact of atmospheric amines on ambient SOA formation. In these experiments, an amine is reacted with atmospheric oxidants including hydroxyl radical (OH) or nitrate radical (NO_3).

In chapter 2 of this dissertation, a systematic theoretical approach was utilized in conjunction with carefully controlled environmental chamber studies to decipher the SOA chemistry occurring in the radical oxidation of aliphatic amines. The approach assumes a simple system at the start of each experiment, i.e. an amine will react with an oxidant. At this point, one can focus on the more likely of several possible reaction routes based on known chemical behavior. For example, a radical will most likely abstract a hydrogen atom from a saturated organic molecule such as an amine (Schade and Crutzen, 1995; Tuazon et al., 1994). The question then becomes, which hydrogen will be abstracted? The answer to that question depends on factors such as bond strength, electronegativity, and steric hindrance (Bruice, 2004). The experimental data is consulted as the various possible mechanisms are identified. In this study, three different mass spectrometric instruments were employed to identify both gas-phase and aerosol-phase oxidation products. With an understanding of how each instrument measures a given sample, certain mechanisms that do not match the results were eliminated. In instances where multiple mechanisms agree with the results, alternative experiments were conducted to confirm or eliminate select chemical mechanisms. Following this approach, a plausible mechanism leading to oligomer products by way of peroxy radical reactions was determined.

In chapter 3 of this dissertation, the aforementioned approach was utilized to investigate the SOA formation from the oxidation of a series of secondary aliphatic amines. Previous work into aliphatic amine reactivity has focused on primary amines (Malloy et al., 2009) and tertiary amines (Silva et al., 2008). However, an in-depth study

on the reactivity of secondary aliphatic amines has not previously been reported. The effect of humidity on the physical properties and chemical composition of the aerosol are reported within this chapter.

Chapter 4 of this dissertation examines the influence of temperature on the physical properties and chemical composition of the aerosol produced from radical oxidation of aliphatic amines. Previous atmospheric chamber studies have investigated the oxidation of alkyl amines only at room temperature (Lee and Wexler, 2013; Malloy et al., 2009; Price et al., 2014; Tang et al., 2013), with studies on the effect of temperature on amine aerosol not previously reported. Earlier temperature work has focused on other biogenic and combustion emissions (Qi et al., 2010; Warren et al., 2009). Even scarcer are atmospheric chamber studies that investigate response of aerosol to changing environmental temperature. The indoor atmospheric chambers at the UC-Riverside College of Engineering – Center for Environmental Research and Technology (UCR/CE-CERT) are ideally suited for this study. The environmental chambers are housed in a 6 m x 6 m x 12 m thermally insulated enclosure that allows for temperature control ranging from 5°C to 45°C. This chapter reports key observed temperature effects for butylamine, diethylamine, and trimethylamine.

Chapter 5 of this dissertation investigates the SOA formation from the atmospheric oxidation of three amino alcohols with OH and NO_3 radicals. Amino alcohols, such as 2-aminoethanol, are used in control technologies designed to capture CO_2 from the flue gas of power plants (Reynolds et al., 2012; Veltman et al., 2010).

Amino alcohols used in carbon capture and sequestration control technologies are volatile compounds that can escape into the atmosphere. Emissions of amino alcohols from CO_2 capture facilities are estimated to be 40 - 160 tons/year depending on process conditions (Karl et al., 2011). Once emitted to the atmosphere, amino alcohols can react with atmospheric oxidants to form SOA. The atmospheric reactivity of amino alcohols, however, is poorly understood. Previous studies have examined the reactions of 2-aminoethanol with hydroxyl radical (OH) or ozone (Borduas et al., 2013; Karl et al., 2012). The oxidation of amino alcohols with nitrate radical (NO_3) is not previously reported. The effect of humidity on the physical properties and chemical composition of the aerosol was also investigated.

1.2. References

Borduas, N., Abbatt, J.P.D., Murphy, J.G., 2013. Gas Phase Oxidation of Monoethanolamine (MEA) with OH Radical and Ozone: Kinetics, Products, and Particles. Environmental Science & Technology 47, 6377-6383.

Bruice, P.Y., 2004. Organic Chemistry, 4th ed. Pearson Prentice Hall, Upper Saddle River.

Cadle, S.H., Mulawa, P.A., 1980. Low-Molecular Weight Aliphatic-Amines in Exhaust from Catalyst-Equipped Cars. Environmental Science & Technology 14, 718-723.

Dockery, D.W., 2009. Health Effects of Particulate Air Pollution. Ann. Epidemiol. 19, 257-263.

Ge, X., Wexler, A.S., Clegg, S.L., 2011. Atmospheric Amines – Part I, A Review. Atmospheric Environment 45, 524-546.

IPCC, 2007. Summary for Policymakers. In: Climate Change 2007: The Physical Science Basis. Contribution of Working Group I to the Fourth Assessment Report of the Intergovernmental Panel on Climate Change. [Solomon, S., D. Qin, M. Manning, Z. Chen, M. Marquis, K.B. Averyt, M. Tignor and H.L. Miller (eds.)]. Cambridge University Press, Cambridge, United Kingdom and New York, NY, USA.

Karl, M., Dye, C., Schmidbauer, N., Wisthaler, A., Mikoviny, T., D'Anna, B., Muller, M., Borras, E., Clemente, E., Munoz, A., Porras, R., Rodenas, M., Vazquez, M., Brauers, T., 2012. Study of OH-initiated degradation of 2-aminoethanol. Atmospheric Chemistry and Physics 12, 1881-1901.

Karl, M., Wright, R.F., Berglen, T.F., Denby, B., 2011. Worst case scenario study to assess the environmental impact of amine emissions from a CO2 capture plant. Int J Greenh Gas Con 5, 439-447.

Lee, D., Wexler, A.S., 2013. Atmospheric amines - Part III: Photochemistry and toxicity. Atmospheric Environment 71, 95-103.

Malloy, Q.G.J., Li, Q., Warren, B., Cocker, D.R., III, Erupe, M.E., Silva, P.J., 2009. Secondary organic aerosol formation from primary aliphatic amines with NO3 radical. Atmospheric Chemistry and Physics 9, 2051-2060.

Mosier, A.R., Andre, C.E., Viets, F.G., Jr., 1973. Identification of Aliphatic Amines Volatilized from Cattle Feedyard. Environmental Science & Technology 7, 642-644.

Murphy, S.M., Sorooshian, A., Kroll, J.H., Ng, N.L., Chhabra, P., Tong, C., Surratt, J.D., Knipping, E., Flagan, R.C., Seinfeld, J.H., 2007. Secondary aerosol formation from

atmospheric reactions of aliphatic amines. Atmospheric Chemistry and Physics 7, 2313-2337.

Pope, C.A., Thun, M.J., Namboodiri, M.M., Dockery, D.W., Evans, J.S., Speizer, F.E., Heath, C.W., 1995. Particulate Air-Pollution as a Predictor of Mortality in a Prospective-Study of Us Adults. Am. J. Respir. Crit. Care Med. 151, 669-674.

Price, D.J., Clark, C.H., Tang, X.C., Cocker, D.R., Purvis-Roberts, K.L., Silva, P.J., 2014. Proposed chemical mechanisms leading to secondary organic aerosol in the reactions of aliphatic amines with hydroxyl and nitrate radicals. Atmos Environ 96, 135-144.

Qi, L., Nakao, S., Tang, P., Cocker, D.R., 2010. Temperature effect on physical and chemical properties of secondary organic aerosol from m-xylene photooxidation. Atmos Chem Phys 10, 3847-3854.

Reynolds, A.J., Verheyen, T.V., Adeloju, S.B., Meuleman, E., Feron, P., 2012. Towards Commercial Scale Postcombustion Capture of CO2 with Monoethanolamine Solvent: Key Considerations for Solvent Management and Environmental Impacts. Environmental Science & Technology 46, 3643-3654.

Schade, G.W., Crutzen, P.J., 1995. Emission of Aliphatic-Amines from Animal Husbandry and Their Reactions - Potential Source of N2o and Hcn. J Atmos Chem 22, 319-346.

Silva, P.J., Erupe, M.E., Price, D.J., Elias, J., Malloy, Q.G.J., Li, Q., Warren, B., Cocker, D.R., III, 2008. Trimethylamine as precursor to secondary organic aerosol formation via nitrate radical reaction in the atmosphere. Environmental Science & Technology 42, 4689-4696.

Tang, X.C., Price, D., Praske, E., Lee, S.A., Shattuck, M.A., Purvis-Roberts, K., Silva, P.J., Asa-Awuku, A., Cocker, D.R., 2013. NO3 radical, OH radical and O-3-initiated secondary aerosol formation from aliphatic amines. Atmospheric Environment 72, 105-112.

Tuazon, E.C., Atkinson, R., Aschmann, S.M., Arey, J., 1994. Kinetics and Products of the Gas-Phase Reactions of O3 with Amines and Related-Compounds. Res. Chem. Intermed. 20, 303-320.

Veltman, K., Singh, B., Hertwich, E.G., 2010. Human and Environmental Impact Assessment of Postcombustion CO2 Capture Focusing on Emissions from Amine-Based Scrubbing Solvents to Air. Environmental Science & Technology 44, 1496-1502.

Warren, B., Austin, R.L., Cocker, D.R., 2009. Temperature dependence of secondary organic aerosol. Atmos Environ 43, 3548-3555.

Watson, J.G., 2002. Visibility: Science and regulation. J Air Waste Manage 52, 628-713.

Westerholm, R., Li, H., Almen, J., 1993. Estimation of Aliphatic Amine Emissions in Automobile Exhausts. Chemosphere 27, 1381-1384.

Chapter 2: Proposed chemical mechanisms leading to secondary organic aerosol in the reactions of aliphatic amines with hydroxyl and nitrate radicals

Reference: Price, D.J., Clark, C.H., Tang, X., Cocker III, D.R., Purvis-Roberts, K.L., Silva, P.J., 2014. *Atmos. Environ*. 96, 135-144.

2.1. Introduction

Atmospheric aerosols are known to cause negative effects on human health, visibility, and the environment (Dockery, 2009; IPCC, 2007; Pope et al., 1995; Watson, 2002). Among these atmospheric pollutants, the formation of secondary organic aerosol (SOA) from alkyl amines has been gaining more attention. There are both anthropogenic and biogenic sources of these amines including agricultural emissions, by-products of selective catalytic reduction control technologies, and biomass burning (Cadle and Mulawa, 1980; Mosier et al., 1973; Westerholm et al., 1993).

Previous studies have suggested that secondary organic aerosol formation from amines is dominated by the production of salt through acid/base reactions with nitric and sulfuric acids (Ge et al., 2011; Murphy et al., 2007). These acid/base reactions alone, however, are not sufficient to explain the total secondary organic aerosol observed from atmospheric aliphatic amine oxidation (Silva et al., 2008; Tang et al., 2013). There has been little attention in the scientific literature given to the importance of peroxy radical chemistry in the formation of secondary organic aerosol from amines. A set of environmental chamber experiments were conducted to ascertain the impact of atmospheric amines on ambient SOA formation. In these experiments, an amine is

reacted with an atmospheric oxidant such as hydroxyl radical (OH) or nitrate radical (NO_3).

To decipher the SOA chemistry occurring in these experiments, a systematic theoretical approach was utilized in conjunction with carefully controlled environmental chamber studies. This approach assumes a simple system at the start of each experiment, i.e. an amine will react with an oxidant. At this point, there are several possible reaction routes. However, one can focus on the more likely routes based on known chemical behavior. For example, a radical will most likely abstract a hydrogen atom from a saturated organic molecule such as an amine (Schade and Crutzen, 1995; Tuazon et al., 1994). The question then becomes, which hydrogen will be abstracted? The answer to that question depends on factors such as bond strength, electronegativity, and steric hindrance (Bruice, 2004). As the various possible mechanisms are presented, the experimental data is consulted. In this study, three different mass spectrometric instruments were employed to identify both gas-phase and aerosol-phase oxidation products. With an understanding of how each instrument measures a given sample, certain mechanisms that do not match the results can be eliminated. In instances where multiple mechanisms agree with the results, alternative experiments are conducted to confirm or eliminate select chemical mechanisms. Following this approach, a plausible mechanism leading to oligomer products by way of peroxy radical reactions was determined.

2.2. Methods

A set of tertiary and secondary aliphatic amines were chosen for this study. These included trimethylamine (TMA, 25 wt.% solution in water, Sigma-Aldrich), triethylamine (TEA, >99.5%, Fluka), dimethylamine (DMA, 40 wt.% solution in water, Sigma-Aldrich) and diethylamine (DEA, >99.5%, Sigma-Aldrich). All experiments were conducted in an environmental chamber located at the College of Engineering - Center for Environmental Research and Technology, University of California - Riverside (CE-CERT/UCR). The amines were reacted in a 12.5 m^3 volume (50.8 μm) Teflon® chamber with hydroxyl radical (OH) and nitrate radical (NO_3). A summary of the experiments with initial concentrations is provided in Table 2.1. The environmental chamber is housed in a 2.5m x 3m x 7.8m reflective aluminum enclosure. Photooxidation, when desired, was driven by 170 40W black lights with peak intensity of 350 nm (350 BL, SYLVANIA) mounted to two of the enclosure walls. Prior to each experiment, the chamber was flushed with purified air (Aadco 737 air purification system) so that background particle concentration, NO_x, and hydrocarbon concentrations are below the detection limits of the instruments used. There were no seed aerosols injected. Only nucleation experiments were conducted in this study. Each experiment was run at room temperature (~295 K) under dry conditions (RH < 0.1%). The amine concentrations in the Teflon chambers were stable before radical injection. Hydroxyl radicals in no NO_x experiments were produced from direct photolysis of hydrogen peroxide (H_2O_2). The nitrate radical was formed from thermal decomposition of dinitrogen pentoxide (N_2O_5).

OH experiments were designed to represent daytime chemistry while the NO_3 experiments represented nighttime chemistry.

Chemical composition of the aerosol products was obtained with a High Resolution Time of Flight Aerosol Mass Spectrometer (HR-ToF-AMS; Aerodyne Research Inc.) (DeCarlo et al., 2006; Jayne et al., 2000). Briefly, an aerosol sample is first drawn through a time-of-flight region where the particles are separated based on their vacuum aerodynamic diameter. The sample is vaporized by a 600°C oven followed by 70 eV electron impact ionization. The resulting ions pass through another time-of-flight section which can be operated in two flight path configurations, V and W. The shorter flight path in the V-mode provides better sensitivity at unit mass resolution. The longer flight path in the W-mode provides separation of isobaric compounds which allows for determination of empirical formulas. For example, the high resolution spectrum (Figure 2.1) shows three ions at m/z 30. The HR-ToF-AMS has a mass resolution of up to 4300 at *m/z* 200 for the W-mode. The mass accuracy is within +/- 5 ppm.

A Particle Into Liquid Sampler – Time of Flight – Mass Spectrometer (PILS-ToF-MS; Brechtel Manufacturing Inc., Agilent Technologies) (Clark et al., 2013) instrument was also used to analyze the particulate matter composition. Particles are collected onto an impactor that is continuously flushed with water. This solution is then pumped to the mass spectrometer where the particles are ionized by electrospray ionization (ESI) and then detected by an accurate mass time of flight mass spectrometer allowing for the

determination of empirical formulas of the detected ions. The PILS-ToF-MS has a mass resolution of 4000 to 7000 from *m/z* 100 to 900 with a mass accuracy within +/- 5 ppm. As ESI is a soft ionization, the observed peaks represent complete molecules plus a proton (M+1). "Whole molecule" empirical formulas can be compared with the "fragment" empirical formulas from the HR-ToF-AMS to help elucidate chemical structures.

In addition to aerosol composition, the gas phase composition of the alkyl amine reaction products was determined with a Selected Ion Flow Tube - Mass Spectrometer (SIFT-MS; Syft Technologies) (Prince et al., 2010). The sample is introduced to a flow tube region where the analyte is ionized by three separate reagent ions (H_3O^+, NO^+, O_2^+) and then detected by a quadrupole mass spectrometer at unit mass resolution (UMR). The SIFT-MS was operated in either the selected ion mode (SIM) scan or the full mass scan. In the SIM scan, specific compounds are tracked and quantified via their product ion masses in real time. In the full mass scan, a mass spectrum is acquired for each reagent ion. As each reagent ion may react differently with a given compound, the identity of isobaric compounds can also be determined.

2.3. Results and Discussion

2.3.1. Peroxy radical mechanisms

It is proposed in this work that peroxy radical chemistry is important to the production of secondary organic aerosol from aliphatic amines. Amine oxidation is initiated by extraction of a hydrogen from the amine to form an alkyl radical that

subsequently reacts with oxygen to form an alkyl peroxy radical (RO_2). This alkyl peroxy radical can then react with another alkyl peroxy radical or hydroperoxyl radical (HO_2). Figure 2.2 gives a summary of three potential alkyl peroxy mechanisms. In the first possible mechanism (*i*), the two alkyl peroxy radicals react to form two alkoxy radicals along with an oxygen molecule. Each of these alkoxy radicals can further react with oxygen to form an aldehyde/ketone and hydroperoxyl radical. The second possible mechanism (*ii*) leads to the formation of an aldehyde, alcohol, and oxygen molecule. The third possible mechanism (*iii*) leads to the formation of a peroxide and oxygen molecule. The reaction of alkyl peroxy radical with HO_2 would either produce an aldehyde/ketone, alcohol, or hydroperoxide. (Finlayson-Pitts and Pitts, 2000; Seinfeld and Pandis, 2006)

2.3.2. Trimethylamine experiments

Figure 2.3 shows the HR-ToF-AMS spectra from the TMA + H_2O_2 and TMA + N_2O_5 experiments. The y-axes of the HR-ToF-AMS spectra are shown in log scale to better observe peaks at lower concentrations. Empirical formulas and possible structure assignments for some of the major fragment ions observed with the HR-ToF-AMS in the TMA experiments are provided in Table 2.2. The spectra are quite similar between the two experiments. This is to be expected, as the initial step for both OH and NO_3 is hydrogen abstraction from the amine. The main difference in the two experiments is that OH abstracts a hydrogen to form H_2O, while NO_3 abstracts a hydrogen to form nitric acid (HNO_3). This HNO_3 then has the ability to further react with the amine to form an amine salt. Salt formation, however, does not appear to be a major pathway, as very little nitrate

salt was observed in the TMA with NO_3 experiment. The minor nitrate formation observed in both experiments is probably due to a small NO_x background present in typical environmental chamber experiments (Carter et al., 2005). Further differences include an increase in the concentration of *m/z* 97 ($C_5H_9N_2^+$) and 111 ($C_6H_{11}N_2^+$) in the NO_3 experiment. The presence of two nitrogen atoms in the molecular formula of both ions indicates the addition of two nitrogen containing molecules. The formation of nitrate salt can be ruled out, as there are no oxygen atoms in the molecular formulas. The most probable explanation for these two ions is the fragmentation of amine dimers/oligomers.

The overall aerosol yield was greater in the NO_3 experiment. This could be due to a greater availability of RO_2 and HO_2 radicals as a result of the apparently faster NO_3 kinetics. Particle formation occurred within 2-3 minutes of N_2O_5 injection, whereas particle formation occurred around 10-12 minutes after photolysis of H_2O_2. An interesting observation in both experiments was the presence of fragment ions at much higher mass than the original amine. Even the formation of TMA salt, with a molecular weight of 122 g/mol, could not explain these higher mass peaks. Clearly, there is an alternate pathway leading to the formation of molecules of high molecular weight. A plausible explanation for these molecules will be discussed later.

Although the molecules undergo a high amount of fragmentation during electron ionization in the HR-ToF-AMS, the charge location and the type of fragmentation can be predicted (McLafferty and Turecek, 1993). Figure 2.4, for example, shows the NO_3

initiated peroxy chemistry along with potential EI fragmentation of the aerosol products. Trimethylamine initially reacts with NO_3 to form an alkyl radical and nitric acid followed by oxygen addition to the alkyl radical to form a peroxy radical. When two peroxy radicals react, they then follow one of three mechanisms (as previously discussed) leading either to gas phase amides and amino alcohols (mech. i and ii) or to an amine peroxide (mech. iii) that may partition to the particle phase. During electron ionization of these products, the charge is expected to occur on the lone pair electrons of the nitrogen atom. Further fragmentation leads to cleavage of the C-C bond of the alpha carbon (α), producing the ion at *m/z* 58 observed by the HR-ToF-AMS. It is also possible for the amide products to further react to form an amide peroxy radical (Barnes et al., 2010). This amide peroxy radical could also engage in peroxy chemistry leading to the formation of an amide peroxide (Figure 2.4). This new amide peroxide could be charged not only on the lone pairs of the nitrogen or peroxide oxygen atoms, but also on the carbonyl oxygen. This ion could then fragment in several ways leading to other *m/z* peaks observed by the HR-ToF-AMS. Not shown in Figure 2.4 is the possibility of an $RO_2 + HO_2$ reaction. However, the resultant amine hydroperoxide would also likely be charged on the amine nitrogen during electron ionization. Therefore, similar fragmentation would occur, leading to the fragment ions shown in Figure 2.4. Based on these fragmentation predictions, the HR-ToF-AMS spectra is consistent with expected products originating through peroxy radical chemistry.

The difficulty, however, with trying to assign fragments to specific molecules in this manner is the increasing complexity of the particle-phase as the experiment

progresses and multiple generation products are produced. Additionally, the likelihood of multiple charge sites on the oxidized products further increases the possible routes of fragmentation. Allowing for the possibility of charge migration and other internal rearrangements of the ion, the ability to make simple predictions fades quickly. There are simply too many possible fragmentation pathways to yield clear certainty of the original molecular structure. Therefore, an instrument with a softer ionization is required to overcome the complexities arising from fragmentation.

The instrument employed in these experiments to meet this need was the PILS-ToF-MS which uses the softer electrospray ionization (ESI). The mass spectrum obtained with the PILS-ToF-MS from the TMA + H_2O_2 experiment (Figure 2.5) shows a series of peaks separated by 103.029 amu. Table 2.3 provides the empirical formula and possible structure assignments for some of the major ions in the spectrum. The chemical pathway in figure 2.6 identifies a route for formation of oligomer compounds to account for the peak series as well as the high mass fragments observed in the HR-ToF-AMS spectra. The radical (OH or NO_3) initiates the peroxy radical reaction to form an amide. An additional radical attack, followed by a hydrogen rearrangement if the carbonyl hydrogen is abstracted, leads to the formation of a monomer-like peroxy radical. That peroxy radical monomer continues to add by RO_2 + RO_2 chemistry to produce oligomer compounds. These reactions start in the gas phase and then continue in the particle phase where surface reactions between the peroxy radical monomer and oligomers occur. There are also HO_2 radicals present that can compete with the peroxy radical monomer. The PILS-ToF-MS observed a series of compounds formed from RO_2 + HO_2 reactions

(*m/z* 104, 207, 310, 413, 516, etc.), though at lower concentrations than the $RO_2 + RO_2$ series. The reaction of the peroxy radical monomer with HO_2 formed a hydroperoxide that was observed at *m/z* 106 (Figure 2.5, Table 2.3).

Another way to view the PILS-ToF-MS data is through a contour plot, such as the one shown in figure 2.7. In this plot, the y-axis is the mass-to-charge ratio, the x-axis is time, and the color scale is the signal intensity. Hypothetically, in an experiment where a nucleation event occurs without subsequent oligomerization, one would expect to see contour lines at specific m/z values appear at the same time (when particles are grown sufficiently to be detected by system) and continue across the graph to the end of the experiment. A similar contour plot could be produced through the clustering of molecules during the ESI process in the PILS-ToF-MS. However, in an oligomerization process, one would expect to see lower m/z compounds appear first with larger compounds separated by specific m/z values fading in over time while smaller compound intensities decrease. This latter behavior is observed in the TMA + H_2O_2 experiment (Figure 2.7) confirming that the large molecular weight compounds are formed through an oligomerization process.

According to the proposed mechanisms for the TMA experiments, amides and amino alcohols should be present and detectable as gas-phase products. The SIFT-MS confirms the presence of these predicted species. Figure 2.8 shows the SIFT-MS mass spectra for the three reagent ions (H_3O^+, NO^+, and O_2^+) in the TMA + H_2O_2 experiment. Table 2.4 provides the empirical formula and possible structure assignments for some of

the major ions observed in the spectra. The spectra taken before photooxidation (light gray) were superimposed on the spectra taken later in the experiment (dark gray, black). This was done to highlight the product compounds as they increased in concentration over time. Dimethylformamide (DMF), N-formyl-N-methylformamide (FMF), and N,N-diformylformamide (DFF) were observed in the H_3O^+ reagent ion spectrum (*m/z* 74, $DMF{\cdot}H^+$; *m/z* 88, $FMF{\cdot}H^+$; and *m/z* 102, $DFF{\cdot}H^+$) as well as the NO^+ reagent ion spectrum (*m/z* 103, $DMF{\cdot}NO^+$; *m/z* 117, $FMF{\cdot}NO^+$; and *m/z* 131, $DFF{\cdot}NO^+$). Fragments of these compounds were observed in the O_2^+ reagent spectrum (*m/z* 72, DMF fragment).

To test the hypothesis that the peroxy chemistry was critical to secondary organic aerosol formation, a repeat of the TMA + H_2O_2 experiment was conducted with the addition of NO. In this experiment, the excess NO was found to consume peroxy radicals to form an alkoxy radical and NO_2, thereby obstructing the peroxy chemistry (Figure 2.9). This also provided a source of HNO_3 that allowed for the formation of amine salts. The resulting HR-ToF-AMS mass spectrum (Figure 2.10B) is more similar to the spectrum from a TMA + HNO_3 experiment (Figure 2.10C) than it is to the spectrum from the original TMA + H_2O_2 experiment (Figure 2.10A).

It was also observed that the fragments from the oligomer molecules disappeared in the TMA + H_2O_2 + NO experiment. This suggests that the RO_2 + RO_2 cross reactions are needed for oligomer formation. To test the importance of peroxy radicals to oligomer formation, an additional experiment was conducted in which TMA was reacted with O_3 followed by NO. In the TMA + O_3 + NO experiment, O_3 reacts with NO to form NO_2,

which reacts further with O_3 to form NO_3 radical. The mass spectra from the TMA + O_3 + NO experiment both before and after NO injection are shown in figure 2.11. The O_3 does react with TMA to form some aerosol (top spectrum). However, more aerosol was produced after the formation of NO_3. Also, the higher mass fragments are seen only after NO injection (bottom spectrum) and are similar to those seen in the TMA + N_2O_5 experiment. This suggests that the oligomer formation requires NO_3 or OH radical hydrogen abstraction. Future field studies in areas with high amine emissions could help determine the atmospheric importance of the RO_2 + RO_2 oligomer chemistry.

2.3.3. Triethylamine experiments

The high molecular weight peaks in the TMA experiment are not observed with the HR-ToF-AMS for the triethylamine (TEA) with N_2O_5 experiment (Figure 2.12), suggesting little to no oligomer formation with TEA as a precursor. The key difference between TMA and TEA is that TMA has only methyl groups attached to the nitrogen, whereas TEA has only ethyl groups attached to the nitrogen (Table 2.1). Therefore, when a radical attacks TMA, the only amides formed are those with an aldehyde functionality [NC(O)H]. When a radical attacks TEA, the only amides formed are those with a ketone functionality [$NC(O)CH_3$]. While it is also possible for the radical to attack the beta-carbons of TEA, the alpha-carbon attack is more probable due to the weaker C-H bond strength at the alpha site and the more stable intermediate radical produced (Bruice, 2004). It would appear that the ketone functionality inhibits oligomer formation. Previous studies with isoprene and butadiene photooxidation have shown the importance

of the aldehyde functionality and molecular structure to oligomer formation (Chan et al., 2010; Surratt et al., 2006).

The largest significant peak in the HR-ToF-AMS mass spectrum is *m/z* 100. This is consistent with the fragmentation of an amine peroxide, following the pathway observed in the TMA experiment (Figure 2.4). The fragmentation of triethylaminium salt ($TEA \cdot HNO_3$ = 164 amu) could also account for the *m/z* 100 peak. The fraction of NO^+ (*m/z* 30) and NO_2^+ (*m/z* 46) to the total aerosol observed by the HR-ToF-AMS was greater in the TEA experiment than in the TMA experiment (9.3% and 7.4% respectively); indicating a greater salt contribution.

2.3.4. Secondary amine experiments

The mass spectrum from the DEA with N_2O_5 experiment is shown in figure 2.13. There are no significant peaks in the high mass range for DEA, suggesting little to no oligomer formation. The largest significant peaks observed in the HR-ToF-AMS mass spectrum are *m/z* 58, 72, and 86. This is consistent with the fragmentation of amine and amide peroxides and salts, following the pathways observed in the TMA experiment (Figure 2.4). The fraction of NO^+ (*m/z* 30) and NO_2^+ (*m/z* 46) to the total aerosol observed by the HR-ToF-AMS was 14.6%; indicating a greater salt contribution in the secondary amine experiments than in the tertiary amine experiments. This is consistent with previous work by Tang et al. (2013), employing particle into liquid sampler – ion chromatography (PILS-IC) and a scanning mobility particle sizer (SMPS), which showed

a greater amine salt contribution with DEA + NO_3 compared to TMA + NO_3 (40-59% and <6% respectively, Tang et al., 2013).

Additional chemistry is observed for the secondary amine experiments, such as the formation of nitramines and imines, possibly due to the availability of the N-H bond. The formation of nitramines is a significant observation as nitramines are known to be carcinogenic (Lindley et al., 1979; Tuazon et al., 1984). Figure 2.14 shows the SIFT-MS mass spectra from the diethylamine with N_2O_5 experiment. Diethylnitramine (DEN) formed within 2 minutes of N_2O_5 injection (*m/z* 119 H_3O^+; *m/z* 148 NO^+; *m/z* 103 and 118 O_2^+). N-ethylethanimine (EEI) also formed quickly in this experiment (*m/z* 72 H_3O^+; *m/z* 71 NO^+; *m/z* 71 O_2^+). The m/z peaks for nitric acid are also observed (*m/z* 30, 46, and 64 H_3O^+; *m/z* 46 O_2^+). Figure 2.15 shows the SIFT-MS mass spectra from the dimethylamine with N_2O_5 experiment. Dimethylnitramine (DMN) formed within 5 minutes of N_2O_5 injection (*m/z* 91 H_3O^+; *m/z* 120 NO^+; *m/z* 90 O_2^+). N-methylmethanimine formed quickly as well (*m/z* 44 H_3O^+; *m/z* 43 NO^+; *m/z* 43 O_2^+). Nitric acid formation was also observed.

2.4. Conclusion

The assembly and fragmentation of molecules were predictable based on an understanding of known chemical behaviors. Combining this knowledge with mass spectral data from both electron and chemical ionization instruments is proven as a powerful tool for determining atmospheric oxidation reaction mechanisms. The HR-ToF-AMS and PILS-ToF-MS are complementary analytical instruments. The HR-ToF-

AMS provides bulk analysis of the particle phase at the expense of fragmentation. The high resolution W-mode data provides the empirical formulas, while the unit resolution V-mode contributes mass concentration and size distribution information. The benefits of the PILS-ToF-MS include the softer electrospray ionization that reduces fragmentation. However, there may be aqueous phase reactions that occur between the PILS sampling and electrospray ionization. Further studies are needed to determine if aqueous phase reactions are significant.

Alkyl peroxy chemistry was observed as an important pathway to the formation of secondary organic aerosol from amine precursors. This chemistry is initiated via hydrogen abstraction from the amine precursor by hydroxyl or nitrate radical. Two alkyl peroxy radicals can react to form amides, amino alcohols, or amine/amide peroxides. Additionally, oligomer formation was observed as a potential significant contributor to secondary organic aerosol from trimethylamine oxidation. This is atmospherically relevant in areas with high amine emissions, where $RO_2 + RO_2$ reactions are more likely to compete with $RO_2 + HO_2$ chemistry. It appears that alkyl peroxy chemistry via radical hydrogen abstraction is fundamental for oligomer growth. In the oligomer mechanism, alkyl peroxy "monomers" continue to add to the base molecule through peroxide linkages. The oligomer mechanism is observed in the trimethylamine experiment, but not the triethylamine or diethylamine experiments. This suggests that the ketone-amide functionality produced in the ethyl-amine reactions inhibits oligomer formation. The availability of N-H bonds in the secondary amines allowed for the formation of nitramines and imines. The formation of carcinogenic nitramines from secondary amines

has negative human health implications in areas with high concentrations of secondary amines.

2.5. References

Barnes, I., Solignac, G., Mellouki, A., Becker, K.H., 2010. Aspects of the Atmospheric Chemistry of Amides. Chemphyschem 11, 3844-3857.

Bruice, P.Y., 2004. Organic Chemistry, 4th ed. Pearson Prentice Hall, Upper Saddle River.

Cadle, S.H., Mulawa, P.A., 1980. Low-Molecular Weight Aliphatic-Amines in Exhaust from Catalyst-Equipped Cars. Environmental Science & Technology 14, 718-723.

Carter, W.P.L., Cocker, D.R., III, Fitz, D.R., Malkina, I.L., Bumiller, K., Sauer, C.G., Pisano, J.T., Bufalino, C., Song, C., 2005. A new environmental chamber for evaluation of gas-phase chemical mechanisms and secondary aerosol formation. Atmos Environ 39, 7768-7788.

Chan, A.W.H., Chan, M.N., Surratt, J.D., Chhabra, P.S., Loza, C.L., Crounse, J.D., Yee, L.D., Flagan, R.C., Wennberg, P.O., Seinfeld, J.H., 2010. Role of aldehyde chemistry and NOx concentrations in secondary organic aerosol formation. Atmos Chem Phys 10, 7169-7188.

Clark, C.H., Nakao, S., Asa-Awuku, A., Sato, K., Cocker III, D.R., 2013. Real-time study of particle-phase products from a-pinene ozonolysis and isoprene photo-oxidation using particle into liquid sampling directly coupled to a time of flight mass spectrometer (PILS-ToF). Aerosol Sci Tech 47, 1374.

DeCarlo, P.F., Kimmel, J.R., Trimborn, A., Northway, M.J., Jayne, J.T., Aiken, A.C., Gonin, M., Fuhrer, K., Horvath, T., Docherty, K.S., Worsnop, D.R., Jimenez, J.L., 2006. Field-deployable, high-resolution, time-of-flight aerosol mass spectrometer. Analytical Chemistry 78, 8281-8289.

Dockery, D.W., 2009. Health Effects of Particulate Air Pollution. Annals of Epidemiology 19, 257-263.

Finlayson-Pitts, B.J., Pitts, J.N., Jr., 2000. Chemistry of the Upper and Lower Atmosphere: Theory, Experiments, and Applications. Academic Press, San Diego.

Ge, X., Wexler, A.S., Clegg, S.L., 2011. Atmospheric Amines – Part I, A Review. Atmos Environ 45, 524-546.

IPCC, 2007. Summary for Policymakers. In: Climate Change 2007: The Physical Science Basis. Contribution of Working Group I to the Fourth Assessment Report of the Intergovernmental Panel on Climate Change. [Solomon, S., D. Qin, M. Manning, Z. Chen, M. Marquis, K.B. Averyt, M. Tignor and H.L. Miller (eds.)]. Cambridge University Press, Cambridge, United Kingdom and New York, NY, USA.

Jayne, J.T., Leard, D.C., Zhang, X.F., Davidovits, P., Smith, K.A., Kolb, C.E., Worsnop, D.R., 2000. Development of an aerosol mass spectrometer for size and composition analysis of submicron particles. Aerosol Sci Tech 33, 49-70.

Lindley, C.R.C., Calvert, J.G., Shaw, J.H., 1979. RATE STUDIES OF THE REACTIONS OF THE (CH3)2N RADICAL WITH O2, NO, AND NO2. Chemical Physics Letters 67, 57-62.

McLafferty, F.W., Turecek, F., 1993. Interpretation of Mass Spectra, 4th ed. University Science Books, Sausalito.

Mosier, A.R., Andre, C.E., Viets, F.G., Jr., 1973. Identification of Aliphatic Amines Volatilized from Cattle Feedyard. Environmental Science & Technology 7, 642-644.

Murphy, S.M., Sorooshian, A., Kroll, J.H., Ng, N.L., Chhabra, P., Tong, C., Surratt, J.D., Knipping, E., Flagan, R.C., Seinfeld, J.H., 2007. Secondary aerosol formation from atmospheric reactions of aliphatic amines. Atmos Chem Phys 7, 2313-2337.

Pope, C.A., Thun, M.J., Namboodiri, M.M., Dockery, D.W., Evans, J.S., Speizer, F.E., Heath, C.W., 1995. Particulate Air-Pollution as a Predictor of Mortality in a Prospective-Study of Us Adults. American Journal of Respiratory and Critical Care Medicine 151, 669-674.

Prince, B.J., Milligan, D.B., McEwan, M.J., 2010. Application of selected ion flow tube mass spectrometry to real-time atmospheric monitoring. Rapid Communications in Mass Spectrometry 24, 1763-1769.

Schade, G.W., Crutzen, P.J., 1995. Emission of Aliphatic-Amines from Animal Husbandry and Their Reactions - Potential Source of N2o and Hcn. Journal of Atmospheric Chemistry 22, 319-346.

Seinfeld, J.H., Pandis, S.N., 2006. Atmospheric Chemistry and Physics: From Air Pollution to Climate Change, 2nd ed. John Wiley & Sons, Inc., Hoboken.

Silva, P.J., Erupe, M.E., Price, D.J., Elias, J., Malloy, Q.G.J., Li, Q., Warren, B., Cocker, D.R., III, 2008. Trimethylamine as precursor to secondary organic aerosol formation via nitrate radical reaction in the atmosphere. Environmental Science & Technology 42, 4689-4696.

Surratt, J.D., Murphy, S.M., Kroll, J.H., Ng, N.L., Hildebrandt, L., Sorooshian, A., Szmigielski, R., Vermeylen, R., Maenhaut, W., Claeys, M., Flagan, R.C., Seinfeld, J.H., 2006. Chemical composition of secondary organic aerosol formed from the photooxidation of isoprene. J Phys Chem A 110, 9665-9690.

Tang, X.C., Price, D., Praske, E., Lee, S.A., Shattuck, M.A., Purvis-Roberts, K., Silva, P.J., Asa-Awuku, A., Cocker, D.R., 2013. NO3 radical, OH radical and O-3-initiated secondary aerosol formation from aliphatic amines. Atmos Environ 72, 105-112.

Tuazon, E.C., Atkinson, R., Aschmann, S.M., Arey, J., 1994. Kinetics and Products of the Gas-Phase Reactions of O3 with Amines and Related-Compounds. Research on Chemical Intermediates 20, 303-320.

Tuazon, E.C., Carter, W.P.L., Atkinson, R., Winer, A.M., Pitts, J.N., 1984. ATMOSPHERIC REACTIONS OF N-NITROSODIMETHYLAMINE AND DIMETHYLNITRAMINE. Environmental Science & Technology 18, 49-54.

Watson, J.G., 2002. Visibility: Science and regulation. J Air Waste Manage 52, 628-713.

Westerholm, R., Li, H., Almen, J., 1993. Estimation of Aliphatic Amine Emissions in Automobile Exhausts. Chemosphere 27, 1381-1384.

2.6. Tables

Table 2.1. Initial conditions of the environmental chamber experiments.

Amine	Structure	[Amine][a] ppb	Oxidant	[Oxidant][a] ppb	[NO_x] ppb	[Ozone] ppb
TMA	$(CH_3)_3N$	100	H_2O_2 (OH)	410	0	0
TMA	$(CH_3)_3N$	100	N_2O_5 (NO_3)	300	0	0
TMA	$(CH_3)_3N$	100	O_3 + NO		100	excess
TMA	$(CH_3)_3N$	100	HNO_3	100	0	0
TMA	$(CH_3)_3N$	225	H_2O_2 + NO	1000	3000	0
TEA	$(CH_3CH_2)_3N$	100	H_2O_2 (OH)	410	0	0
TEA	$(CH_3CH_2)_3N$	100	N_2O_5 (NO_3)	300	0	0
DMA	$(CH_3)_2NH$	100	H_2O_2 (OH)	410	0	0
DMA	$(CH_3)_2NH$	100	N_2O_5 (NO_3)	300	0	0
DEA	$(CH_3CH_2)_2NH$	100	H_2O_2 (OH)	410	0	0
DEA	$(CH_3CH_2)_2NH$	100	N_2O_5 (NO_3)	300	0	0

a) Initial amine, H_2O_2, and N_2O_5 concentrations were calculated using the injected volume.

Table 2.2. Some of the major fragment ions observed by the HR-ToF-AMS in the TMA experiments along with their proposed molecular structure in SYBYL line notation.

m/z	Empirical Formula	Possible structure (SYBYL line notation)
58.066	$C_3H_8N^+$	N[+](CH3)(CH3)=CH2
88.040	$C_3H_6NO_2^+$	HC(=O)N(CH3)CH=O[+]H
97.077	$C_5H_9N_2^+$	N[1]HC(CH3)HCH=N[+]HCH=CH@1
104.035	$C_3H_6NO_3^+$	HC(=O)N(CH3)CH2O[+]=O
111.092	$C_6H_{11}N_2^+$	N[1]HC(CH3)HCH=N[+]HC(CH3)=CH@1
133.061	$C_4H_9N_2O_3^+$	HC(=O)N(H)CH2OOCH2N[+](H)=CH2
145.061	$C_5H_9N_2O_3^+$	HC(=O)N[+](=CH2)CH2OOCH2N=CH2
161.056	$C_5H_9N_2O_4^+$	HC(=O)N(CH3)CH2OOC(=O)N[+](H)=CH2
191.067	$C_6H_{11}N_2O_5^+$	HC(=O)N(CH3)CH2OOC(=O)N(CH3)CH=O[+]H
207.062	$C_6H_{11}N_2O_6^+$	HC(=O)N(CH3)CH2OOC(=O)N(CH3)CH2O[+]=O

Table 2.3. Empirical formula and possible structure assignments for some of the major PILS-ToF-MS ions in the trimethylamine with OH experiment.

m/z	Empirical Formula	Possible structure
60.081	$C_3H_{10}N^+$	Trimethylamine (TMA)
74.061	$C_3H_8NO^+$	Dimethylformamide (DMF)
88.048	$C_3H_6NO_2^+$	N-formyl-N-methylformamide (FMF)
106.051	$C_3H_8NO_3^+$	Peroxy monomer + $HO_2^\cdot$ → ROOH
191.068	$C_6H_{11}N_2O_5^+$	FMF + 1 monomer
294.097	$C_9H_{16}N_3O_8^+$	FMF + 2 monomers
397.125	$C_{12}H_{21}N_4O_{11}^+$	FMF + 3 monomers
500.154	$C_{15}H_{26}N_5O_{14}^+$	FMF + 4 monomers
603.181	$C_{18}H_{31}N_6O_{17}^+$	FMF + 5 monomers
706.211	$C_{21}H_{36}N_7O_{20}^+$	FMF + 6 monomers

Table 2.4. Empirical formula and possible structural assignments for some of the major ions observed by the SIFT-MS for each of the three reagent ions in the TMA with OH experiment. *SIFT-MS reagent ions.

m/z	Ion*	Empirical Formula	Possible structure
60	H_3O+	$C_3H_9N \cdot H^+$	Trimethylamine (TMA)
74	H_3O+	$C_3H_7NO \cdot H^+$	Dimethylformamide (DMF)
88	H_3O+	$C_3H_5NO_2 \cdot H^+$	N-formyl-N-methylformamide (FMF)
102	H_3O+	$C_3H_3NO_3 \cdot H^+$	N,N-diformylformamide (DFF)
59	NO+	$C_3H_9N^+$	Trimethylamine
103	NO+	$C_3H_7NO \cdot NO^+$	Dimethylformamide + NO
117	NO+	$C_3H_5NO_2 \cdot NO^+$	N-formyl-N-methylformamide + NO
131	NO+	$C_3H_3NO_3 \cdot NO^+$	N,N-diformylformamide + NO
58	O_2+	$C_3H_8N^+$	TMA fragment
59	O_2+	$C_3H_9N^+$	Trimethylamine
72	O_2+	$C_3H_6NO^+$	DMF fragment

2.7. Figures

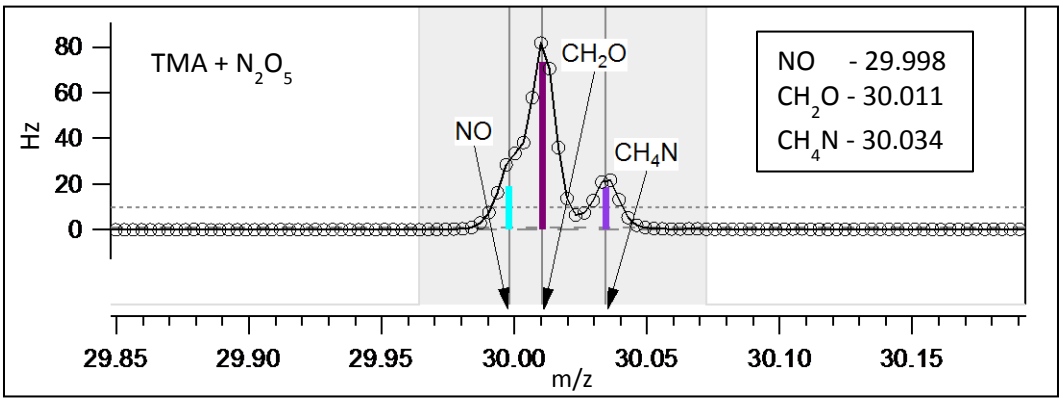

Figure 2.1. High resolution mass spectrum of m/z 30 from the TMA + N_2O_5 experiment.

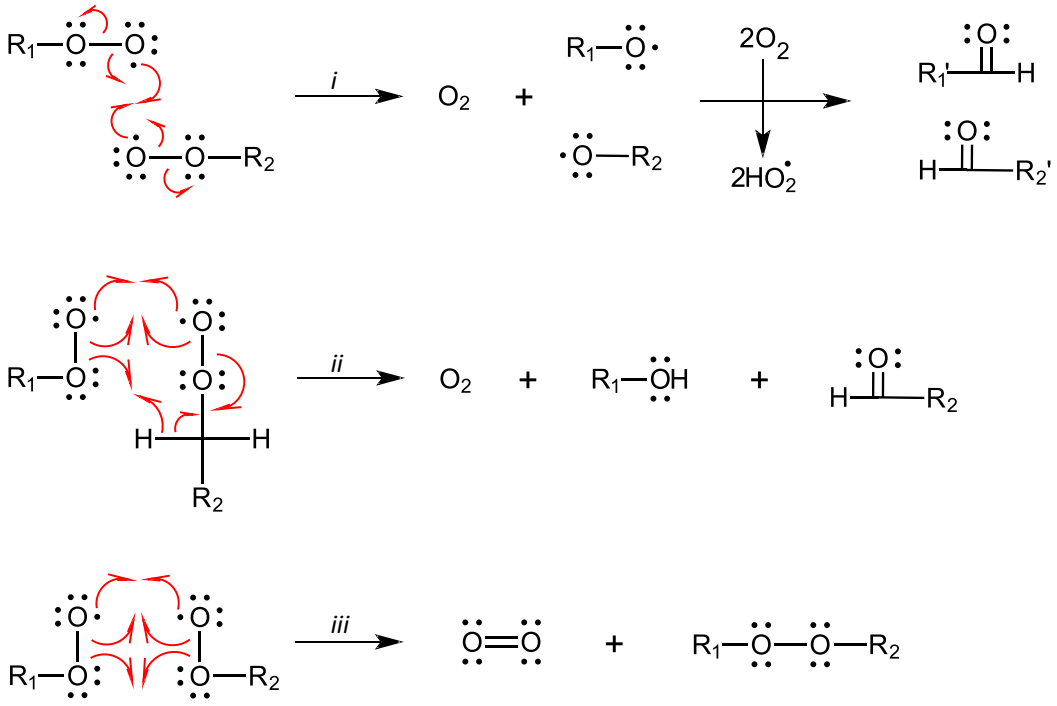

Figure 2.2. Three possible mechanisms for peroxy radical chemistry.

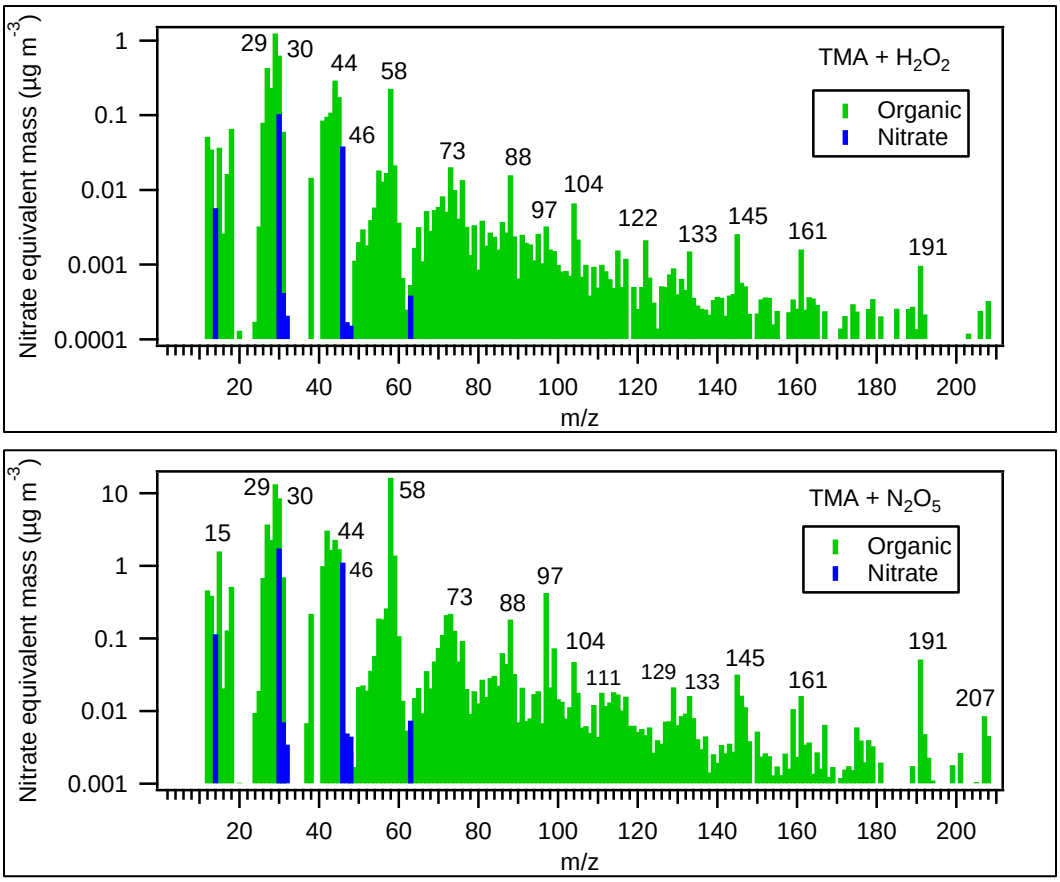

Figure 2.3. HR-ToF-AMS mass spectra from the reaction of TMA with H_2O_2 (top) and N_2O_5 (bottom).

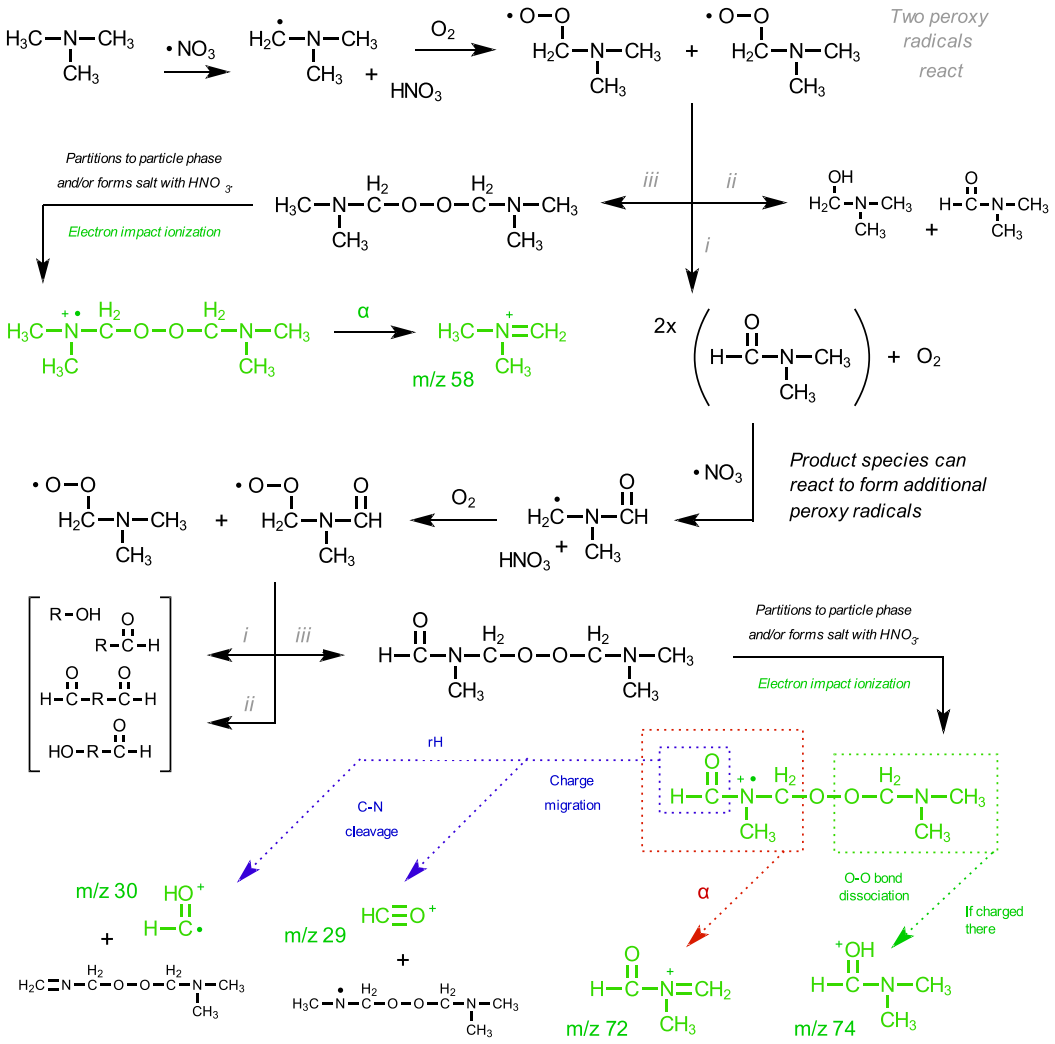

Figure 2.4. Possible chemical pathways in the TMA + N_2O_5 experiment. The compounds in green with corresponding *m/z* values are ions observed by the HR-ToF-AMS.

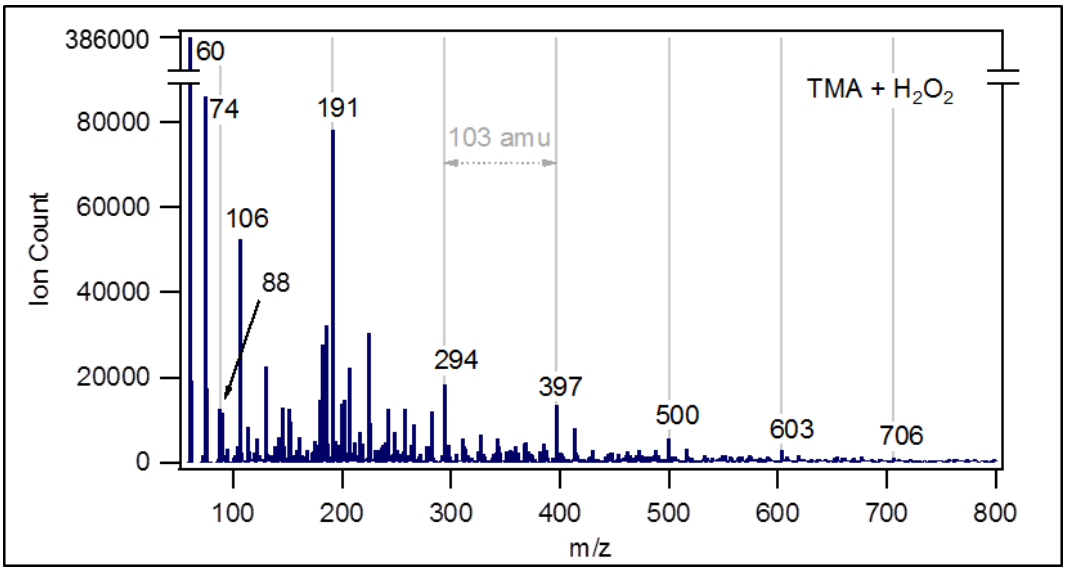

Figure 2.5. PILS-ToF-MS mass spectrum from the reaction of TMA with H_2O_2.

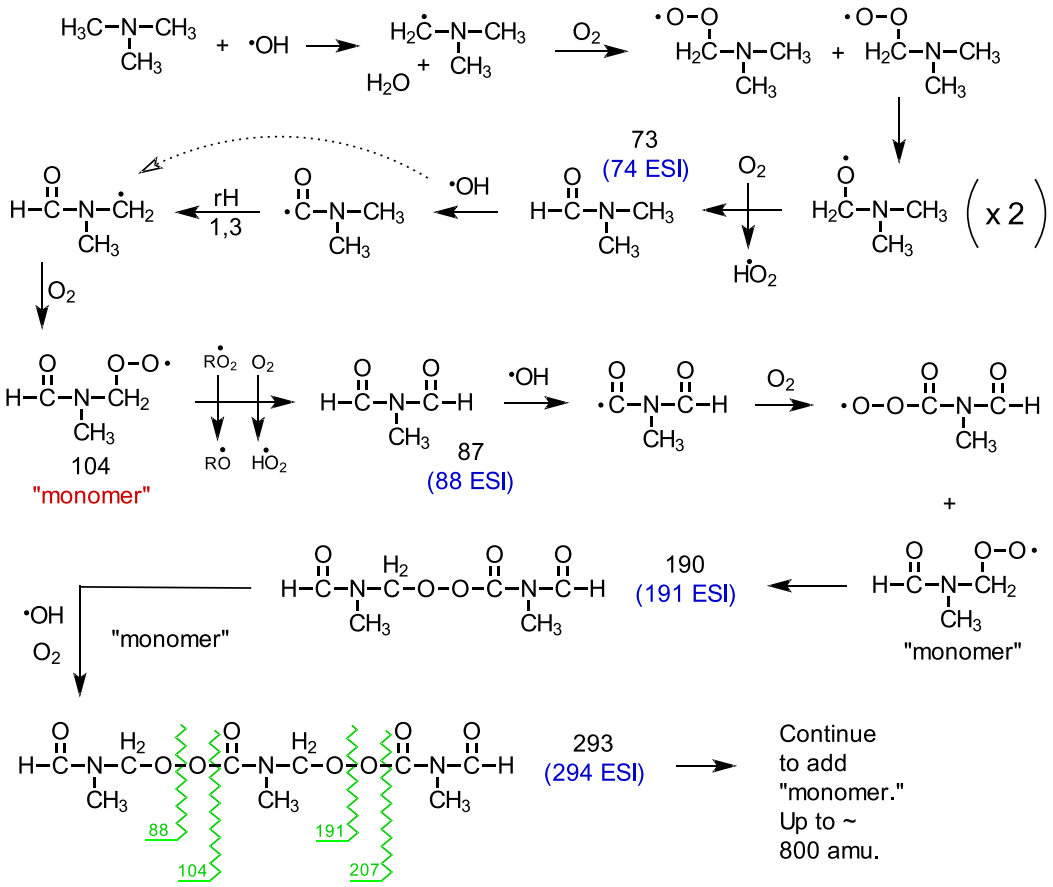

Figure 2.6. Proposed pathway for oligomer aerosol formation. The blue numbers represent peaks observed with the PILS-ToF-MS. The green numbers represent the fragment peaks observed by the HR-ToF-AMS.

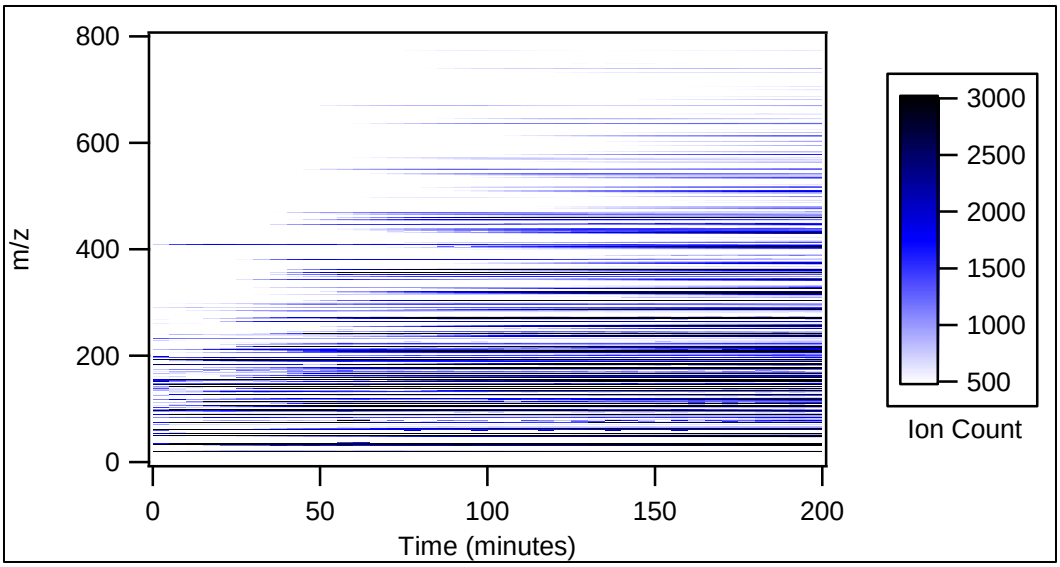

Figure 2.7. Contour plot of PILS-ToF-MS data over time for the reaction of TMA with OH radical.

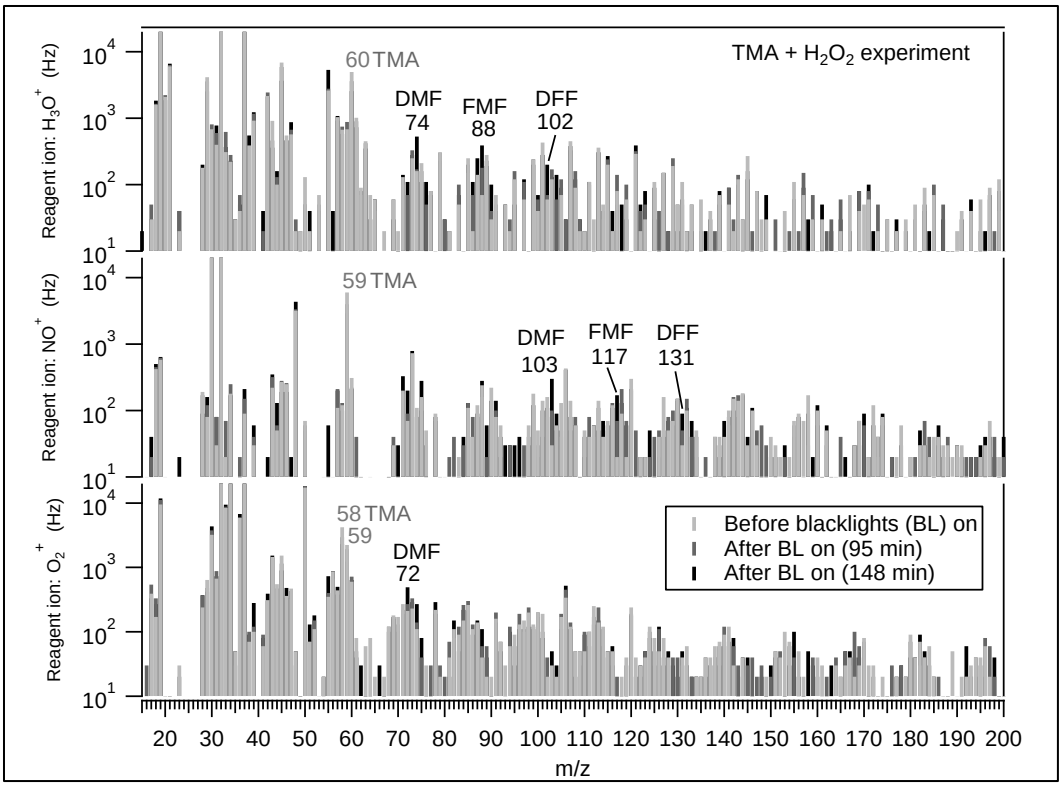

Figure 2.8. SIFT-MS mass spectra from the TMA + H_2O_2 experiment.

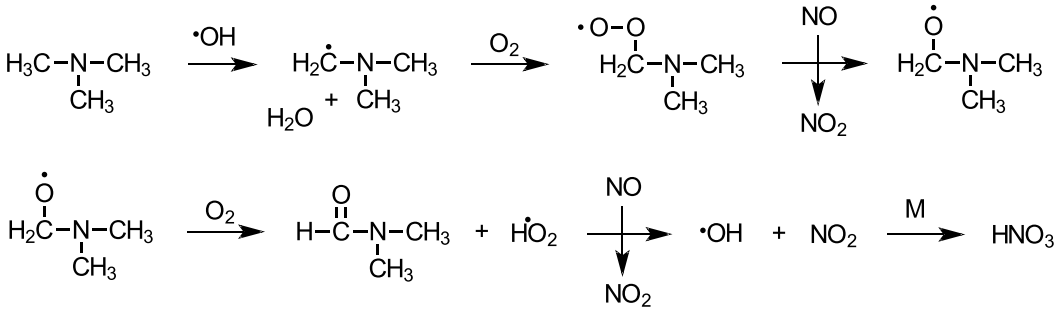

Figure 2.9. Pathway for nitric acid formation in the TMA + H_2O_2 + NO experiment.

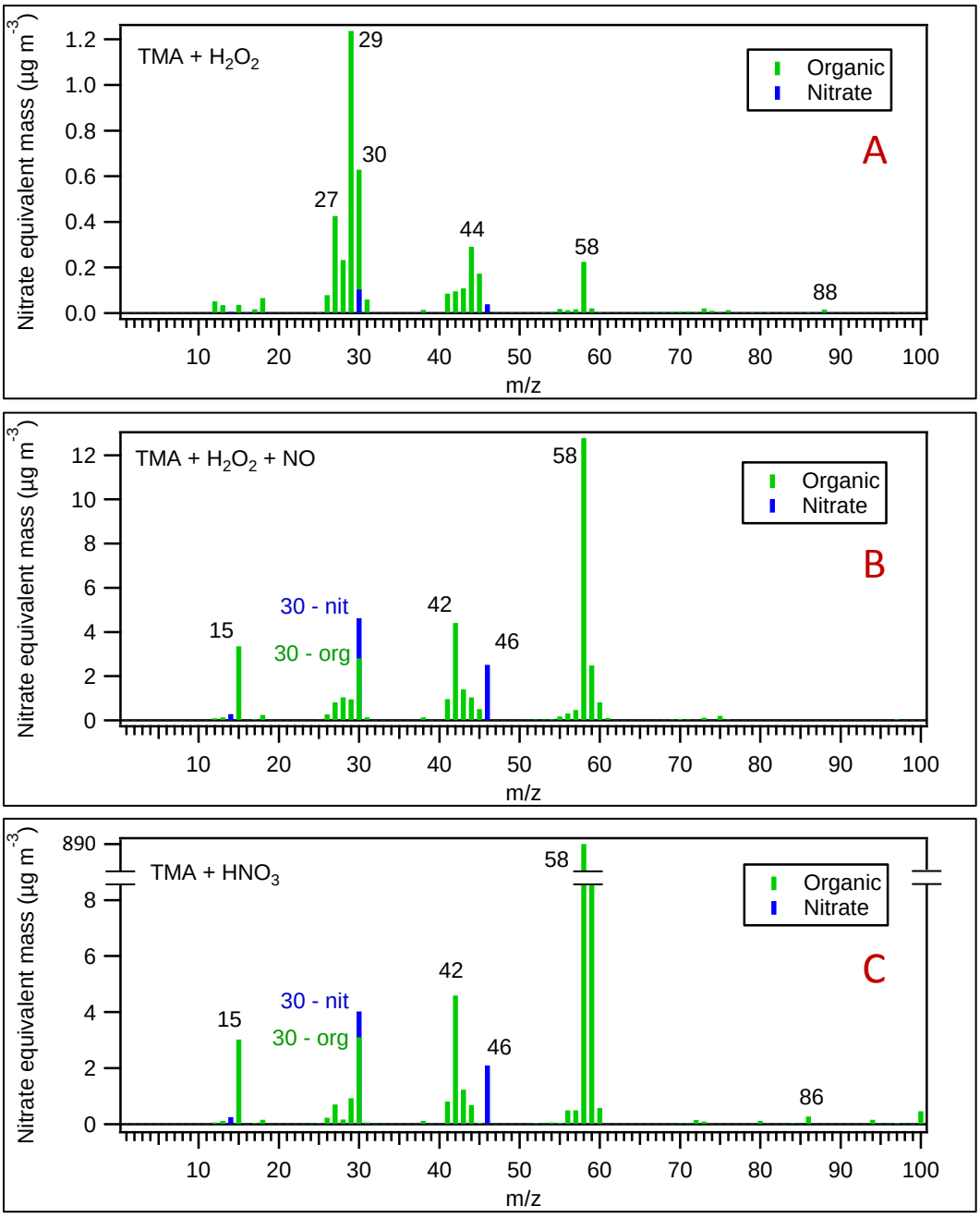

Figure 2.10. HR-ToF-AMS mass spectra from the A) TMA + H_2O_2, B) TMA + H_2O_2 + NO and C) TMA + HNO_3 experiments.

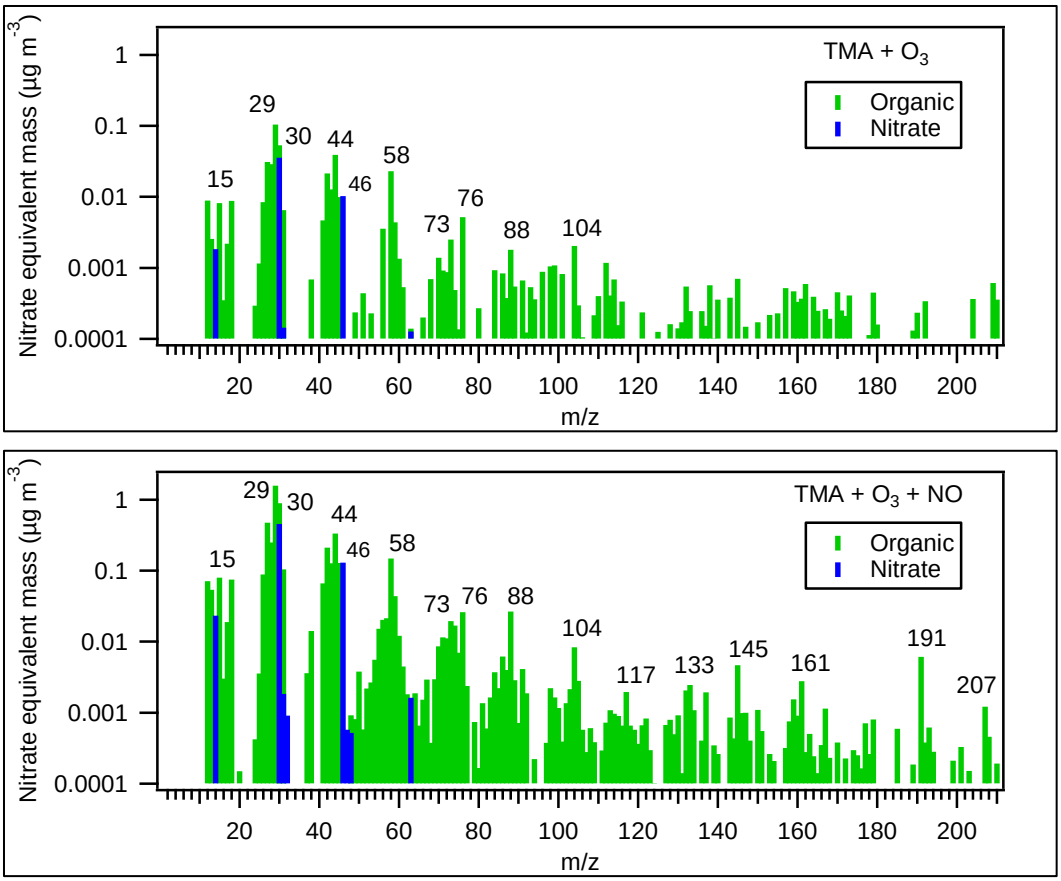

Figure 2.11. HR-ToF-AMS mass spectra from the TMA + O_3 + NO experiment. TMA + ozone only (Top). TMA + ozone + NO (Bottom).

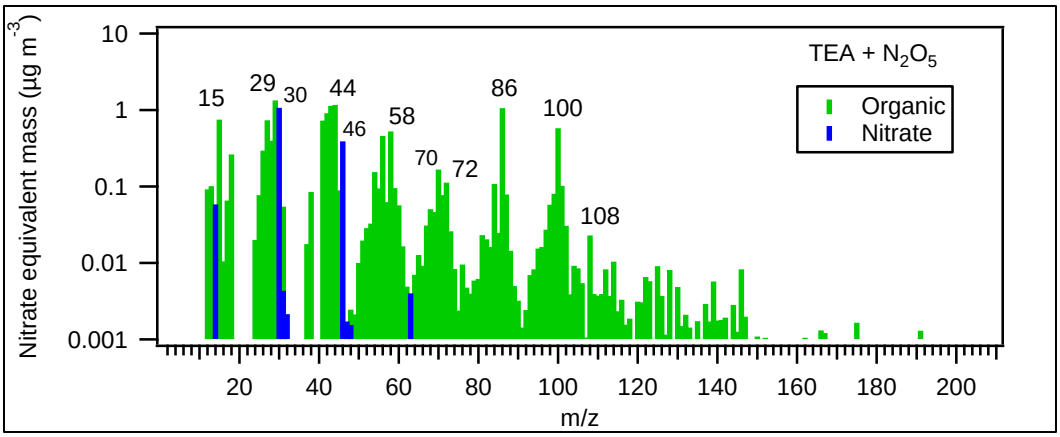

Figure 2.12. HR-ToF-AMS mass spectrum from the TEA + N_2O_5 experiment.

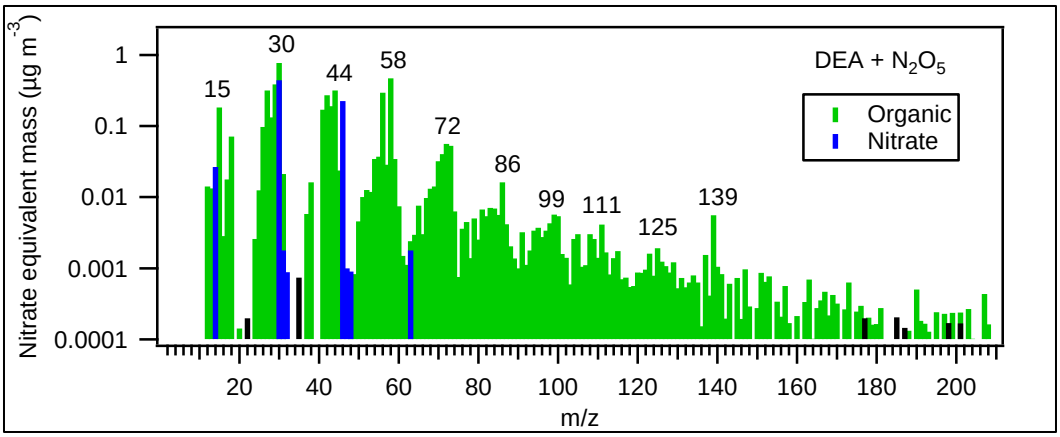

Figure 2.13. HR-ToF-AMS mass spectrum from the DEA + N_2O_5 experiment.

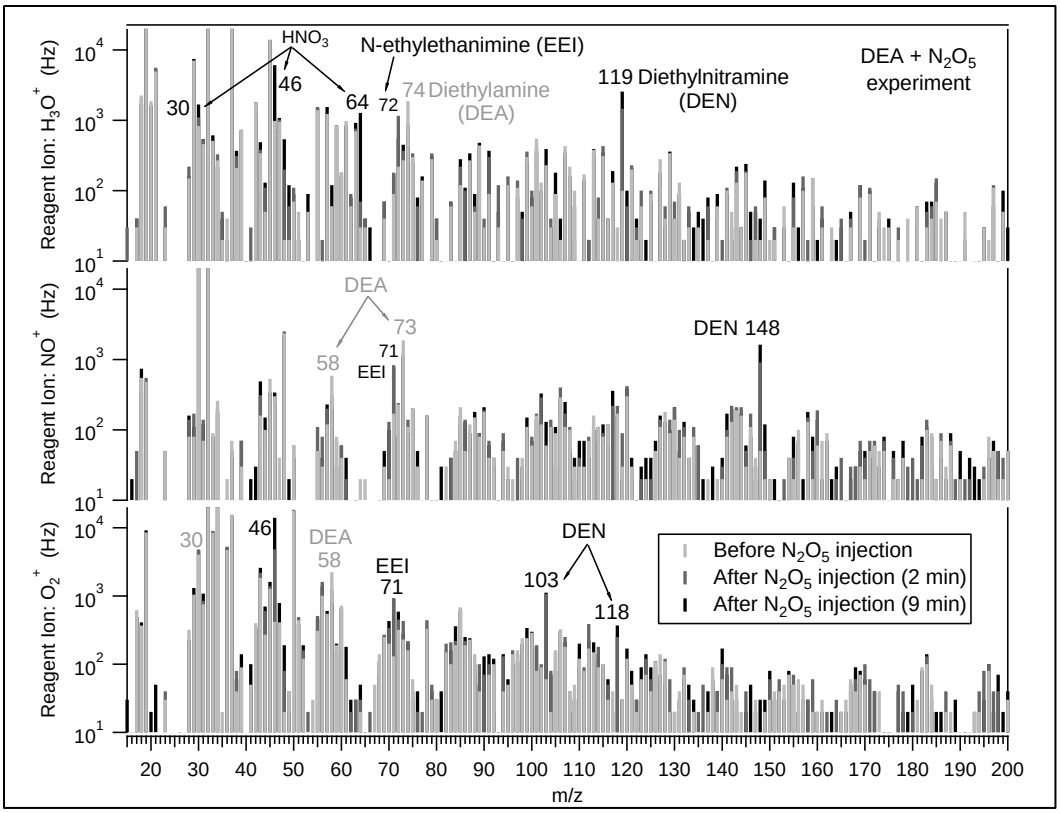

Figure 2.14. SIFT-MS mass spectra from the DEA + N_2O_5 experiment.

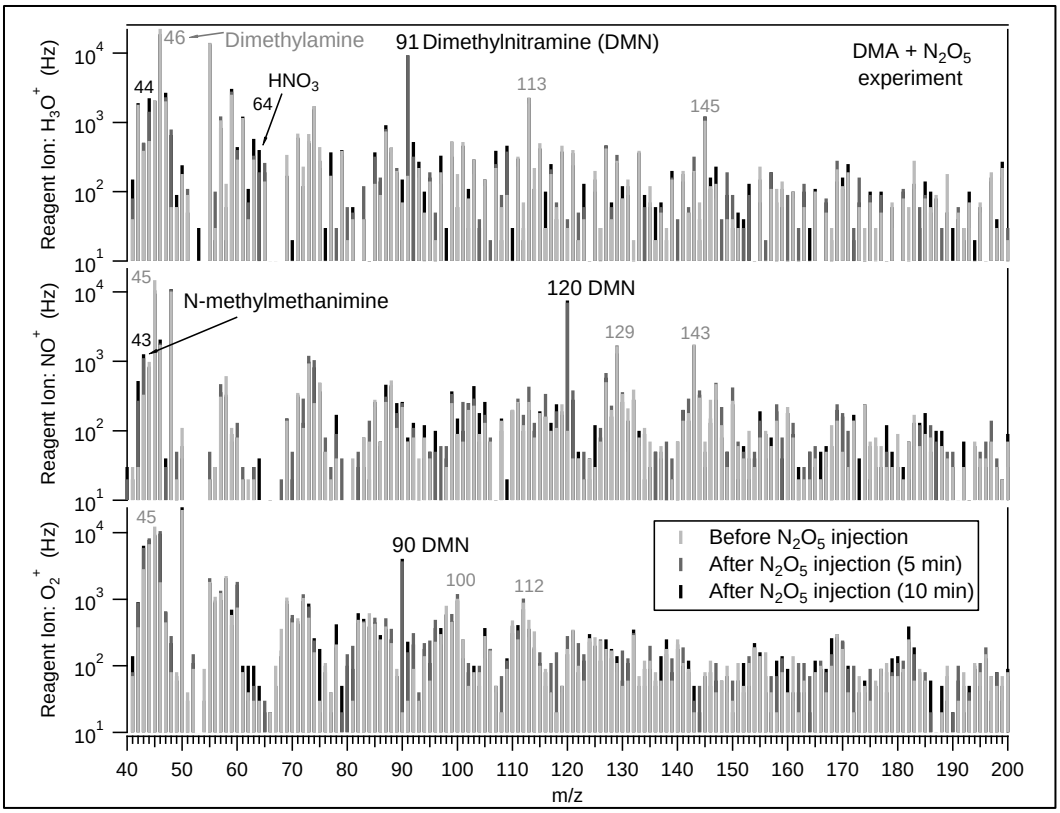

Figure 2.15. SIFT-MS mass spectra from the DMA + N_2O_5 experiment.

Chapter 3: Secondary Organic Aerosol Formation from the Reaction of Secondary Aliphatic Amines with Hydroxyl and Nitrate Radicals

3.1. Introduction

Secondary organic aerosol (SOA) and fine particulate matter negatively impact human health, air quality, visibility, and directly and indirectly influence radiative climate forcing (Dockery, 2009; IPCC, 2013; Pope et al., 1995; Watson, 2002). Significant precursors to aerosol formation in the atmosphere include reduced nitrogen compounds such as ammonia and amines (Ge et al., 2011). Anthropogenic and biogenic sources of amines include agricultural emissions, by-products of selective catalytic reduction and carbon capture control technologies, and biomass burning (Borduas et al., 2013; Cadle and Mulawa, 1980; Ge et al., 2011; Mosier et al., 1973; Westerholm et al., 1993).

The importance of amines in new particle formation is gaining attention. Previous studies have investigated the formation of organic salt aerosol through the reactions of atmospherically relevant acids (HNO_3, H_2SO_4) with alkyl amines (Barsanti et al., 2009). In addition to organic salt formation, field studies have observed that a significant portion of new particle growth is due to oxidized organic amine aerosol (Silva et al., 2008; Smith et al., 2008). The atmospheric reactions of alkyl amines, however, remain poorly understood. Previous work into aliphatic amine reactivity has focused on primary amines (Malloy et al., 2009a) and tertiary amines (Silva et al., 2008). An in-depth study on the reactivity of secondary aliphatic amines has not previously been reported. This study investigates the atmospheric oxidation of four secondary alkyl

amines leading to SOA formation. The effect of humidity on the physical properties and chemical composition of the aerosol is also investigated.

3.2. Methods

A set of secondary aliphatic amines were chosen for this study: dimethylamine (DMA, 40 wt.% solution in water, Sigma-Aldrich), diethylamine (DEA, >99.5%, Sigma-Aldrich), dipropylamine (DPA, >99.0%, Fluka), and dibutylamine (DBA, >99.0%, Fluka). All experiments were conducted in an atmospheric chamber located at the College of Engineering - Center for Environmental Research and Technology, University of California - Riverside (CE-CERT/UCR). The amines were oxidized in a 37.5 m^3 volume Teflon® film (50.8 μm) chamber with hydroxyl (OH) and nitrate (NO_3) radicals. The environmental chamber is housed in a 2.5m x 3m x 7.8m reflective aluminum enclosure.

Photooxidation, when desired, was driven by 170 40W black lights with peak intensity of 350 nm (350 BL, Sylvania) mounted to two of the enclosure walls. Excess ozone was injected into the chamber with black lights on prior to each experiment to clean and purge the chamber of any background hydrocarbons. Additionally, the injection glassware was washed with methanol to remove any residual amine from previous experiments. The chamber was flushed with purified air (Aadco 737 air purification system) prior to each experiment so that background particle concentration, NO_x, and hydrocarbon concentrations were below the detection limits of the instruments used. No seed aerosols were used for these experiments. Each experiment was

performed at room temperature (~295 K). Experiments were performed at both dry (RH < 0.001%) and humid (RH ~ 30%) conditions. A summary of the experiments with initial concentrations is provided (Table 3.1). Amine concentrations were allowed to stabilize in the Teflon chambers prior to radical injection. Hydroxyl radicals (no NO_x experiments) were produced from direct photolysis of hydrogen peroxide (H_2O_2) in the chamber. The nitrate radical was formed from thermal decomposition of dinitrogen pentoxide (N_2O_5) in the chamber. OH experiments were designed to represent daytime chemistry while the NO_3 experiments represented nighttime chemistry.

The chemical composition of the aerosol products was measured by a High Resolution Time of Flight Aerosol Mass Spectrometer (HR-ToF-AMS; Aerodyne Research Inc.) (DeCarlo et al., 2006; Jayne et al., 2000). Briefly, an aerosol sample was drawn through a time-of-flight region where the particles were separated based on their vacuum aerodynamic diameter. The sample was subsequently vaporized by a 600°C oven followed by 70 eV electron impact ionization. The resulting ions passed through another time-of-flight section, which can be operated in two (V and W) flight path configurations. The shorter flight path (V-mode) provides better sensitivity at unit mass resolution. The longer flight path (W-mode) provides sufficient mass spectral resolution (4300 at *m/z* 200) to separate isobaric compounds and determine empirical formulas.

A custom built scanning mobility particle sizer (SMPS) (Cocker et al., 2001) was used to measure the concentration and size distribution (27 - 712 nm) of the aerosol formed during the experiments. The SMPS also communicates size distribution values in

real-time to an Aerosol Particle Mass Analyzer (APM, Kanomax model 3600) in series with an SMPS used to measure effective density (Ehara et al., 1996; Malloy et al., 2009b). Briefly, the mass of the particle is selected by the APM based on the peak number electrical mobility diameter identified by the independent SMPS. The mass selected particles are then measured by an in-series SMPS to obtain the peak number electrical mobility diameter transmitted by the APM. Density measurements were taken every 85 seconds.

In addition to aerosol composition, the gas phase composition of the alkyl amine reaction products was determined with a Selected Ion Flow Tube - Mass Spectrometer (SIFT-MS; Syft Technologies) (Prince et al., 2010). The sample is introduced to a flow tube region where the analyte is ionized by three separate reagent ions (H_3O^+, NO^+, O_2^+) and then detected by a quadrupole mass spectrometer at unit mass resolution (UMR). The SIFT-MS was operated in either the selected ion mode (SIM) scan or the full mass scan. In the SIM scan, specific compounds are tracked and quantified via their product ion masses in real time. In the full mass scan, a mass spectrum is acquired for each reagent ion. As each reagent ion may react differently with a given compound, the identity of isobaric compounds can also be determined.

3.3. Results and Discussion

3.3.1. Gas Phase

The gas-phase chemical composition for the nitrate radical (NO_3) oxidation experiments of DMA (dry) and dry and humid DEA, DPA, and DBA was measured by

SIFT-MS (Figures 3.1 – 3.7). Each of the SIFT-MS figures show three background subtracted spectra for each of the reagent ions (H_3O^+, NO^+, and O_2^+). The spectra taken earlier in the experiment (before and within 1 hour of oxidation) are superimposed on top of the later spectra (after 2 hours of oxidation) to identify reaction products through progression of reaction. The formation of a nitramine (R_2NNO_2) was observed, as well as nitrous and nitric acids (HONO, HNO_3) in each of the dry experiments (Figures 3.1, 3.2, 3.4, and 3.6). The formation of primary aldimines (RCH=NH) were observed in the diethylamine (DEA), dipropylamine (DPA), and dibutylamine (DBA) experiments (Figures 3.2, 3.4, and 3.6, respectively).

The formation of a nitramine, a primary aldimine, and nitrous acid was observed in each of the humid experiments (Figures 3.3, 3.5, and 3.7). The humid dimethylamine (DMA) + NO_3 spectra are not shown due to a malfunction of the instrument during that experiment. Nitric acid formation was not observed in the humid experiments with the exception of the DBA experiment. Additionally, the concentrations of the gas-phase products including the nitramines and primary aldimines were lower in the humid experiments. This suggests the uptake of gas-phase products and nitric acid into water, which could lead to acid catalyzed aqueous phase chemistry in the humid experiments.

3.3.2. Particle Phase - Density

An overall trend of decreasing density with increasing carbon number is observed for the aerosol produced in both the OH and NO_3 oxidation experiments (Figure 3.8). The low salt density suggests formation of fractal-like particles. Further investigation

with SEM imaging would be required to confirm the formation of fractal-like particles. A wider density spread is observed in the NO_3 oxidation experiments (DBA, 0.98 g/cm^3 – DMA, 1.53 g/cm^3) compared to the OH oxidation experiments (DBA, 1.22 g/cm^3 – DMA, 1.50 g/cm^3). Humidity did not significantly affect density.

3.3.3. Dimethylamine Experiments

Particle formation, with and without wall loss correction (WLC), for the DMA experiments are shown (Figure 3.9). Overall mass-based aerosol yields were calculated for each experiment assuming complete consumption of the gas-phase precursor amine (Table 3.2). The OH oxidation reactions produced similar amounts of aerosol for the dry and humid experiments (8.9% and 8.0%, respectively). More aerosol formed in the NO_3 experiments than in the OH experiments. Further, unlike the OH oxidation experiments, much more aerosol formed in the humid NO_3 oxidation experiment than in the dry experiment (200.8% and 28.3%, respectively). The maximum possible mass-based yield was estimated for each experiment (Table 3.2). An average increase of three oxygen atoms for the OH oxidation experiments and formation of amine nitrate salts is assumed when estimating the maximum mass-based yield. Therefore, the maximum possible yield for the DMA + NO_3 oxidation experiments is 240%, assuming complete conversion of gas-phase DMA to dimethylammonium nitrate salt ($DMA{\cdot}HNO_3$).

While the calculated aerosol yield for the humid DMA + NO_3 experiment is within reason, it is still far greater than the aerosol yield in the dry DMA + NO_3 experiment. Further investigation revealed some interesting trends in the aerosol

produced from the NO_3 oxidation experiments. A large particle burst (4.0×10^5 cm^{-3}) occurred at the start of the dry NO_3 experiment, which then quickly decayed and continued to decline over time. The rapid loss of particles at the beginning is indicative of particle coagulation. Little to no particle wall loss is observed in the non-wall loss corrected (NWLC) concentration profile for the humid DMA + NO_3 oxidation experiment (Figure 3.9). The suspended aerosol concentration plateaus quickly with little to no decay over time, atypical of atmospheric chamber experiments. A possible explanation is that the amine salt aerosol is not stable on the Teflon surface of the chamber and partitions back to the gas phase components (DMA + HNO_3), which then quickly partitions back to the amine salt aerosol. The wall loss correction, therefore, over-predicts the aerosol formation in the humid NO_3 oxidation experiment. The overall NWLC mass-based aerosol yields are also reported (Table 3.2).

The mass concentration profiles of the organic and nitrate components of the aerosol measured by the HR-ToF-AMS (Figure 3.10) are consistent with those trends observed by the SMPS. These include observations of: slightly more aerosol formation in the dry OH experiment than in the humid OH experiment; more aerosol formation in the NO_3 experiments than in the OH experiments; more aerosol formation in the humid than dry NO_3 experiment; and large particle nucleation at the start of the dry NO_3 experiment which then decayed over time. Finally, the little to no wall loss observed in the humid NO_3 experiment is confirmed by the AMS measurements. The ripple effect observed in the concentration profile is consistent with small oscillations in the chamber relative humidity profile. This suggests that humidity has an immediate effect on the

produced aerosol. The organic to nitrate mass ratios (Org/NO_3) are reported in Table 3.2. The Org/NO_3 is higher in the dry NO_3 experiment (4.8 dry vs 1.2 humid).

The HR-ToF-AMS organic mass spectra for the DMA experiments are presented (Figure 3.11). The organic spectra from the dry and humid experiments are plotted together for both OH and NO_3 oxidation. The mass spectra for the secondary amine experiments are shown in logarithmic scale to highlight the higher mass peaks, i.e., peaks greater than that of the amine precursor (DMA = 45 amu). A correlation plot of the dry organic mass versus the humid organic mass with respect to *m/z* is presented to highlight the differences between the two spectra. The good correlation ($r^2 = 0.941$) between the dry and humid OH oxidation experiments indicates a similar aerosol chemical composition for both experiments. A slope greater than 1.0 in the linear regression equation (m = 1.772) indicates that more organic mass formed in the dry OH experiment. The higher *m/z* peaks (> 45) at 58 ($C_3H_8N^+$, $C_2H_4NO^+$), 72 ($C_4H_{10}N^+$, $C_3H_6NO^+$, $C_2H_2NO_2^+$), 86 ($C_4H_8NO^+$, $C_3H_4NO_2^+$), and 132 ($C_4H_6NO_4^+$) are fragment ions indicative of oligomer compounds. The lower *m/z* peaks (< 45) at 29 (CHO^+), 30 (CH_2O^+, CH_4N^+), 42 ($C_2H_4N^+$, $C_2H_2O^+$), and 44 (CO_2^+, $C_2H_6N^+$, CH_2NO^+) are smaller aldehyde and amide fragment ions also expected from the oligomer compounds.

The poor correlation ($r^2 = 0.463$) between the dry and humid NO_3 oxidation experiments indicates significant differences in the chemical composition between the experiments. A slope less than 1.0 in the linear regression equation (m = 0.268) indicates that more organic mass formed in the humid NO_3 experiment. The lower *m/z* peaks (<

45) at 30 (CH_4N^+), 44 ($C_2H_6N^+$) and 45 ($C_2H_7N^+$) are fragments of the unoxidized parent amine, consistent with fragmentation of dimethylammonium nitrate salt ($DMA{\cdot}HNO_3$). The *m/z* peaks at 29 (CHO^+), 58 ($C_3H_8N^+$, $C_2H_4NO^+$), 72 ($C_4H_{10}N^+$, $C_3H_6NO^+$, $C_2H_2NO_2^+$), and 86 ($C_4H_8NO^+$, $C_3H_4NO_2^+$) are fragment ions indicative of oligomer compounds. The series of higher *m/z* peaks (> 45) at 97, 101, 109, 111, 123, 125, 137, 139, 151, 153, 165, and 167 are fragments of highly reduced aerosol with three nitrogen and two oxygen separated by CH_2 groups ($CH_{11}N_3O_2^+$ – $C_6H_{21}N_3O_2^+$). More oligomer (*m/z* 29 and 58) and highly-reduced fragmentation series (*m/z* 97 and 101) aerosol formation is observed in the dry NO_3 experiment while more amine nitrate salt (*m/z* 30, 44, and 45) formation is observed in the humid NO_3 experiment.

The elemental analyses for the DMA (H/C = 3.5; N/C = 0.5; O/C = 0.0) experiments are shown (Figure 3.12). The aerosol produced in both the humid and dry OH experiments was oxidized (O/C ≈ 0.36) with carbonyl functional groups (H/C ≈ 1.92). The aerosol formed in the humid NO_3 experiment has a high H/C (2.65) and N/C (0.48) and low O/C (0.08) suggesting fragmentation of reduced amine nitrate salts. However, the H/C is lower than expected for the fragmentation of $DMA{\cdot}HNO_3$ ($CH_2{=}N^+HCH_3$; H/C = 3.0) indicating the formation of larger reduced oligomer salts. The dry NO_3 experiment has more influence from the highly-reduced fragmentation series (containing 3 nitrogen and 2 oxygen atoms). Therefore, higher H/C, O/C, and OM/OC ratios are expected in the dry NO_3 experiment.

3.3.4. Diethylamine Experiments

Particle formation, WLC and NWLC, for the DEA experiments are shown (Figure 3.13). The overall mass-based aerosol yield for each experiment is reported (Table 3.2). The concentration trends observed in the DEA experiments were similar to those observed in the DMA experiments. More aerosol formed in the humid OH experiment than in the dry experiment (5.8% and 1.1%, respectively). More aerosol formed in the NO_3 experiments than in the OH experiments. As with the OH oxidation experiments, much more aerosol formed in the humid NO_3 oxidation experiment than in the dry experiment (342.0% and 78.3%, respectively). As with the DMA experiment, the aerosol in the dry DEA + NO_3 oxidation experiment nucleates quickly (4.0×10^5 cm^{-3}) and then abruptly decays due to particle coagulation. The coagulation is less intense than the DMA experiment. The maximum possible yield for the DEA + NO_3 oxidation experiments, assuming complete conversion of gas-phase DEA to diethylammonium nitrate salt ($DEA \cdot HNO_3$), is 186%. The WLC aerosol yield in the humid NO_3 experiment is greater than the maximum possible yield and, therefore, over-predicts the aerosol formation. As in the DMA experiment, there is little to no particle wall loss observed in the NWLC concentration profile for the humid DEA + NO_3 oxidation experiment (Figure 3.13). The NWLC aerosol yield of 132% is close to the maximum (186%), suggesting that most of the precursor amine reacts to form $DEA \cdot HNO_3$ aerosol.

The mass concentration profiles of the organic and nitrate components of the aerosol measured by the HR-ToF-AMS (Figure 3.14) confirm the trends observed by the

SMPS in the DEA experiments: more aerosol formed in the humid OH experiment than in the dry OH experiment; more aerosol formed in the NO_3 experiments than in the OH experiments; more aerosol formed in the humid NO_3 experiment than in the dry NO_3 experiment; and large particle nucleation at the start of the dry NO_3 experiment which then decayed over time. Again, little to no wall loss was observed in the humid NO_3 experiment. The ripple effect observed in the concentration profile is consistent with small oscillations in the relative humidity profile. The Org/NO_3 is higher in the dry NO_3 experiment (4.4 vs 3.2 humid), indicating the formation of more organic aerosol in the dry experiments.

The HR-ToF-AMS organic mass spectra and correlation plots for the DEA experiments are presented (Figure 3.15). Aerosol had difficulty forming in the dry DEA + OH experiment, even for twice the amount of precursor amine (200 ppb). The small amount of aerosol formed was not much above the typical background chamber SOA formed during photooxidation. Therefore, poor correlation ($r^2 = 0.703$) between the dry and humid OH oxidation experiments is observed due to background fragments. The linear regression slope (m = 0.172) confirms that more organic mass formed in the humid OH experiment. The lower *m/z* peaks (< 73) at 30 (CH_4N^+, CH_2O^+), 44 (CO_2^+, $C_2H_6N^+$, CH_2NO^+), 58 ($C_3H_8N^+$, $C_2H_4NO^+$), and 72 ($C_4H_{10}N^+$, $C_3H_6NO^+$) are fragment ions of oxidized amines. Oxidized amine (*m/z* 86) and the highly-reduced aerosol series (*m/z* 97, 109, 111, 123, and 125) fragment ions were observed in the humid OH experiment.

There was good correlation ($r^2 = 0.987$) between the dry and humid NO_3 oxidation experiments, indicating similar chemical composition between the experiments. The linear regression slope (m = 0.462) confirms that more organic mass was formed in the humid NO_3 experiment. Most of the aerosol fragments are the lower *m/z* peaks (≤ 73) at 30 (CH_4N^+), 44 ($C_2H_6N^+$), 58 ($C_3H_8N^+$), 72 ($C_4H_{10}N^+$), and 73 ($C_2H_7N^+$) consistent with the fragmentation of diethylammonium nitrate salt ($DMA{\cdot}HNO_3$). Oxidized amine (*m/z* 86) and the highly-reduced aerosol series (*m/z* 97, 109, 111, 123, 125, 137, 139, 151, 153, 165, 167, 179, and 181) fragment ions were observed in both the dry and humid NO_3 experiments. More oxidized amine / highly-reduced fragmentation series aerosol formed in the dry NO_3 experiment. More amine nitrate salt formed in the humid NO_3 experiment. This suggests that the amine nitrate salt mechanism is enhanced in the humid experiment while there is more time for oxidation in the dry experiment prior to aerosol formation.

The elemental analyses for the DEA (H/C = 2.75; N/C = 0.25; O/C = 0.00) experiments are shown (Figure 3.16). The aerosol produced in the OH experiments consists of oxidized amines (O/C = 0.28; N/C = 0.25) with carbonyl functional groups (H/C = 2.10). The elemental ratios were slightly different for the dry OH experiment due to the influence from the background photooxidation aerosol (O/C = 0.22; N/C = 0.16). The aerosol formed in the NO_3 oxidation experiments have high H/C (2.75) and N/C (0.42) and low O/C (0.02), suggesting fragmentation of $DEA{\cdot}HNO_3$ ($H_2C{=}N^+HCH_2CH_3$). In the dry NO_3 experiment, the H/C drops (2.48) and the O/C

increases (0.07) over the course of the experiment, indicating the formation of more oxidized aerosol in the dry experiment.

3.3.5. Dipropylamine Experiments

Particle formation, WLC and NWLC, for the DPA experiments are shown (Figure 3.17). The overall mass-based aerosol yield for each experiment is reported (Table 3.2). The concentration trends observed in the DPA experiments were similar to those observed in the DMA and DEA experiments. More aerosol formed in the humid OH experiment than in the dry experiment (6.1% and 5.6%, respectively). More aerosol formed in the NO_3 experiments than in the OH experiments. As with the OH oxidation experiments, more aerosol formed in the humid NO_3 oxidation experiment than in the dry experiment (290.0% and 123.0%, respectively). Unlike the previous amine experiments, there was little particle coagulation in the dry DPA + NO_3 oxidation experiment. The maximum possible yield for the DPA + NO_3 oxidation experiments, assuming complete conversion of gas-phase DPA to dipropylammonium nitrate salt (DPA·HNO_3), is 162%. As with the DEA experiment, the WLC aerosol yield in the humid DPA + NO_3 experiment is greater than the maximum possible yield and, therefore, over-predicts the aerosol formation. As in the previous amine experiments, there is little to no particle wall loss observed in the NWLC concentration profile for the humid DPA + NO_3 oxidation experiment (Figure 3.17). The NWLC aerosol yield is 140%. This yield is close to the maximum (162%), suggesting that most of the precursor amine reacts to form DPA·HNO_3 aerosol.

The mass concentration profiles of the organic and nitrate components of the aerosol measured by the HR-ToF-AMS (Figure 3.18) confirm the trends observed by the SMPS in the DPA experiments: slightly more aerosol formed in the humid OH experiment than in the dry OH experiment; more aerosol formed in the NO_3 experiments than in the OH experiments; and more aerosol formed in the humid NO_3 experiment than in the dry NO_3 experiment. Again, no wall loss is observed in the humid NO_3 experiment. The ripple effect observed in the concentration profile is consistent with oscillation seen in the relative humidity profile. This suggests that humidity has an immediate effect on the produced aerosol. The Org/NO_3 is higher in the dry NO_3 experiment (5.8 vs 5.1 humid), indicating the formation of more organic aerosol in the dry experiments.

The HR-ToF-AMS organic mass spectra and correlation plots for the DPA experiments are presented (Figure 3.19). Good correlation ($r^2 = 0.966$) is observed between the dry and humid OH oxidation experiments. The linear regression slope (m = 0.779) confirms that more organic mass formed in the humid OH experiment. The higher *m/z* peaks (> 101) at 114 ($C_6H_{12}NO^+$), 130 ($C_6H_{12}NO_2^+$), and 146 ($C_6H_{12}NO_3^+$) are the fragment ions of oxidized amines. The lower *m/z* peaks (< 101) at 30 (CH_4N^+, CH_2O^+), 44 (CO_2^+, $C_2H_6N^+$, CH_2NO^+), 58 ($C_3H_8N^+$, $C_2H_4NO^+$), 72 ($C_4H_{10}N^+$, $C_3H_6NO^+$) and 86 ($C_4H_8NO^+$) are smaller fragment ions of the oxidized amines.

The excellent correlation ($r^2 = 0.995$) between the dry and humid NO_3 oxidation experiments indicates similar chemical composition between the experiments. The linear

regression slope (m = 0.465) confirms that more organic mass was formed in the humid NO_3 experiment. The bulk of the aerosol is with the lower *m/z* peaks (≤ 101) at 30 (CH_4N^+), 44 ($C_2H_6N^+$), 58 ($C_3H_8N^+$), 72 ($C_4H_{10}N^+$), 86 ($C_5H_{12}N+$), 100 ($C_6H_{14}N+$), and 101 ($C_6H_{15}N^+$) consistent with the fragmentation of dipropylammonium nitrate salt ($DPA{\cdot}HNO_3$). The higher *m/z* peak (> 101) at 114 ($C_6H_{12}NO^+$) in the dry NO_3 experiment is a fragment ion of oxidized amine nitrate salt.

The elemental analyses for the DPA (H/C = 2.5; N/C = 0.17; O/C = 0.00) experiments are shown (Figure 3.20). The aerosol produced in the OH experiments consisted of oxidized amines (O/C = 0.22; N/C = 0.17) with carbonyl functional groups (H/C = 2.05). No significant difference was observed between the dry and humid OH experiments, indicating similar chemical composition. Reduced aerosol is formed in the NO_3 oxidation experiments with high H/C (2.55) and N/C (0.32) and low O/C (0.02), suggesting the fragmentation of $DPA{\cdot}HNO_3$ ($H_2C{=}N^+H(CH_2)_2CH_3$). There is a slight increase in O/C (0.022) observed in the dry NO_3 experiment due to oxidized amine nitrate salt fragments.

3.3.6. Dibutylamine Experiments

Particle formation, WLC and NWLC, for the DBA experiments are shown (Figure 3.21). The overall mass-based aerosol yield for each experiment is reported (Table 3.2). The concentration trends observed in the DBA experiments were similar to those observed in the previous amine experiments. More aerosol formed in the humid OH experiment than in the dry experiment (15.3% and 11.3%, respectively). More

aerosol formed in the NO_3 experiments than in the OH experiments. As with the OH oxidation experiments, more aerosol formed in the humid NO_3 oxidation experiment than in the dry experiment (223.0% and 121.0%, respectively). As with the DPA experiments, little particle coagulation is observed in the dry DBA + NO_3 oxidation experiment. The maximum possible yield for the DBA + NO_3 oxidation experiments, assuming complete conversion of gas-phase DBA to dibutylammonium nitrate salt ($DBA{\cdot}HNO_3$), is 149%. As with the DEA and DPA experiments, the WLC aerosol yield in the humid DBA + NO_3 experiment is greater than the maximum possible yield and over-predicts the aerosol formation. Also, as in the previous amine experiments, there is little to no particle wall loss observed in the NWLC concentration profile for the humid DBA + NO_3 oxidation experiment (Figure 3.21). The NWLC aerosol yield is 115%. This yield is close to the maximum (149%), suggesting that most of the precursor amine reacts to form $DBA{\cdot}HNO_3$ aerosol.

The mass concentration profiles of the organic and nitrate aerosol components measured by the HR-ToF-AMS (Figure 3.22) confirm the trends observed by the SMPS in the DBA experiments: slightly more aerosol formed in the humid OH experiment than in the dry OH experiment; more aerosol formed in the NO_3 experiments than in the OH experiments; and more aerosol formed in the humid NO_3 experiment than in the dry NO_3 experiment. Again, little to no wall loss measured by HR-ToF-AMS is confirmed for the humid NO_3 experiment. The Org/NO_3 is higher in the dry NO_3 experiment (9.1 vs 6.9 humid), indicating the formation of more organic aerosol in the dry experiments.

The HR-ToF-AMS organic mass spectra and correlation plots for the DBA experiments are presented (Figure 3.23). Good correlation ($r^2 = 0.915$) is observed between the dry and humid OH oxidation experiments. The linear regression slope (m = 0.893) confirms that more organic mass formed in the humid OH experiment. The higher *m/z* peaks (> 129) at 142 ($C_8H_{16}NO^+$), 158 ($C_8H_{16}NO_2^+$), and 174 ($C_8H_{16}NO_3^+$) are the fragment ions of oxidized amines. The lower *m/z* peaks (< 129) at 29 (CHO^+, $C_2H_5^+$), 41 ($C_2H_3N^+$, $C_3H_5^+$), 43 ($C_3H_7^+$, $C_2H_3O^+$, $C_2H_5N^+$, $CHNO^+$), 58 ($C_3H_8N^+$, $C_2H_4NO^+$), 72 ($C_4H_{10}N^+$, $C_3H_6NO^+$, $C_4H_8O^+$), 88 ($C_3H_6NO_2^+$, $C_4H_{10}NO^+$), 104 ($C_4H_{10}NO_2^+$, $C_3H_6NO_3^+$), and 114 ($C_6H_{12}NO^+$, $C_5H_8NO_2^+$) are smaller fragment ions of the oxidized amines.

Excellent correlation ($r^2 = 0.975$) between the dry and humid NO_3 oxidation experiments indicates a similar chemical composition between the experiments. The linear regression slope (m = 0.695) confirms that more organic mass was formed in the humid NO_3 experiment. The bulk of the aerosol is with the lower *m/z* peaks (≤ 129) at 30 (CH_4N^+), 44 ($C_2H_6N^+$), 57 ($C_4H_9^+$, $C_3H_7N^+$), 72 ($C_4H_{10}N^+$), 86 ($C_5H_{12}N+$), 98 ($C_6H_{12}N+$), 112 ($C_7H_{14}N+$), 128 ($C_8H_{18}N+$), and 129 ($C_8H_{19}N^+$), consistent with fragmentation of dibutylammonium nitrate salt ($DBA{\cdot}HNO_3$). The higher *m/z* peaks (> 129) at 142 ($C_8H_{16}NO^+$), 156 ($C_8H_{14}NO_2^+$), 171 ($C_8H_{13}NO_3^+$), 185 ($C_9H_{17}N_2O_2^+$), and 203 ($C_8H_{13}NO_5^+$) in the dry NO_3 experiment are oxidized amine nitrate salt fragment ions.

The elemental analyses for the DBA (H/C = 2.375, N/C = 0.125; O/C = 0.000) experiments are shown (Figure 3.24). The aerosol produced in the OH experiments consisted of oxidized amines (O/C = 0.23; N/C = 0.12) with carbonyl functional groups

(H/C = 1.95). No significant difference was observed between the dry and humid OH experiments, indicating similar chemical composition. Reduced aerosol is formed in the NO_3 oxidation experiments with high H/C (2.45) and N/C (0.25) and low O/C (0.01), suggesting the fragmentation of DBA·HNO_3 ($H_2C=N^+H(CH_2)_3CH_3$). There is a slight increase in O/C (0.02) observed in the dry NO_3 experiment due to the oxidized amine nitrate salt fragments.

3.4. Conclusion

The availability of the N-H bonds in the secondary alkyl amines allowed for the formation of nitramines and imines. The formation of carcinogenic nitramines from the oxidation secondary alkyl amines may have negative human health implications in areas with high concentrations of secondary amines. The addition of humidity to the system allows for the uptake of reaction products (amine products, HNO_3, etc.) into water, thereby introducing additional aqueous phase reactions leading to SOA formation under humid conditions.

In general, more aerosol was produced in the humid oxidation experiments than in the dry oxidation experiments. Also, the reactions with NO_3 produced far more aerosol than the OH reactions. The addition of humidity in the NO_3 oxidation experiments had the effect of inhibiting particle coagulation and loss to the walls. This is possibly due to the formation of amine nitrate salts that are unstable on surfaces, partitioning to the gas-phase and then returning to the suspended particle phase.

Oligomer formation was observed in the dimethylamine oxidation experiments, which is not seen in experiments with the other secondary amines. More oxidized oligomer compounds were formed in the DMA + OH oxidation experiments while reduced oligomer salt formation occurred in the NO_3 oxidation experiments. The fragmentation of highly reduced aerosol containing three nitrogen and two oxygen atoms was measured by HR-ToF-AMS in the DMA and DEA oxidation experiments. In general, the OH reactions produced highly oxidized organic aerosol while the NO_3 reactions produced reduced amine nitrate salt aerosol. The Org/NO_3 ratio increases with increasing carbon number. Humidity lowers the Org/NO_3 ratio in most of the secondary amine experiments. Humidity enhances the amine nitrate salt mechanism, which leads to increased aerosol concentration while limiting the time for oxidation of the precursor amine.

3.5. References

Barsanti, K.C., McMurry, P.H., Smith, J.N., 2009. The potential contribution of organic salts to new particle growth. Atmos Chem Phys 9, 2949-2957.

Borduas, N., Abbatt, J.P.D., Murphy, J.G., 2013. Gas Phase Oxidation of Monoethanolamine (MEA) with OH Radical and Ozone: Kinetics, Products, and Particles. Environ Sci Technol 47, 6377-6383.

Cadle, S.H., Mulawa, P.A., 1980. Low-Molecular Weight Aliphatic-Amines in Exhaust from Catalyst-Equipped Cars. Environ Sci Technol 14, 718-723.

Cocker, D.R., Flagan, R.C., Seinfeld, J.H., 2001. State-of-the-art chamber facility for studying atmospheric aerosol chemistry. Environ Sci Technol 35, 2594-2601.

DeCarlo, P.F., Kimmel, J.R., Trimborn, A., Northway, M.J., Jayne, J.T., Aiken, A.C., Gonin, M., Fuhrer, K., Horvath, T., Docherty, K.S., Worsnop, D.R., Jimenez, J.L., 2006. Field-deployable, high-resolution, time-of-flight aerosol mass spectrometer. Analytical Chemistry 78, 8281-8289.

Dockery, D.W., 2009. Health Effects of Particulate Air Pollution. Annals of Epidemiology 19, 257-263.

Ehara, K., Hagwood, C., Coakley, K.J., 1996. Novel method to classify aerosol particles according to their mass-to-charge ratio - Aerosol particle mass analyser. J Aerosol Sci 27, 217-234.

Ge, X., Wexler, A.S., Clegg, S.L., 2011. Atmospheric Amines – Part I, A Review. Atmos Environ 45, 524-546.

IPCC, 2013. Climate change 2013: The physical science basis. Contribution of working group I to the fifth assessment report of the Intergovernmental Panel on Climate Change [Stocker, T.F., D. Qin, G.-K. Plattner, M. Tignor, S.K. Allen, J. Boschung, A. Nauels, Y. Xia, V. Bex and P.M. Midgley (eds.)]. Cambridge University Press, Cambridge, United Kingdom and New York, NY, USA, p. 1535 pp.

Jayne, J.T., Leard, D.C., Zhang, X.F., Davidovits, P., Smith, K.A., Kolb, C.E., Worsnop, D.R., 2000. Development of an aerosol mass spectrometer for size and composition analysis of submicron particles. Aerosol Sci Tech 33, 49-70.

Malloy, Q.G.J., Li, Q., Warren, B., Cocker, D.R., III, Erupe, M.E., Silva, P.J., 2009a. Secondary organic aerosol formation from primary aliphatic amines with NO3 radical. Atmospheric Chemistry and Physics 9, 2051-2060.

Malloy, Q.G.J., Nakao, S., Qi, L., Austin, R., Stothers, C., Hagino, H., Cocker, D.R., 2009b. Real-Time Aerosol Density Determination Utilizing a Modified Scanning

Mobility Particle SizerAerosol Particle Mass Analyzer System. Aerosol Sci Tech 43, 673-678.

Mosier, A.R., Andre, C.E., Viets, F.G., Jr., 1973. Identification of Aliphatic Amines Volatilized from Cattle Feedyard. Environ Sci Technol 7, 642-644.

Pope, C.A., Thun, M.J., Namboodiri, M.M., Dockery, D.W., Evans, J.S., Speizer, F.E., Heath, C.W., 1995. Particulate Air-Pollution as a Predictor of Mortality in a Prospective-Study of Us Adults. American Journal of Respiratory and Critical Care Medicine 151, 669-674.

Prince, B.J., Milligan, D.B., McEwan, M.J., 2010. Application of selected ion flow tube mass spectrometry to real-time atmospheric monitoring. Rapid Communications in Mass Spectrometry 24, 1763-1769.

Silva, P.J., Erupe, M.E., Price, D.J., Elias, J., Malloy, Q.G.J., Li, Q., Warren, B., Cocker, D.R., III, 2008. Trimethylamine as precursor to secondary organic aerosol formation via nitrate radical reaction in the atmosphere. Environ Sci Technol 42, 4689-4696.

Smith, J.N., Dunn, M.J., VanReken, T.M., Iida, K., Stolzenburg, M.R., McMurry, P.H., Huey, L.G., 2008. Chemical composition of atmospheric nanoparticles formed from nucleation in Tecamac, Mexico: Evidence for an important role for organic species in nanoparticle growth. Geophys Res Lett 35.

Watson, J.G., 2002. Visibility: Science and regulation. J Air Waste Manage 52, 628-713.

Westerholm, R., Li, H., Almen, J., 1993. Estimation of Aliphatic Amine Emissions in Automobile Exhausts. Chemosphere 27, 1381-1384.

3.6. Tables

Table 3.1. Initial conditions of the environmental chamber experiments.

Amine	Structure	Humidity	[Amine] ppb	Oxidant	[Oxidant] ppb
DMA	$(CH_3)_2NH$	<0.001%	100	H_2O_2 (OH)	415
DMA	$(CH_3)_2NH$	30%	100	H_2O_2 (OH)	415
DMA	$(CH_3)_2NH$	<0.001%	100	N_2O_5 (NO_3)	310
DMA	$(CH_3)_2NH$	30%	100	N_2O_5 (NO_3)	310
DEA	$(CH_3CH_2)_2NH$	<0.001%	200	H_2O_2 (OH)	415
DEA	$(CH_3CH_2)_2NH$	30%	100	H_2O_2 (OH)	415
DEA	$(CH_3CH_2)_2NH$	<0.001%	100	N_2O_5 (NO_3)	310
DEA	$(CH_3CH_2)_2NH$	30%	100	N_2O_5 (NO_3)	310
DPA	$(CH_3C_2H_4)_2NH$	<0.001%	100	H_2O_2 (OH)	415
DPA	$(CH_3C_2H_4)_2NH$	30%	100	H_2O_2 (OH)	415
DPA	$(CH_3C_2H_4)_2NH$	<0.001%	100	N_2O_5 (NO_3)	310
DPA	$(CH_3C_2H_4)_2NH$	30%	100	N_2O_5 (NO_3)	310
DBA	$(CH_3C_3H_6)_2NH$	<0.001%	100	H_2O_2 (OH)	415
DBA	$(CH_3C_3H_6)_2NH$	30%	100	H_2O_2 (OH)	415
DBA	$(CH_3C_3H_6)_2NH$	<0.001%	100	N_2O_5 (NO_3)	310
DBA	$(CH_3C_3H_6)_2NH$	30%	100	N_2O_5 (NO_3)	310

Table 3.2. Mass-based aerosol yield values and HR-ToF-AMS organic to nitrate ratios.

Amine	Oxidant	Humidity	Y_{max} (%)[a,b]	Y_{wlc} (%)[c]	Y_{nwlc} (%)[c]	Org/NO_3
DMA	OH	dry	207	8.9	7.3	4.9
DMA	OH	humid	207	8.0	6.6	5.6
DMA	NO_3	dry	240	28.3	11.9	4.8
DMA	NO_3	humid	240	200.8	103.8	1.2
DEA	OH	dry	166	1.1	0.8	7.8
DEA	OH	humid	166	5.8	4.8	5.4
DEA	NO_3	dry	186	78.3	36.7	4.4
DEA	NO_3	humid	186	342.0	132.0	3.2
DPA	OH	dry	148	5.6	5.5	10.0
DPA	OH	humid	148	6.1	5.2	8.3
DPA	NO_3	dry	162	123.0	58.0	5.8
DPA	NO_3	humid	162	290.0	140.0	5.1
DBA	OH	dry	137	11.3	8.1	97.4
DBA	OH	humid	137	15.3	11.8	19.8
DBA	NO_3	dry	149	121.0	59.0	9.1
DBA	NO_3	humid	149	223.0	115.0	6.9

a) Maximum possible yield assuming the addition of three oxygen atoms. (OH experiments)
b) Maximum possible yield assuming the formation of amine nitrate salt. (NO_3 experiments)
c) Assuming complete conversion of the precursor amine.

3.7. Figures

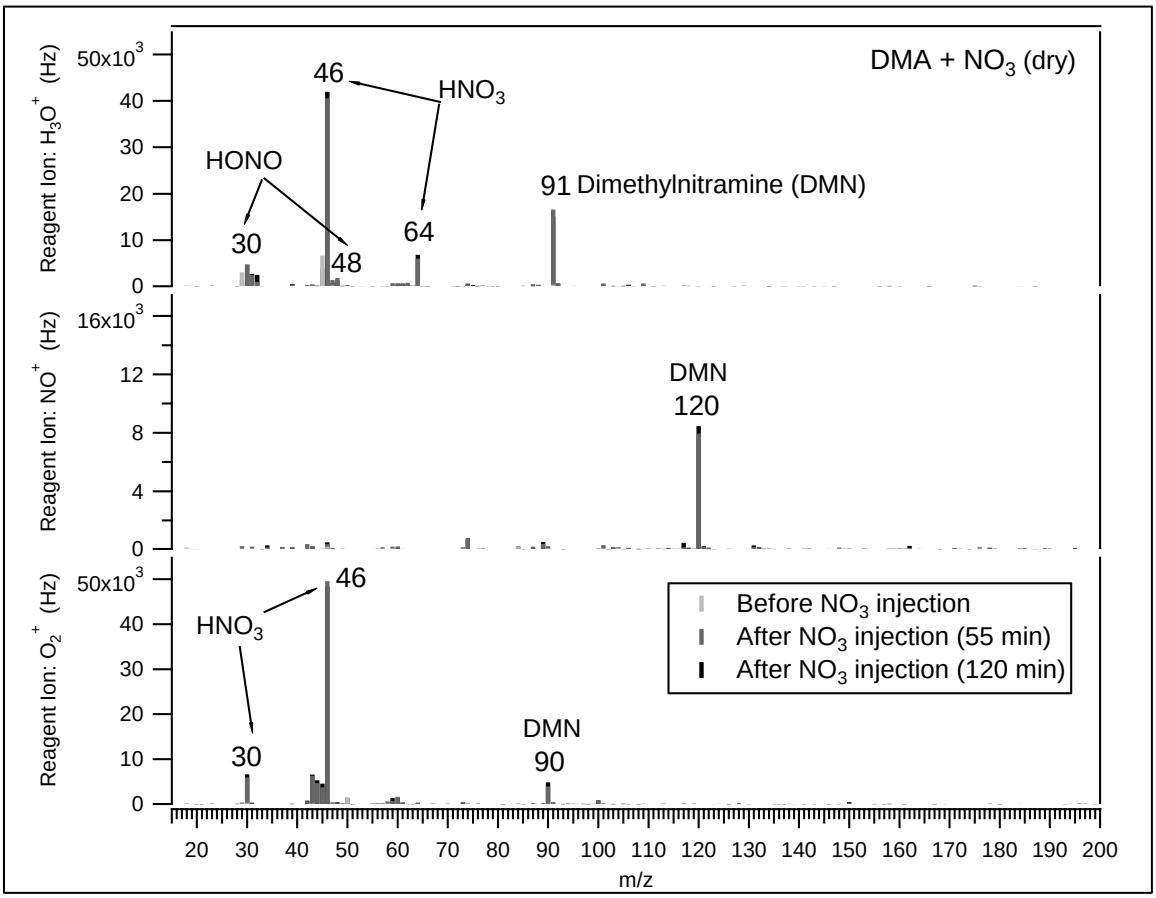

Figure 3.1. SIFT-MS mass spectra for the dry dimethylamine with nitrate radical oxidation experiment.

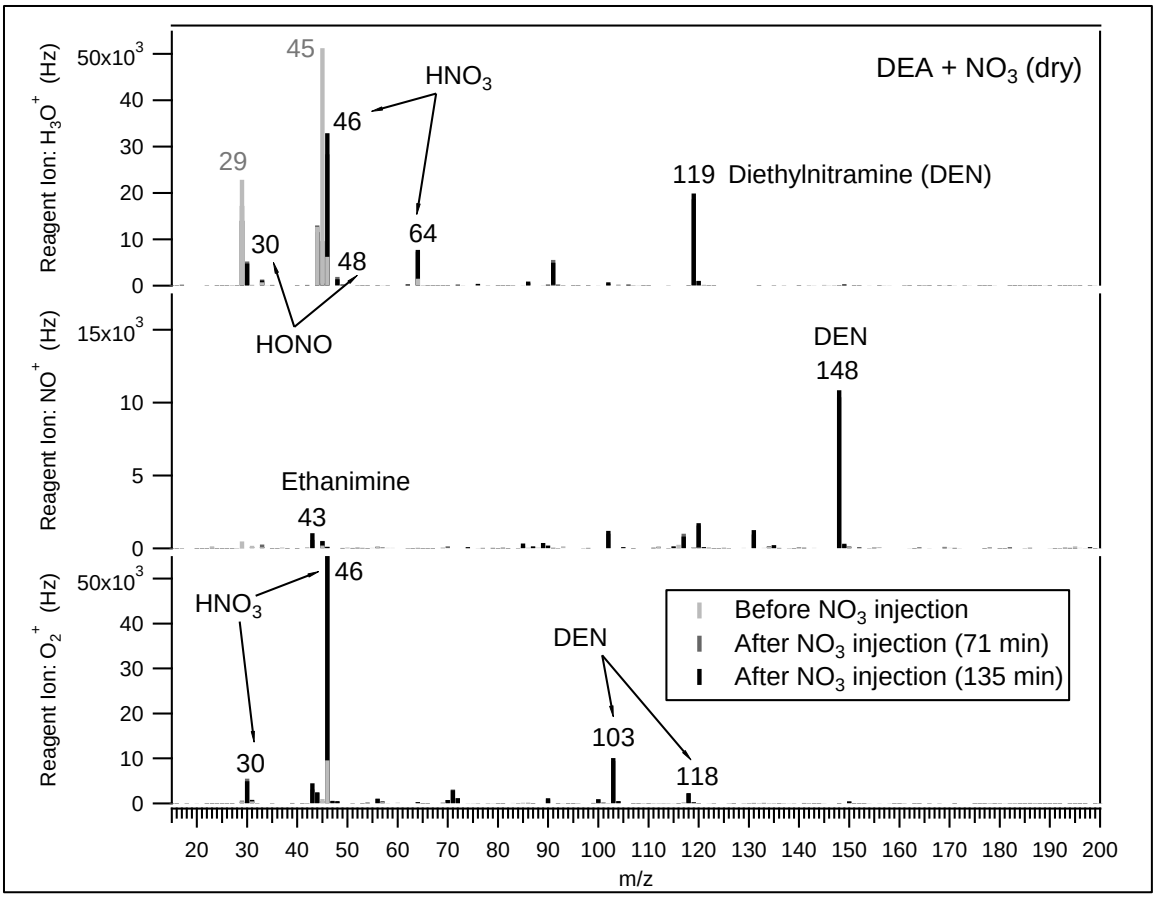

Figure 3.2. SIFT-MS mass spectra for the dry diethylamine with nitrate radical oxidation experiment.

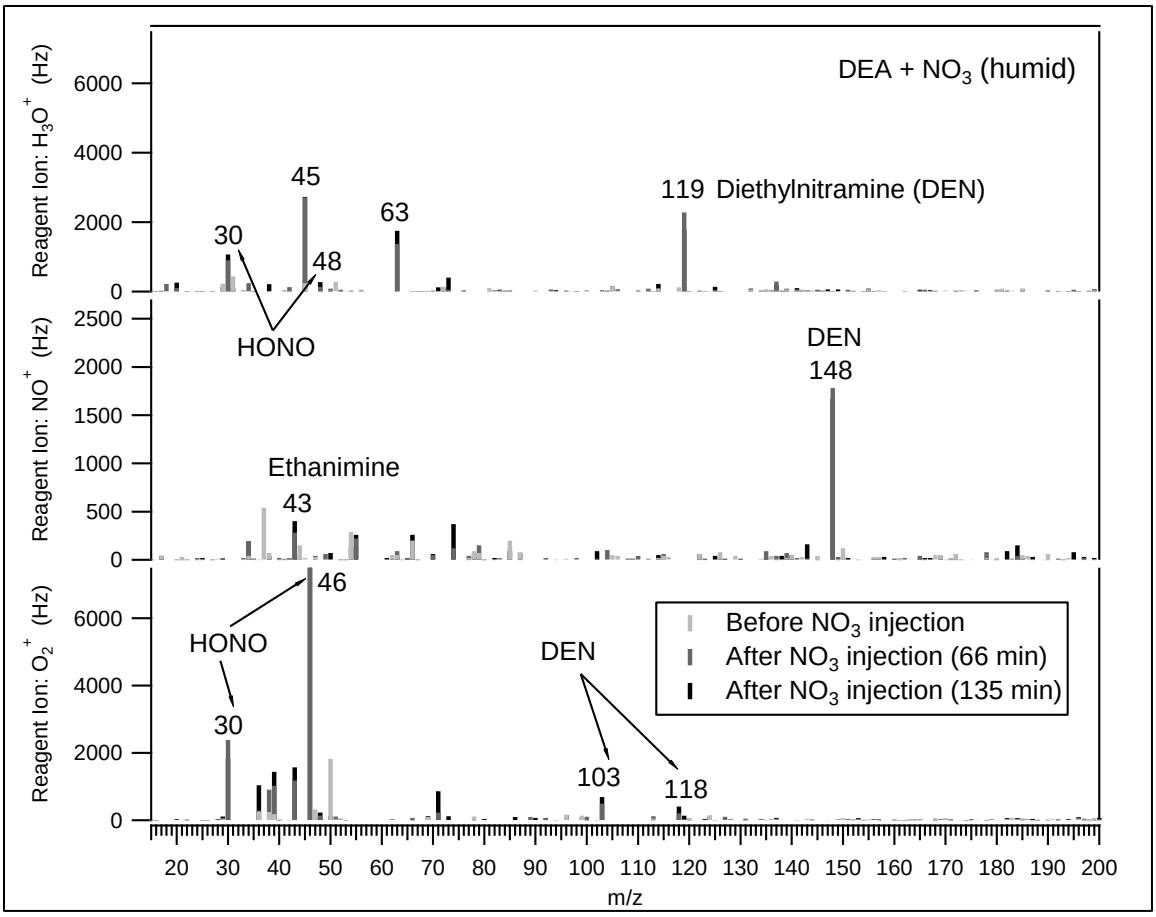

Figure 3.3. SIFT-MS mass spectra for the humid diethylamine with nitrate radical oxidation experiment.

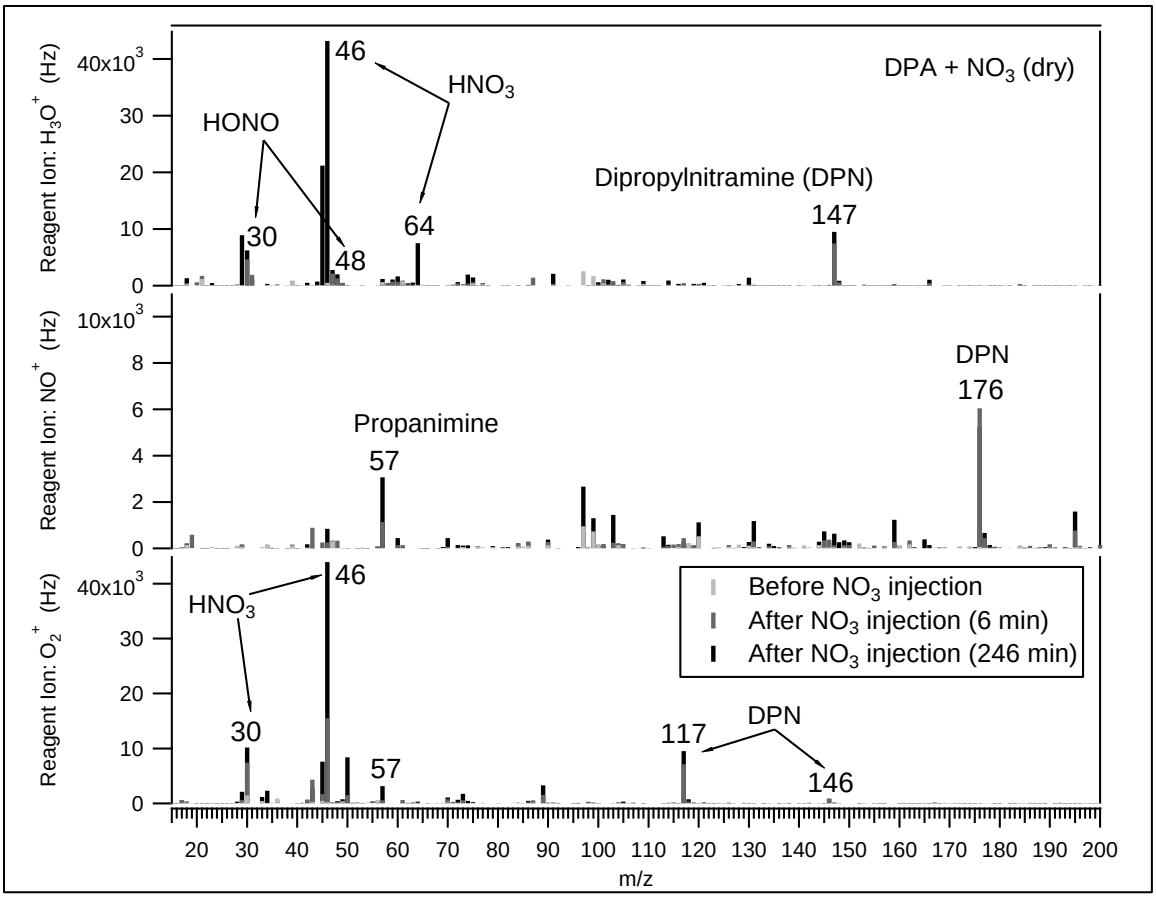

Figure 3.4. SIFT-MS mass spectra for the dry dipropylamine with nitrate radical oxidation experiment.

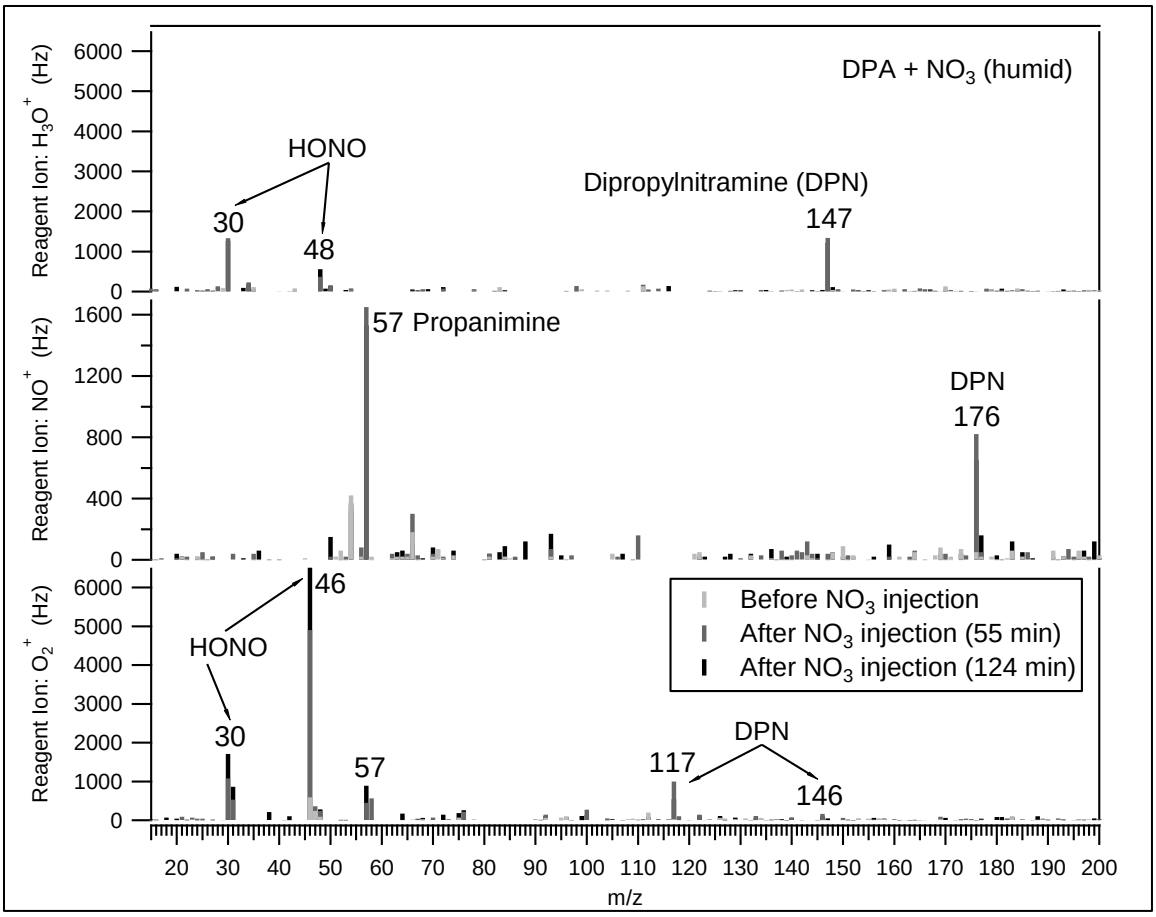

Figure 3.5. SIFT-MS mass spectra for the humid dipropylamine with nitrate radical oxidation experiment.

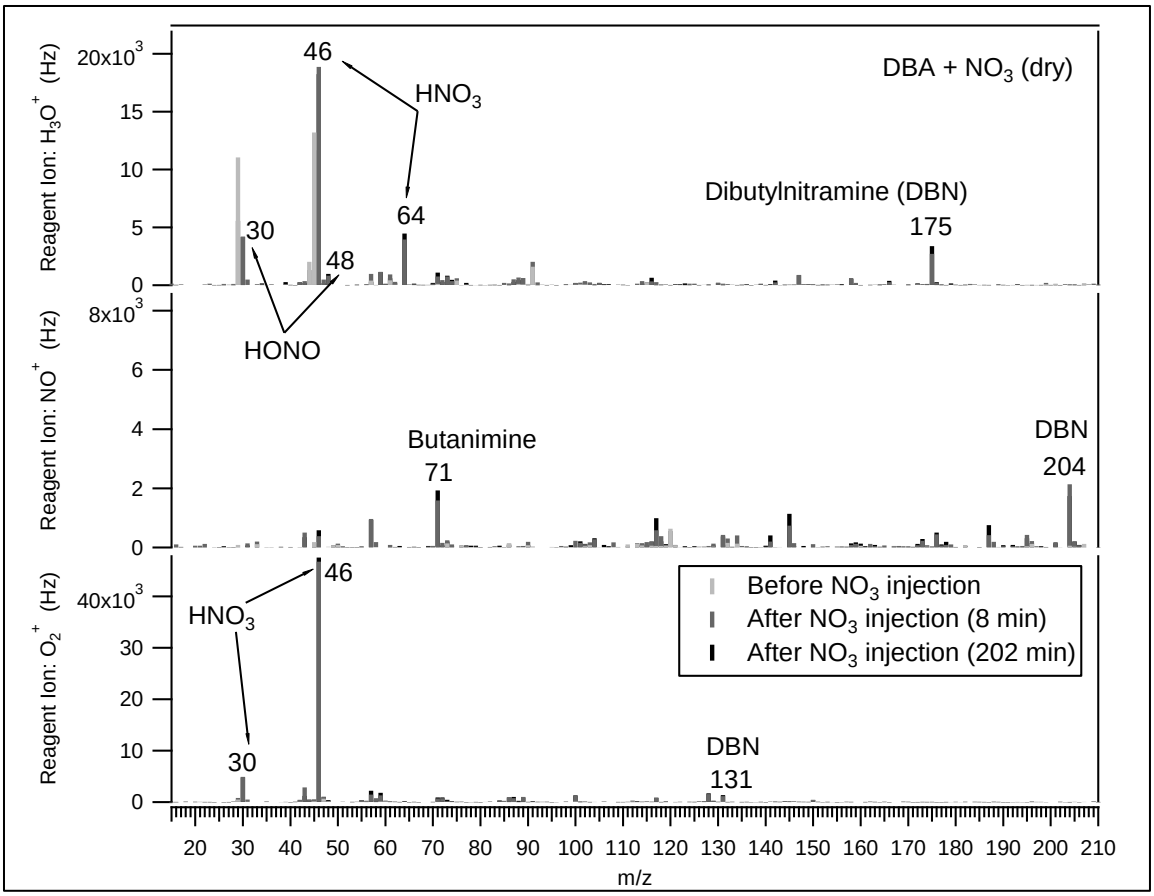

Figure 3.6. SIFT-MS mass spectra for the dry dibutylamine with nitrate radical oxidation experiment.

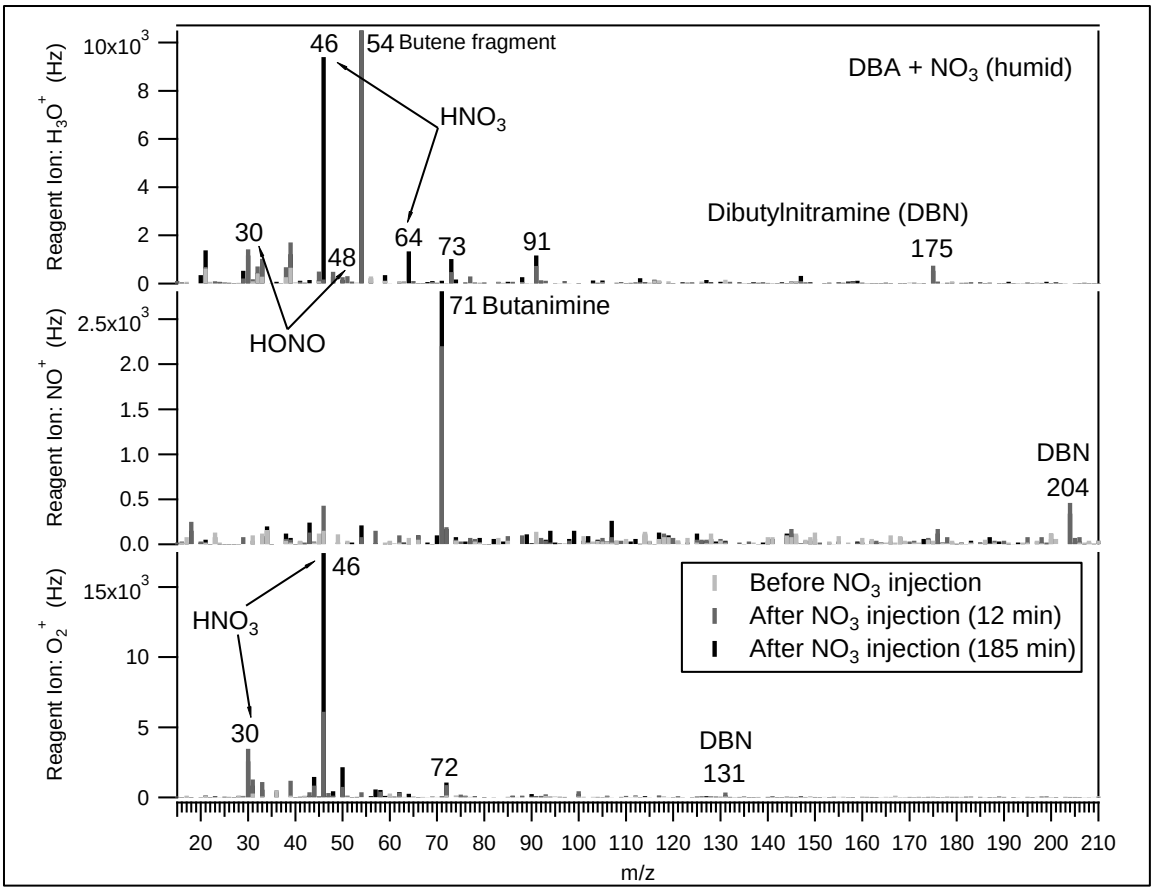

Figure 3.7. SIFT-MS mass spectra for the humid dibutylamine with nitrate radical oxidation experiment.

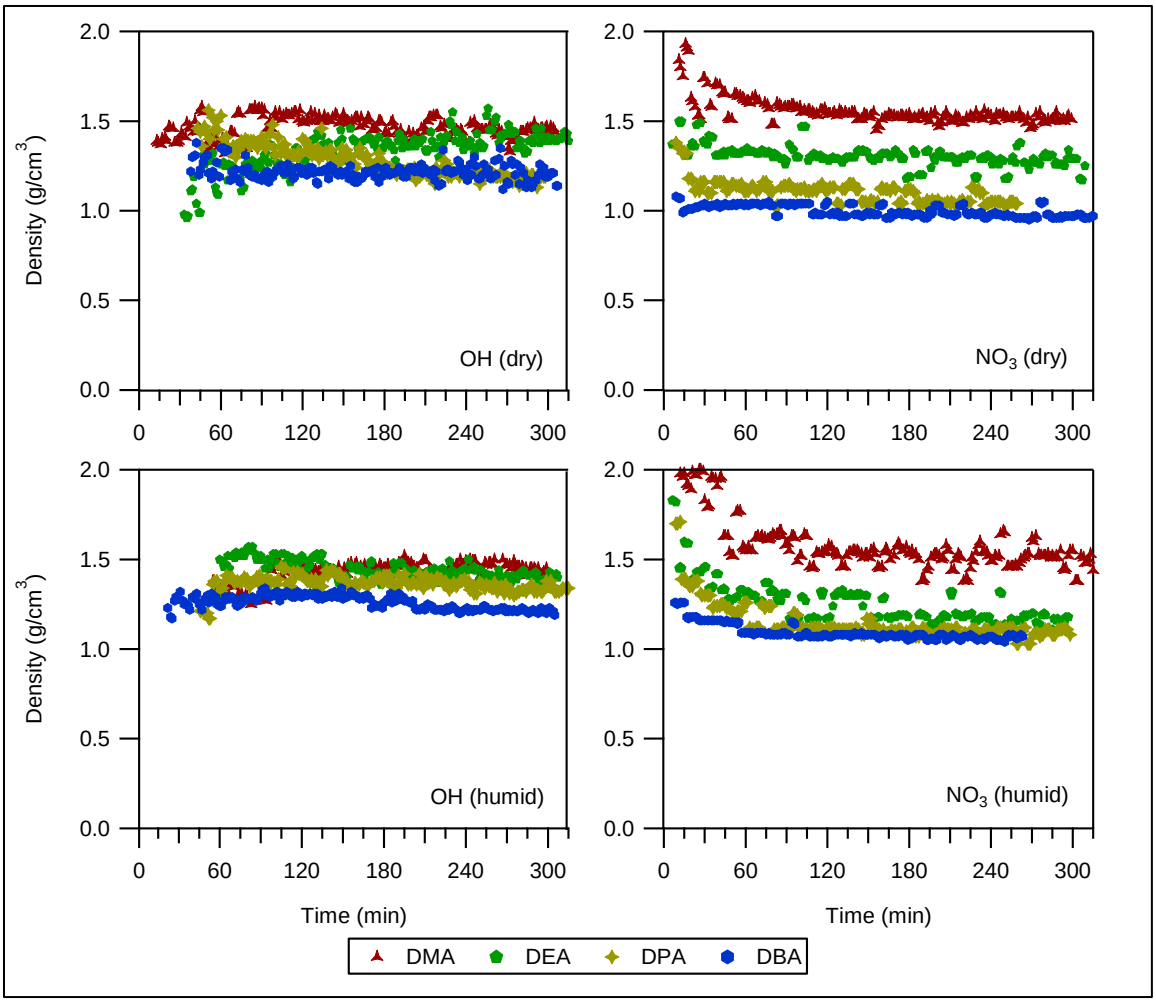

Figure 3.8. Density profiles for the aerosol produced in the secondary amine oxidation experiments.

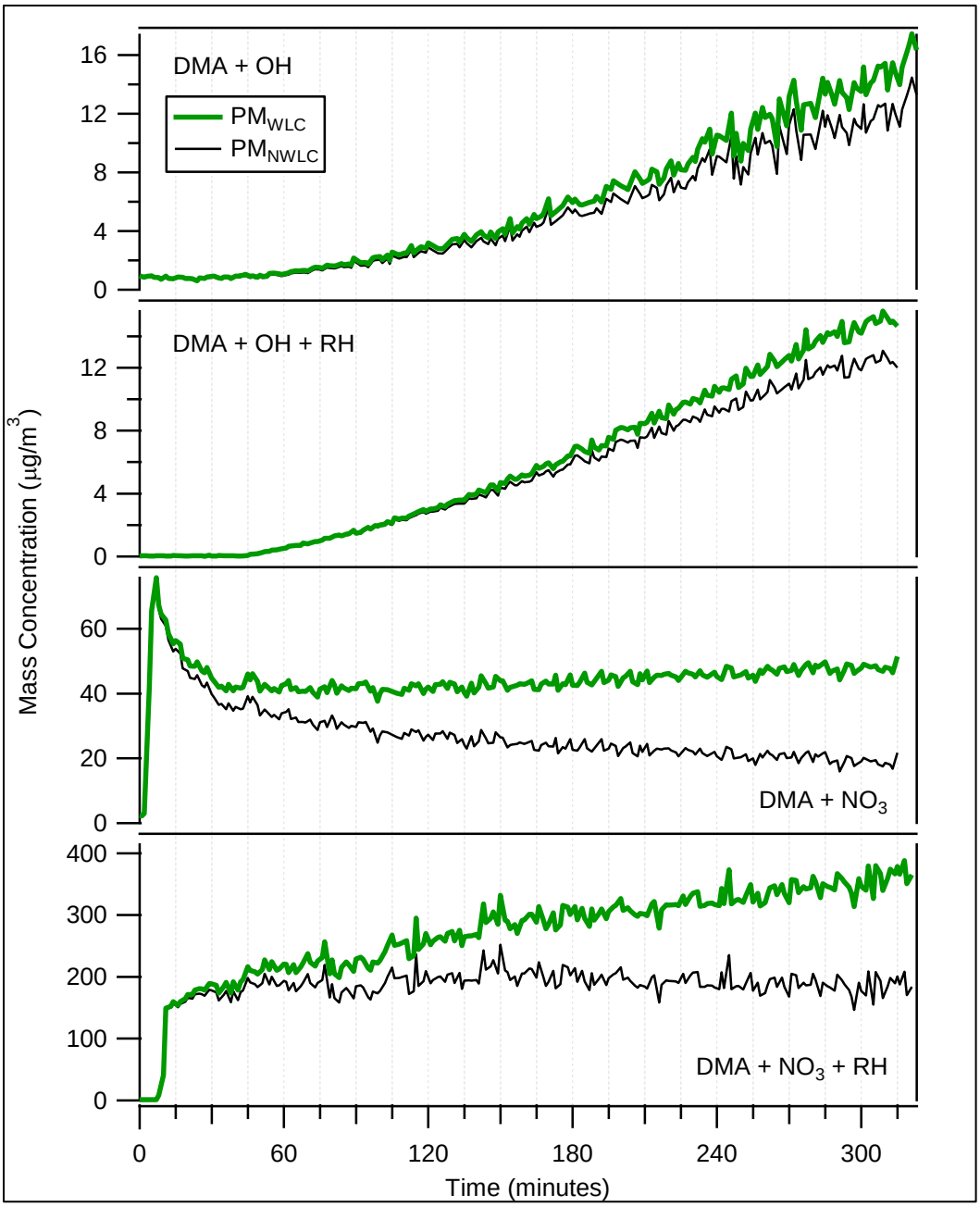

Figure 3.9. Particulate matter (PM) profiles for the dimethylamine oxidation experiments. (WLC = wall loss correction, NWLC = non-wall loss corrected)

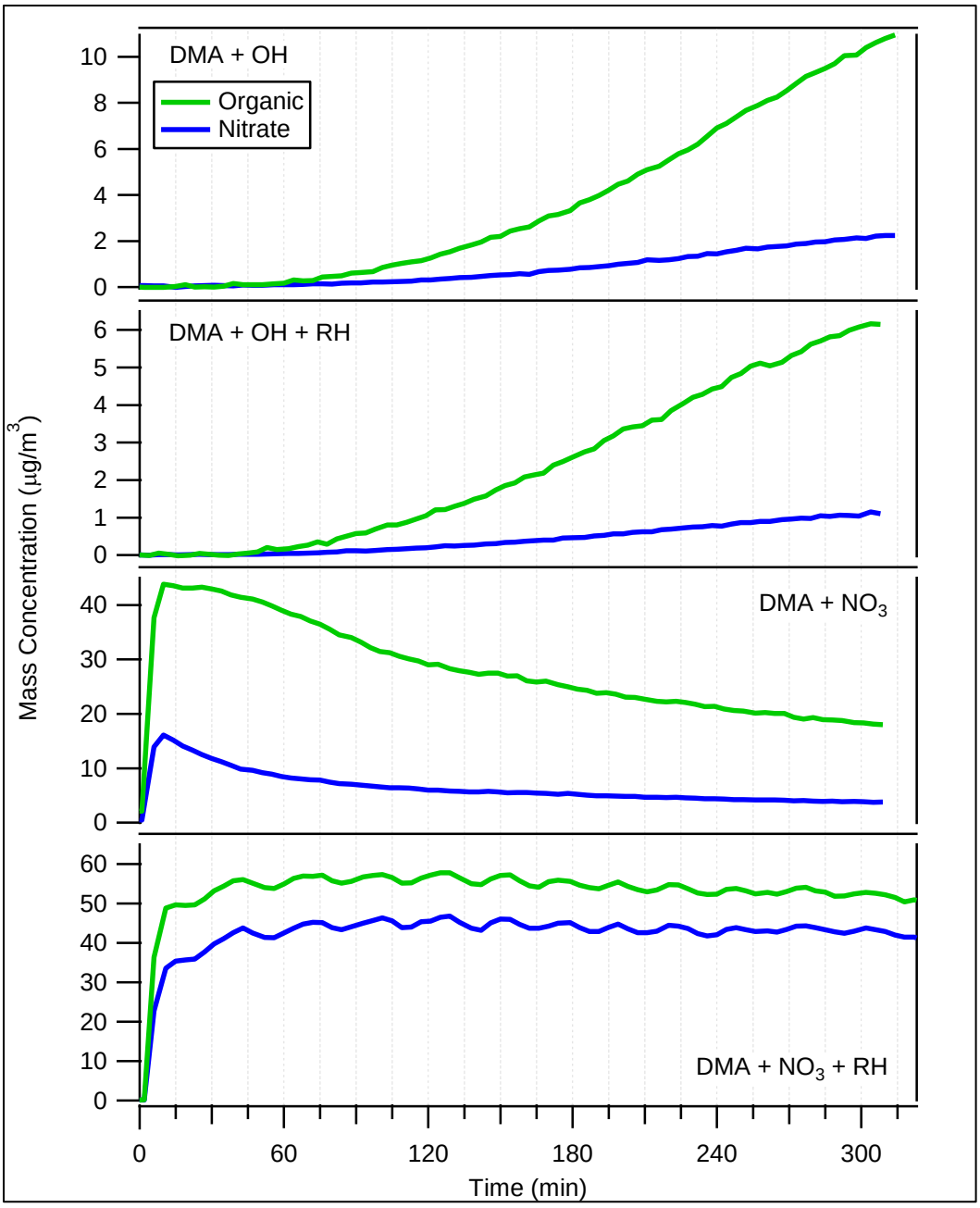

Figure 3.10. HR-ToF-AMS organic and nitrate concentration profiles for the dimethylamine oxidation experiments.

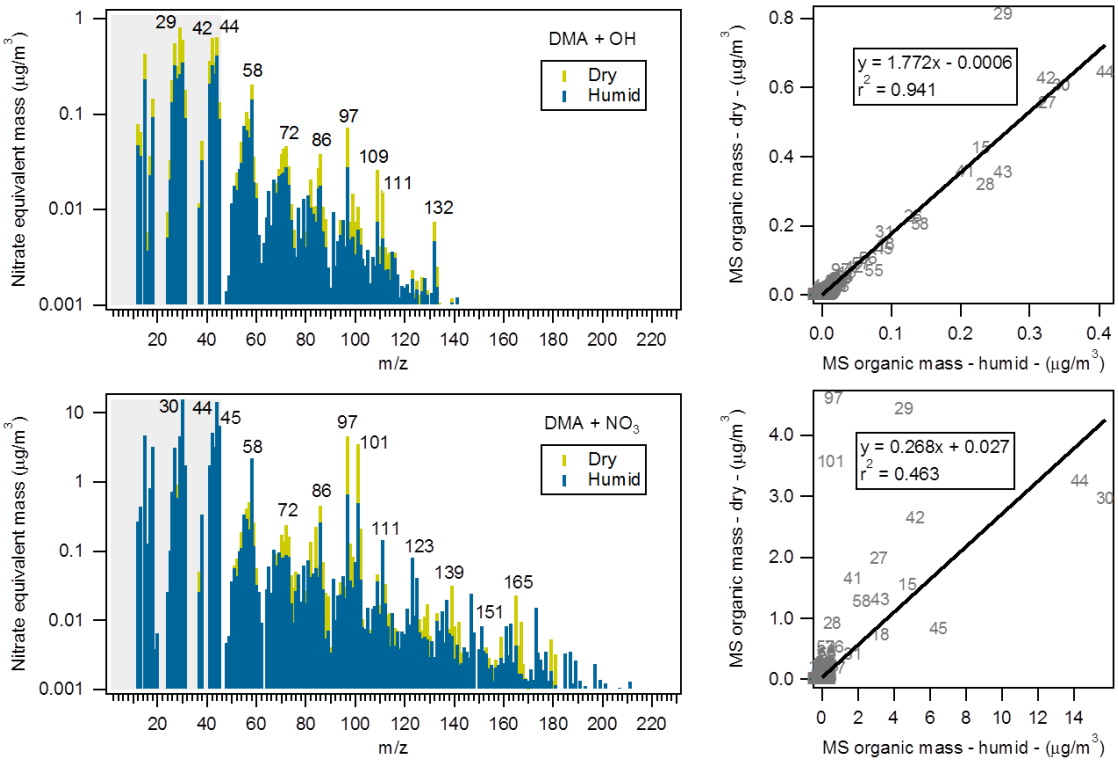

Figure 3.11. HR-ToF-AMS mass spectra and correlation plots for the dry and humid dimethylamine oxidation experiments. The shaded area represents the precursor amine *m/z* range.

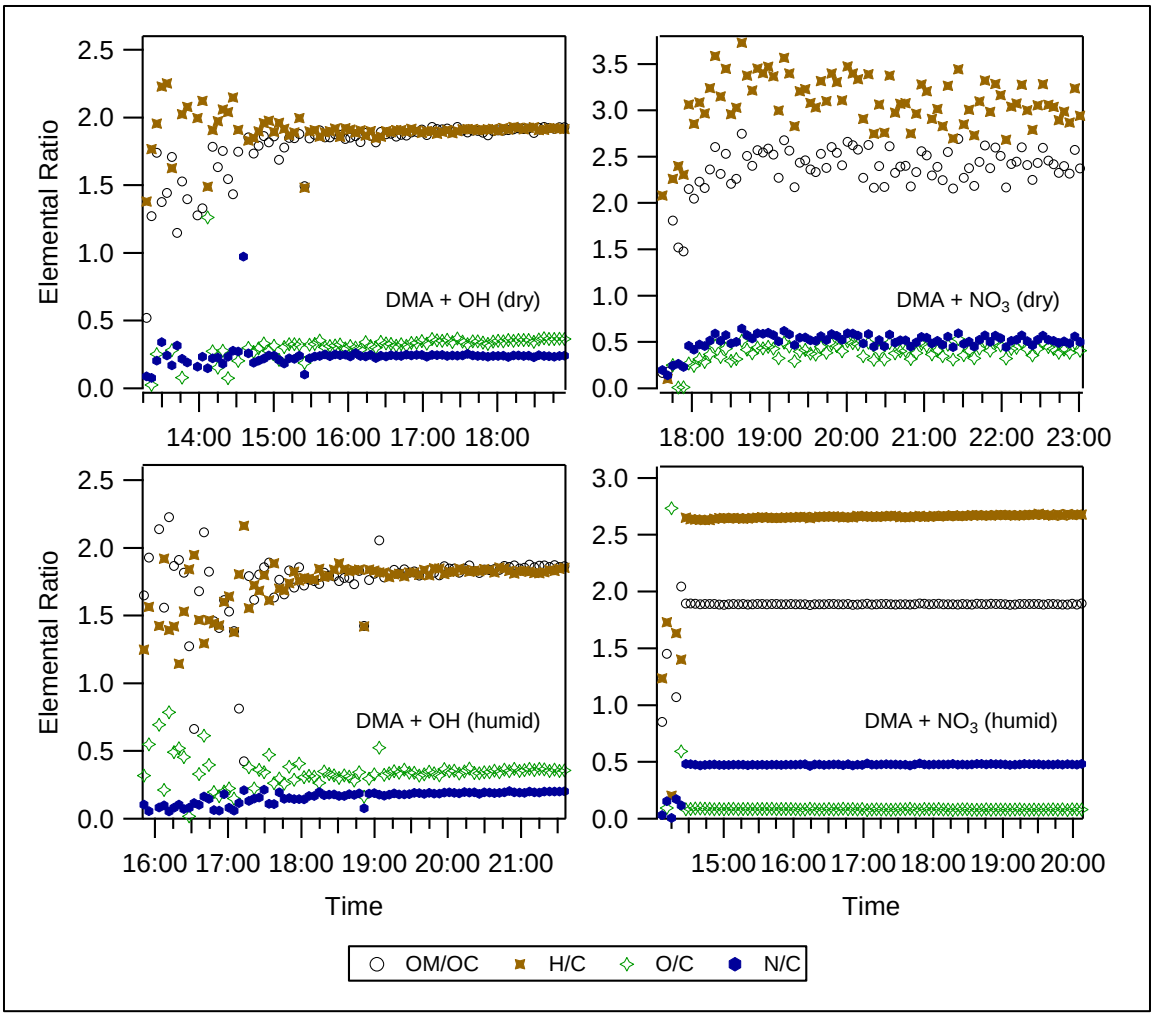

Figure 3.12. The elemental analyses for the aerosol formed in the dimethylamine oxidation experiments.

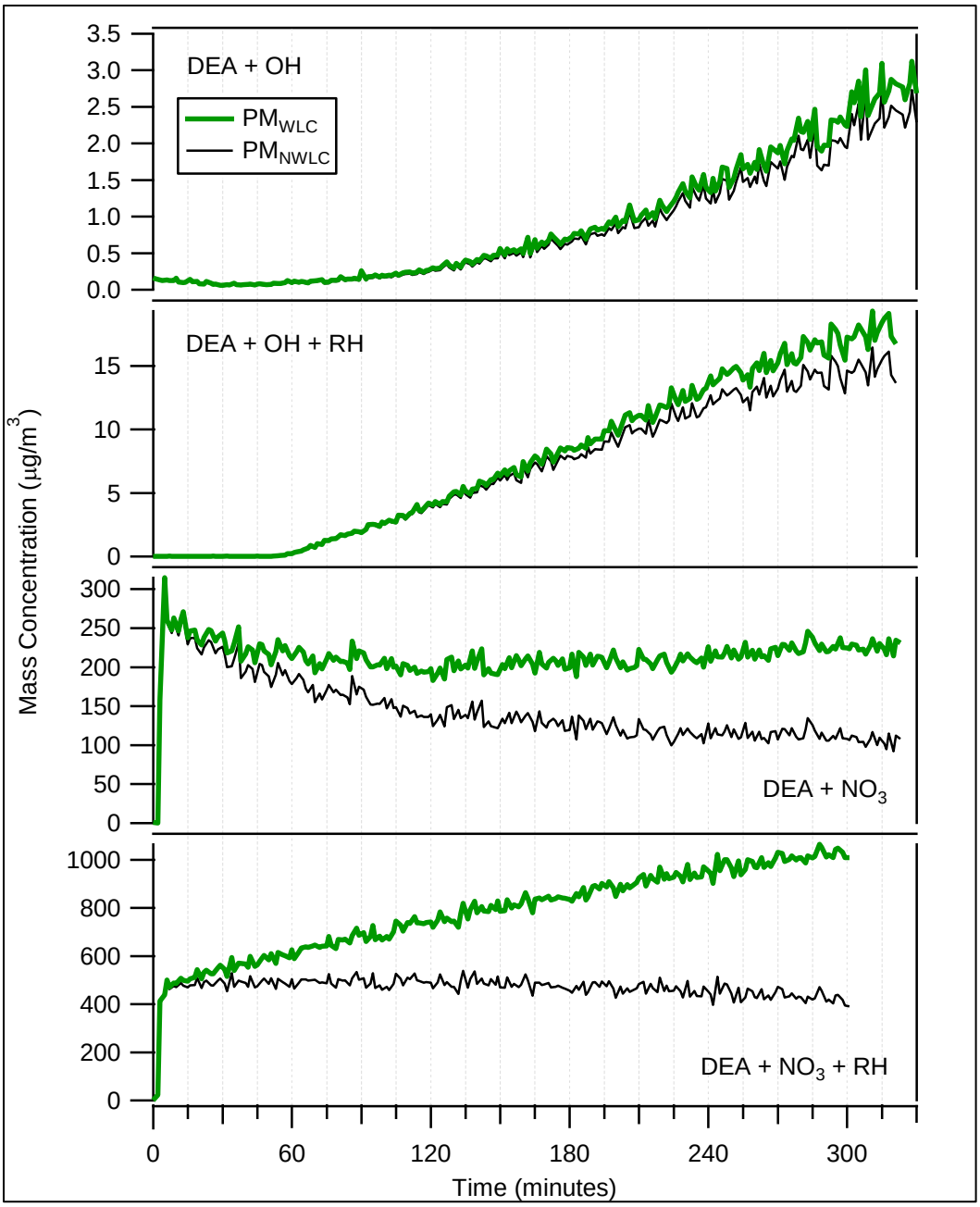

Figure 3.13. Particulate matter (PM) profiles for the diethylamine oxidation experiments. (WLC = wall loss correction, NWLC = non-wall loss corrected)

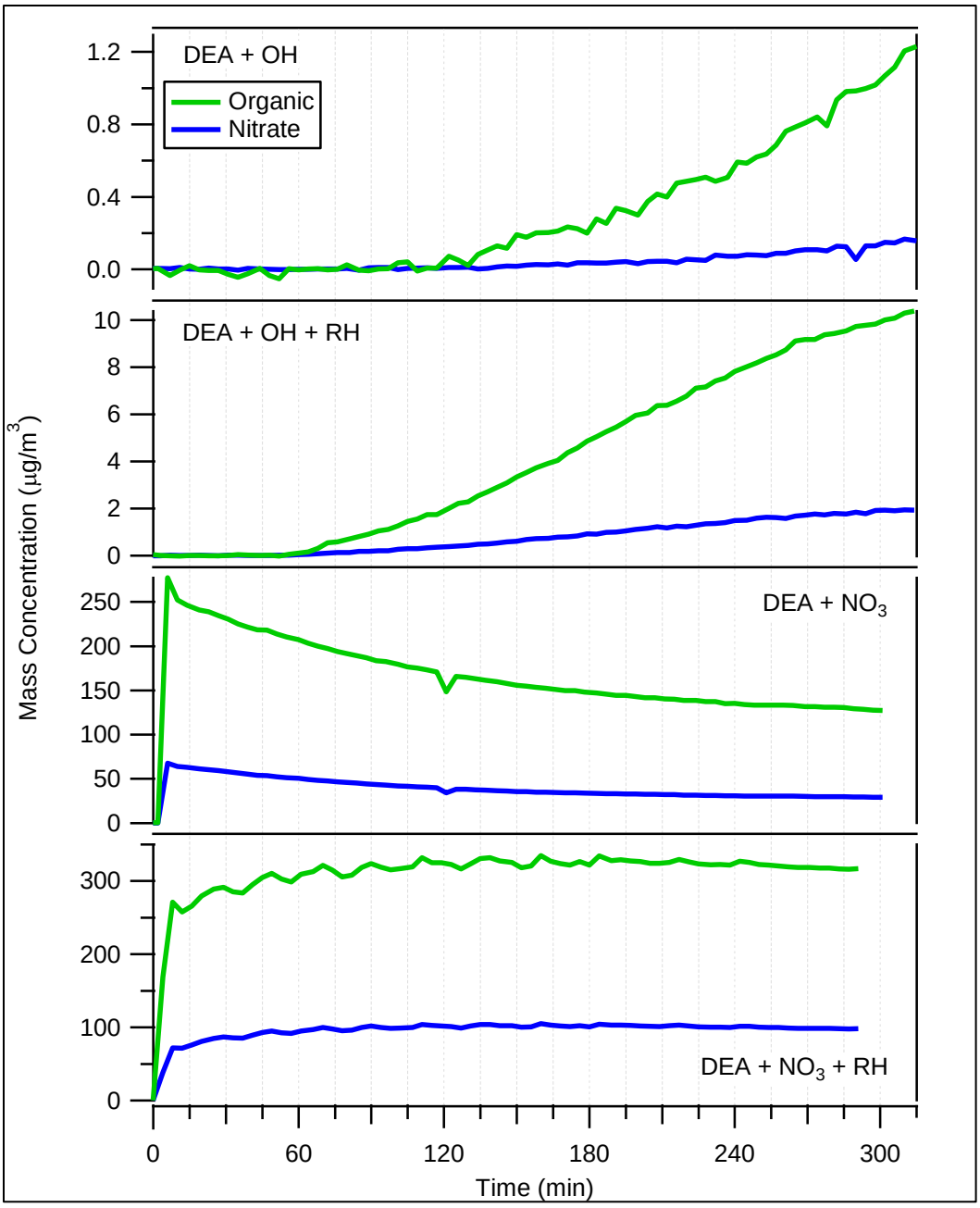

Figure 3.14. HR-ToF-AMS organic and nitrate concentration profiles for the diethylamine oxidation experiments.

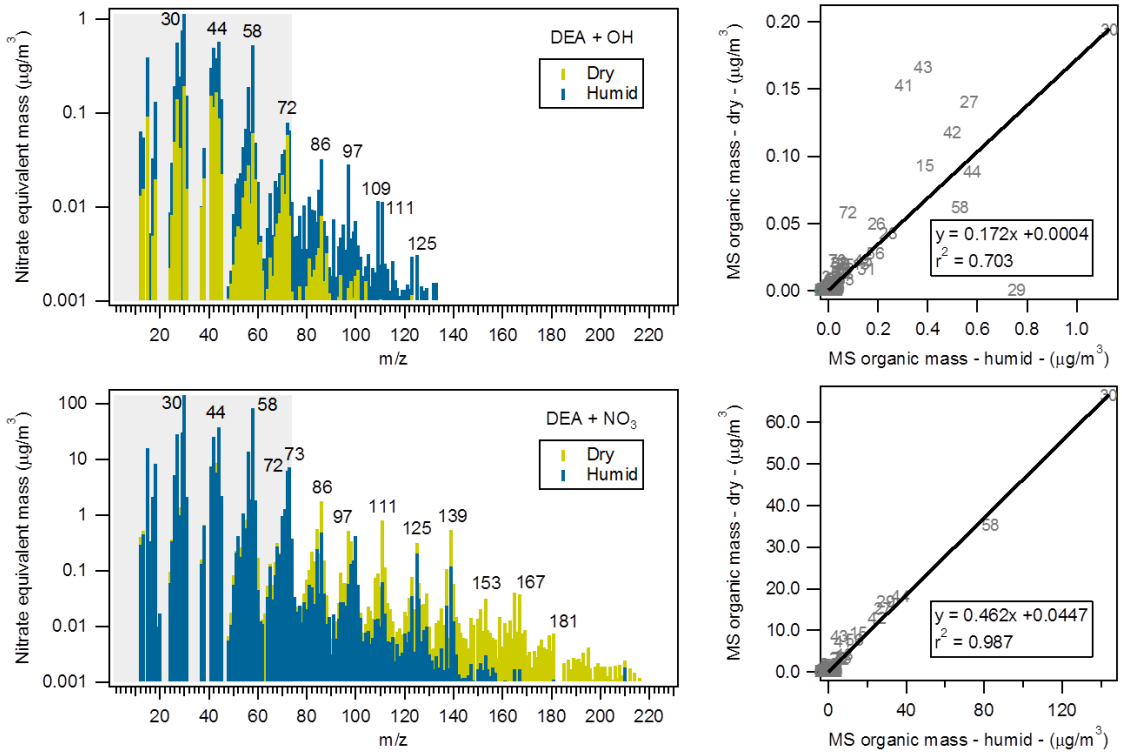

Figure 3.15. HR-ToF-AMS mass spectra and correlation plots for the dry and humid diethylamine oxidation experiments. The shaded area represents the precursor amine *m/z* range.

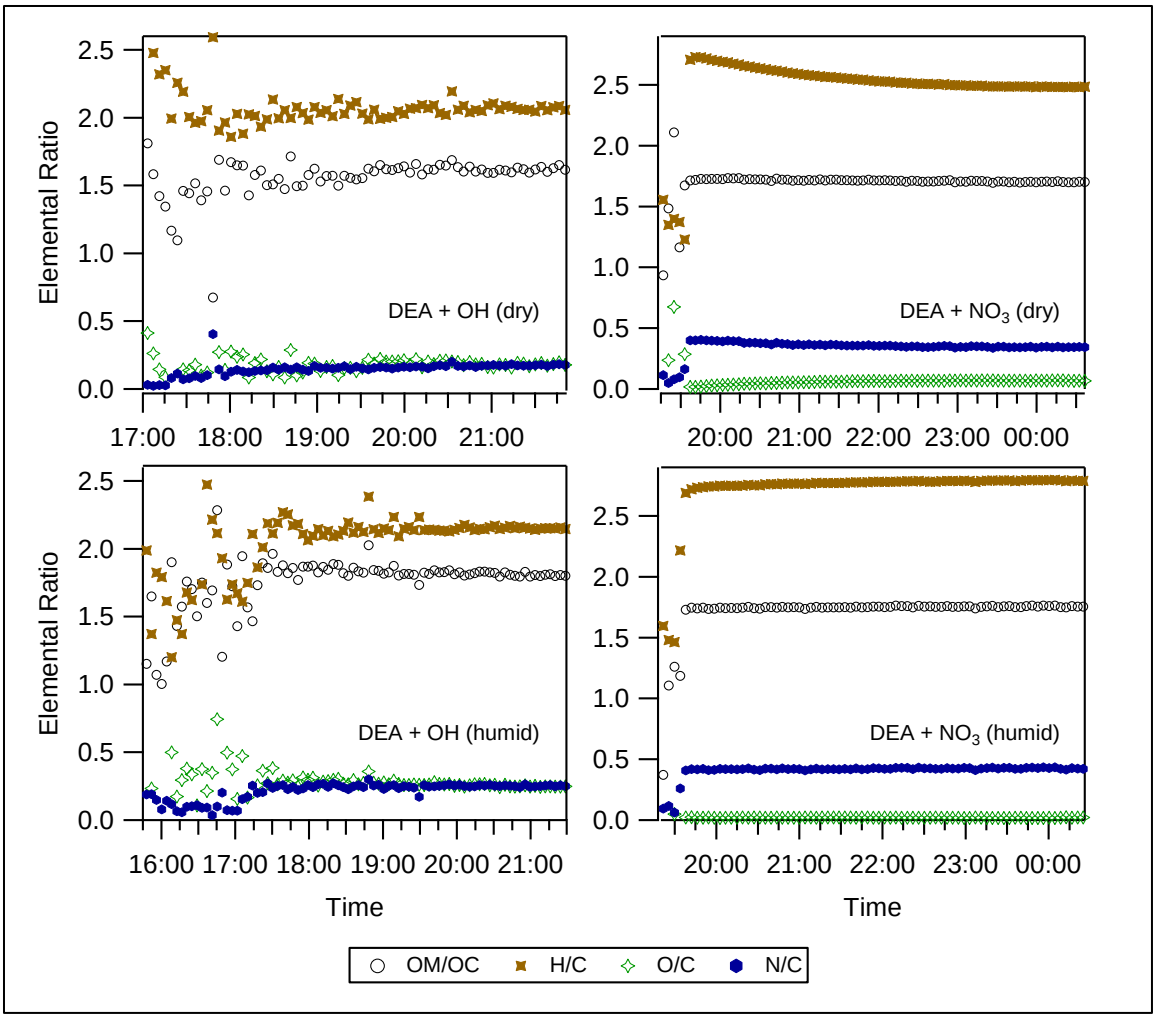

Figure 3.16. The elemental analyses for the aerosol formed in the diethylamine oxidation experiments.

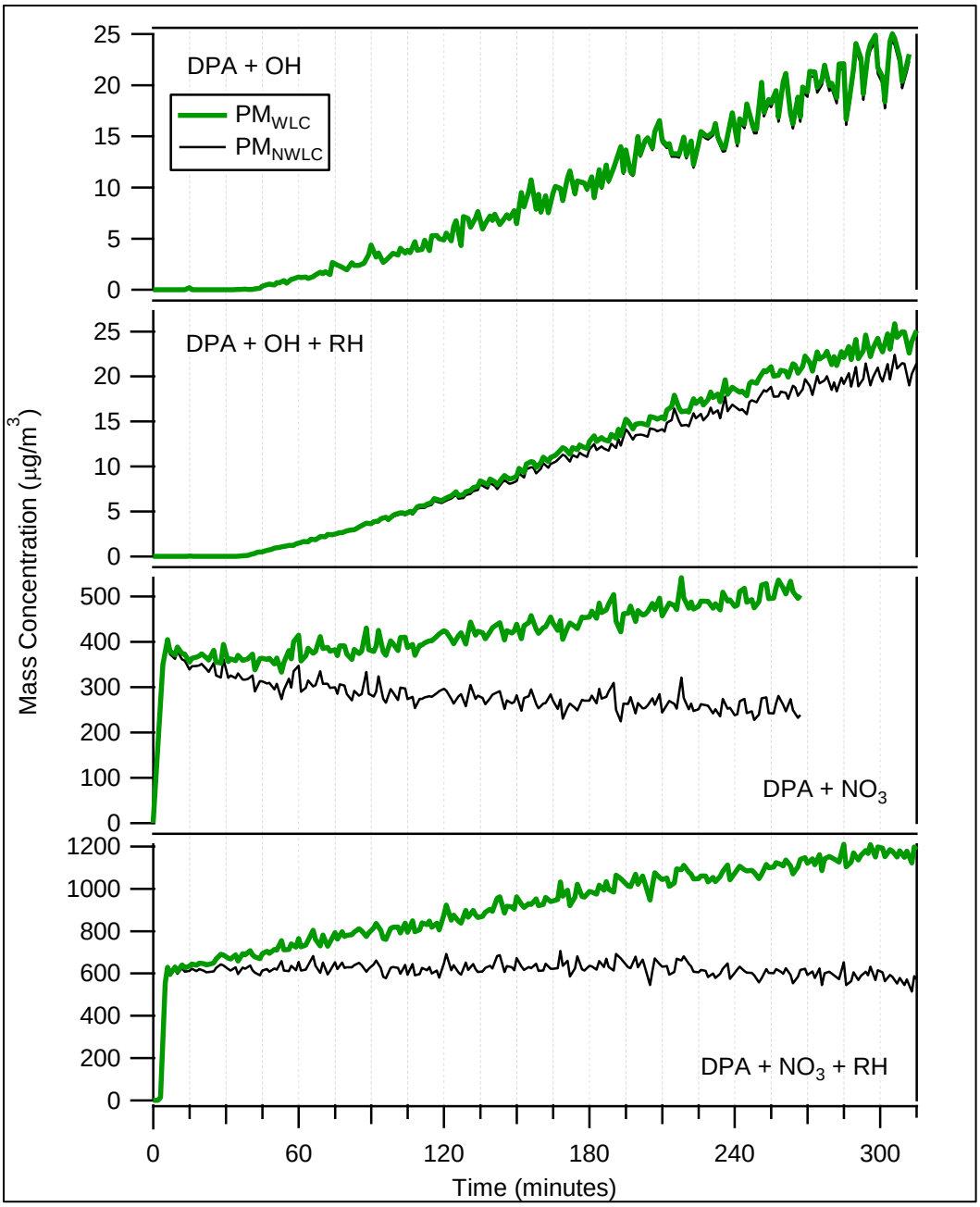

Figure 3.17. Particulate matter (PM) profiles for the dipropylamine oxidation experiments. (WLC = wall loss correction, NWLC = non-wall loss corrected)

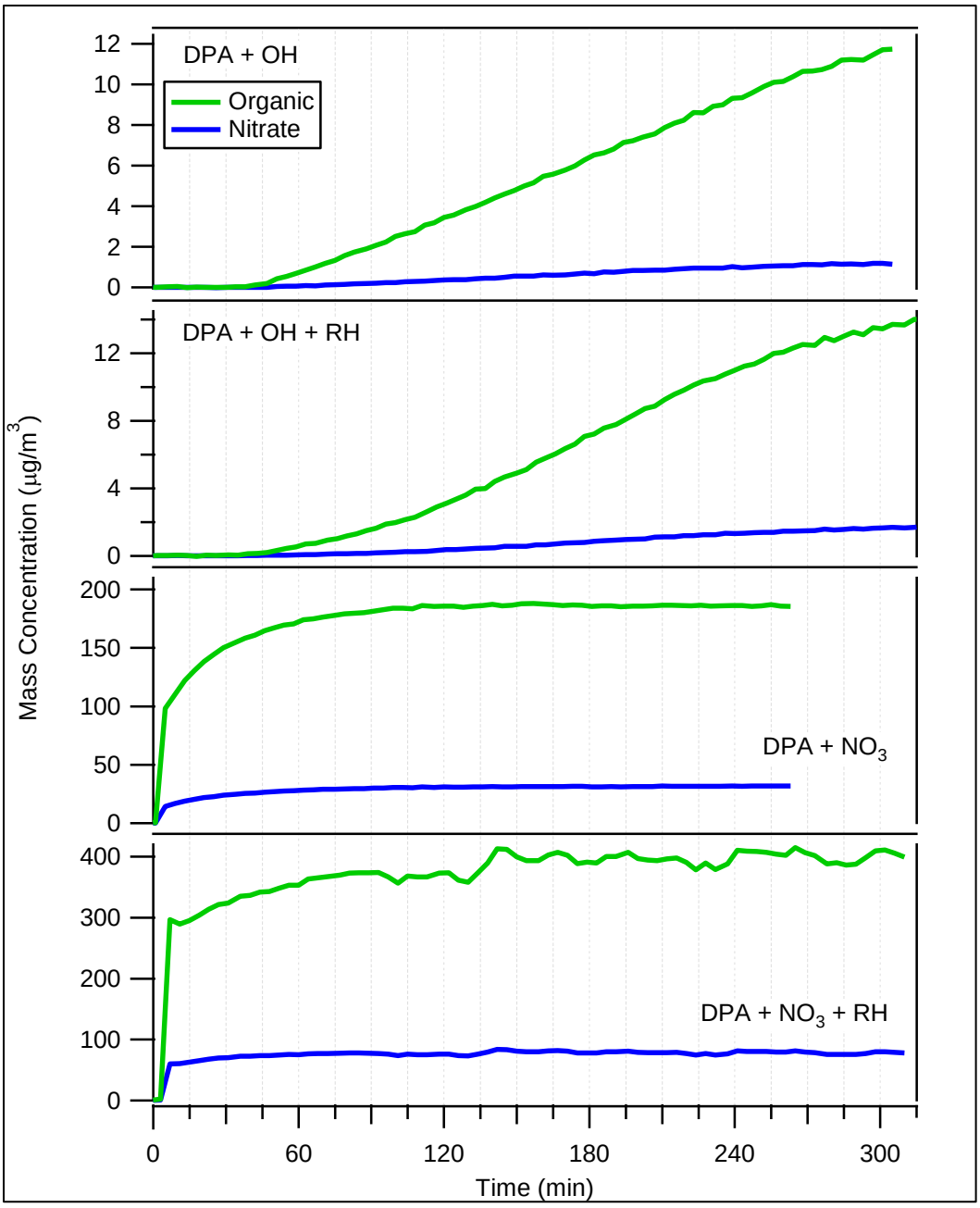

Figure 3.18. HR-ToF-AMS organic and nitrate concentration profiles for the dipropylamine oxidation experiments.

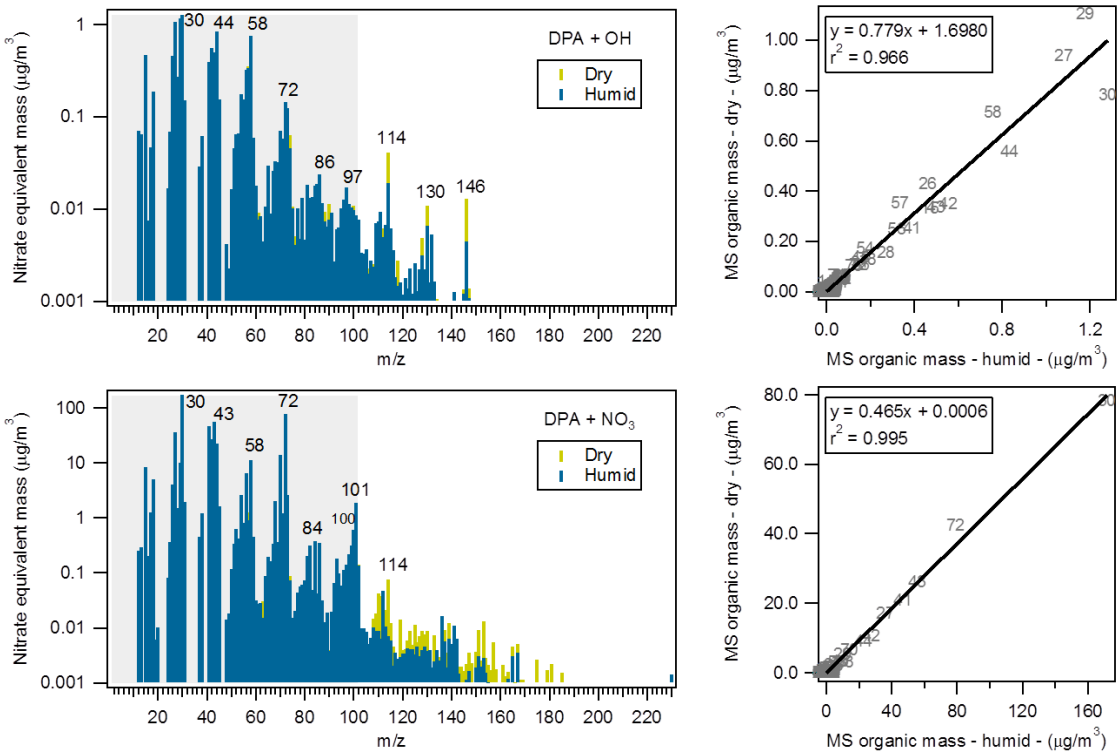

Figure 3.19. HR-ToF-AMS mass spectra and correlation plots for the dry and humid dipropylamine oxidation experiments. The shaded area represents the precursor amine *m/z* range.

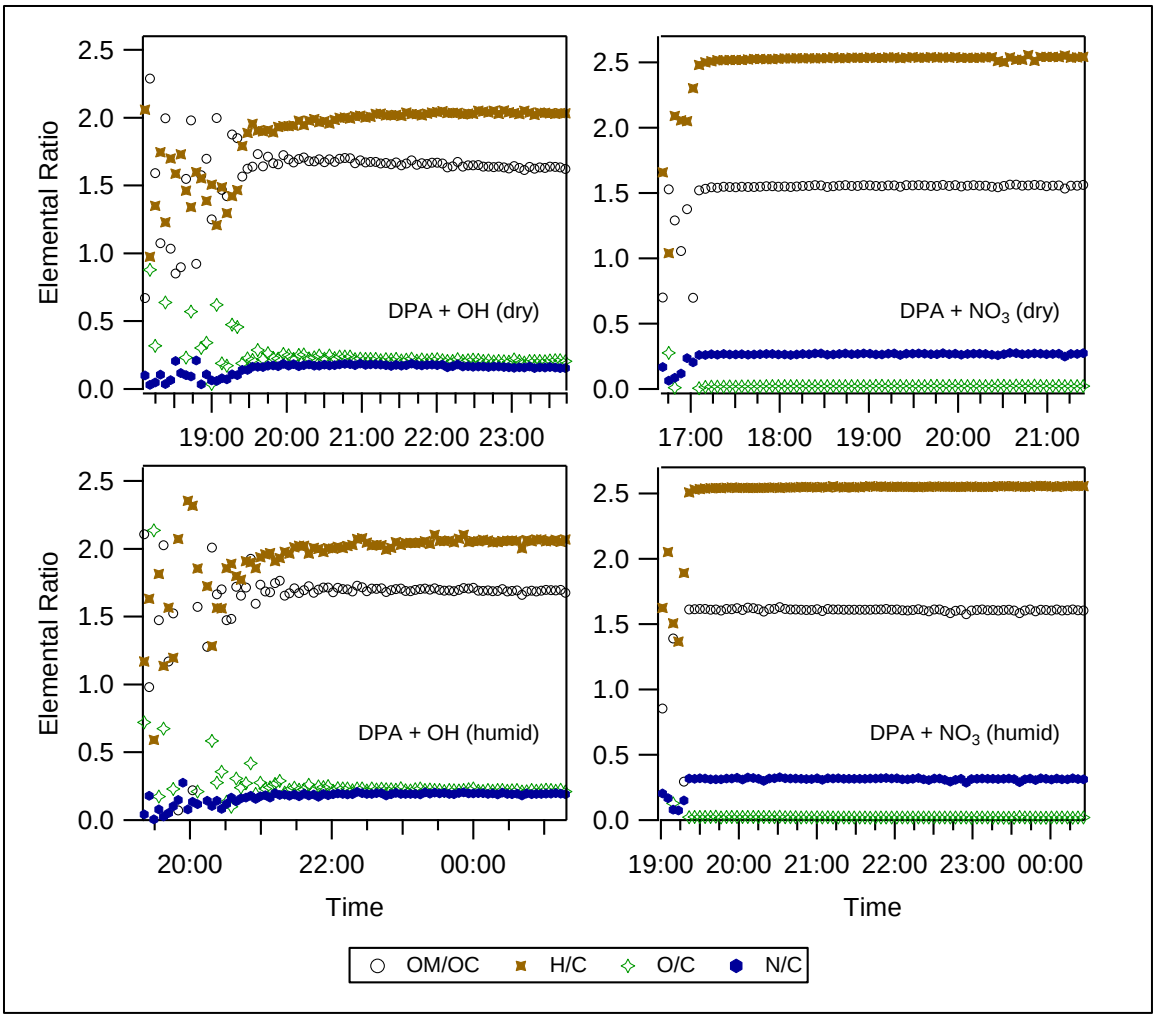

Figure 3.20. The elemental analyses for the aerosol formed in the dipropylamine oxidation experiments.

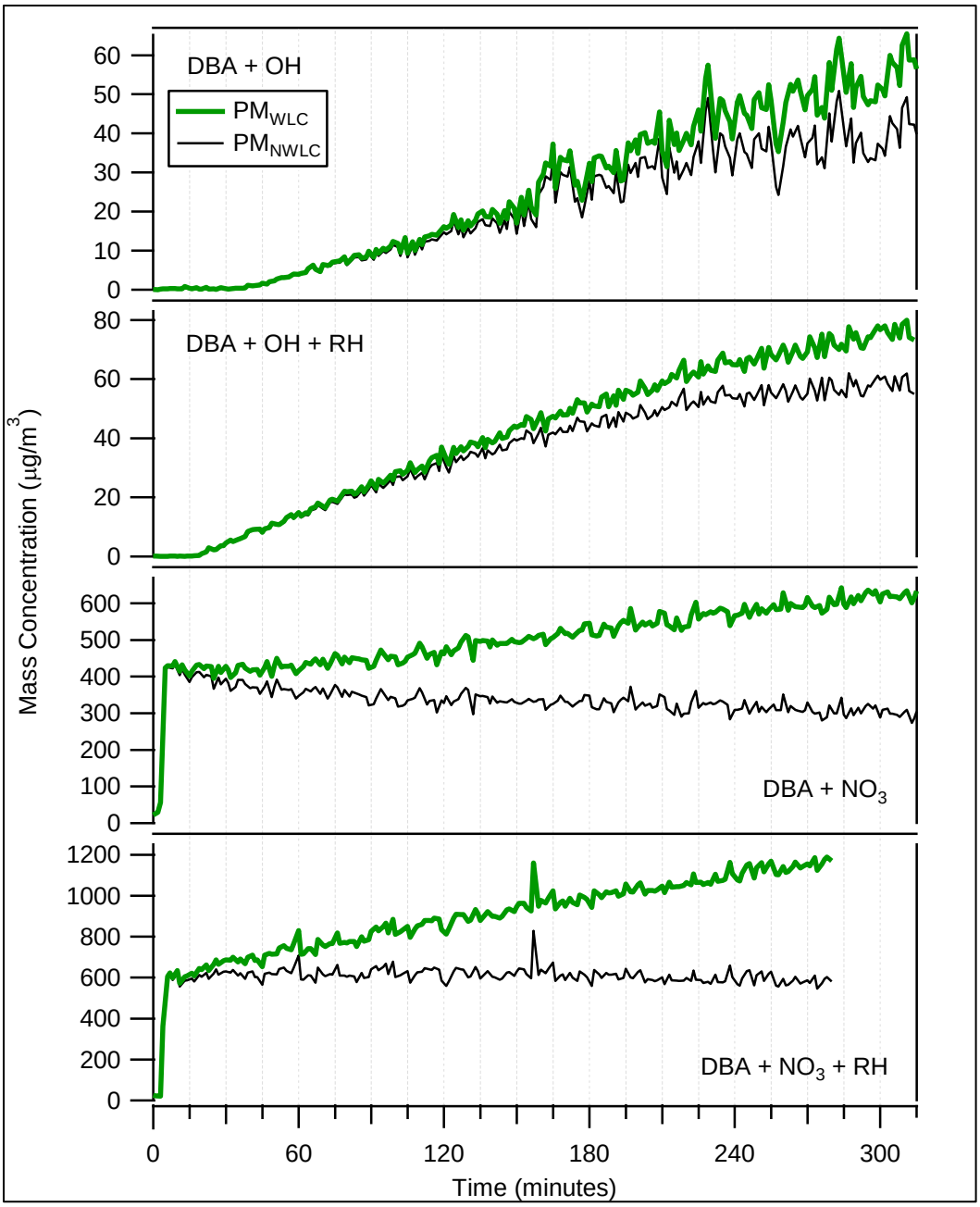

Figure 3.21. Particulate matter (PM) profiles for the dibutylamine oxidation experiments. (WLC = wall loss correction, NWLC = non-wall loss corrected)

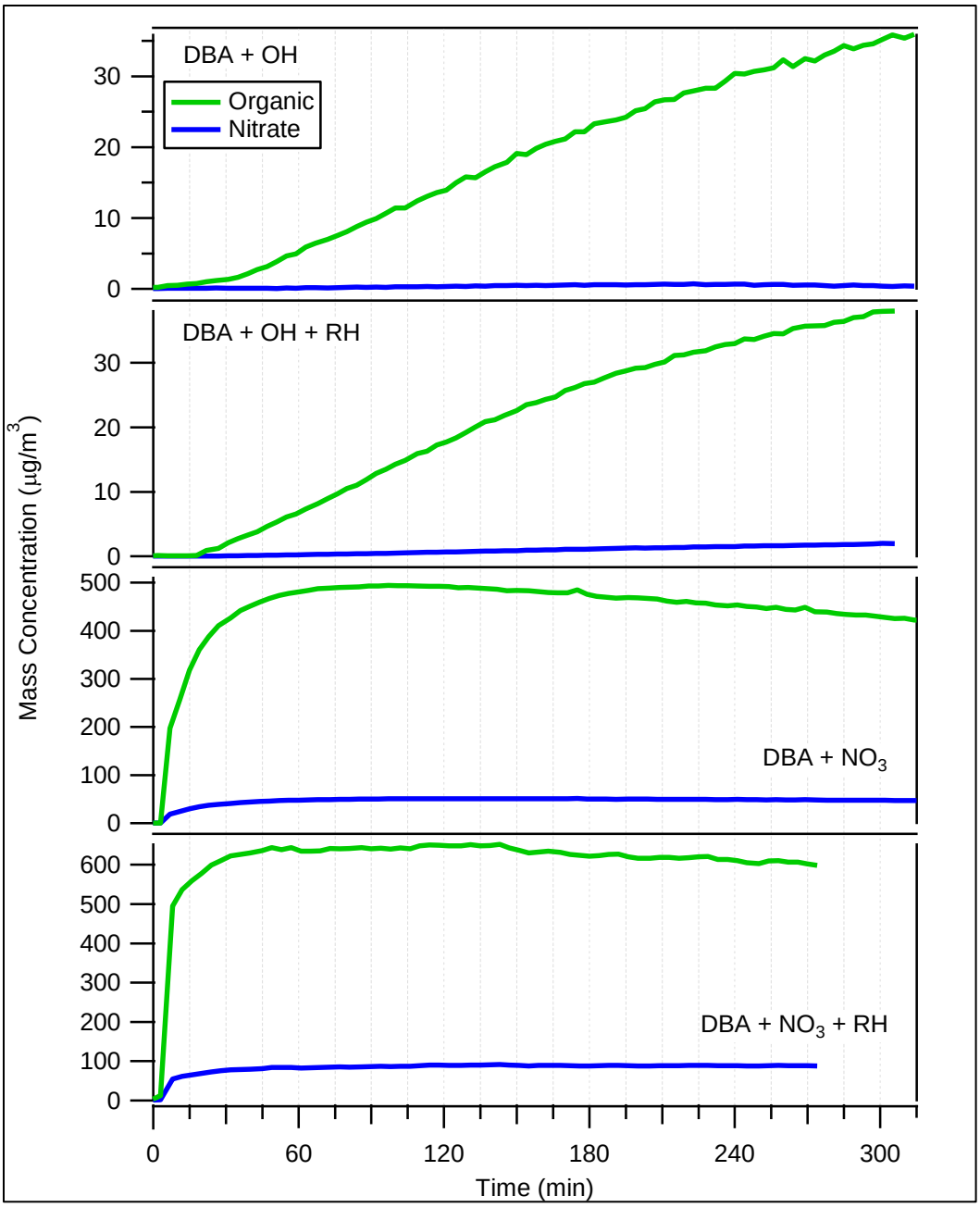

Figure 3.22. HR-ToF-AMS organic and nitrate concentration profiles for the dibutylamine oxidation experiments.

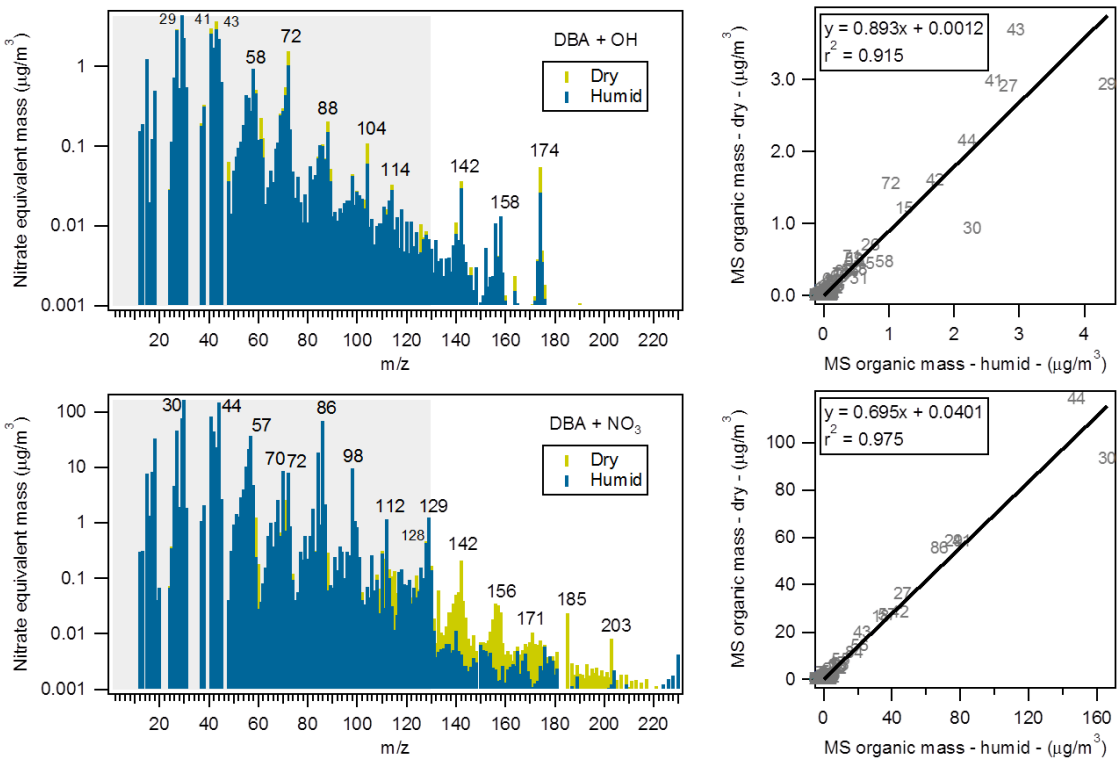

Figure 3.23. HR-ToF-AMS mass spectra and correlation plots for the dry and humid dibutylamine oxidation experiments. The shaded area represents the precursor amine *m/z* range.

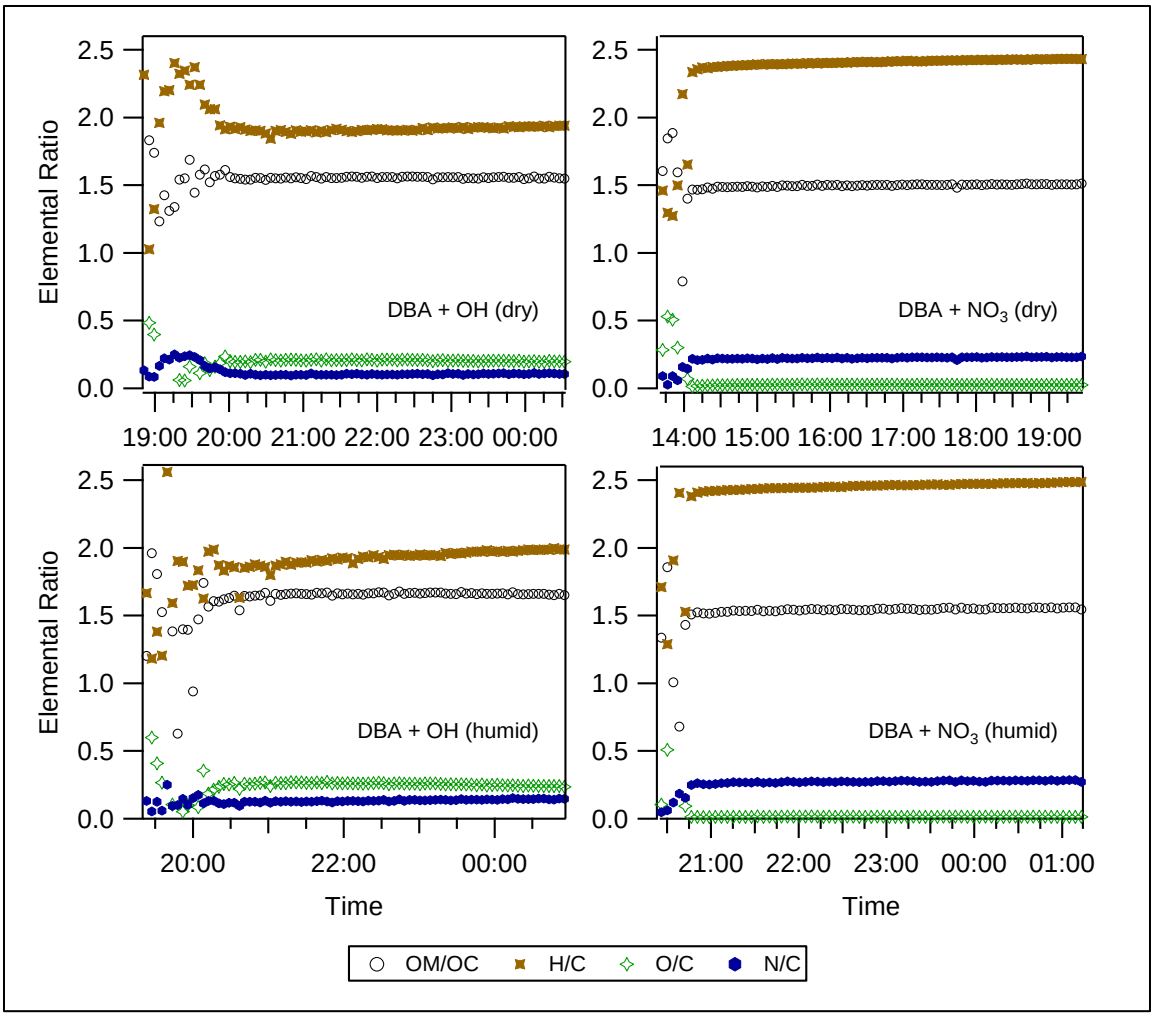

Figure 3.24. The elemental analyses for the aerosol formed in the dibutylamine oxidation experiments.

Chapter 4: Effects of Temperature on the Formation of Secondary Organic Aerosol from Amine Precursors

4.1. Introduction

Secondary organic aerosol (SOA) and fine particulate matter have negative effects on human health, air quality, visibility, and climate (Dockery, 2009; IPCC, 2013; Pope et al., 1995; Watson, 2002). Significant precursors to aerosol formation in the atmosphere are reduced nitrogen compounds including ammonia and amines (Ge et al., 2011). There are both anthropogenic and biogenic sources of amines including agricultural emissions, by-products of selective catalytic reduction and carbon capture control technologies, and biomass burning (Borduas et al., 2013; Cadle and Mulawa, 1980; Ge et al., 2011; Mosier et al., 1973; Westerholm et al., 1993).

The importance of amines in new particle formation is gaining attention. Previous studies have investigated the formation of organic salt aerosol through the reactions of atmospherically relevant acids (HNO3, H2SO4) with alkyl amines (Barsanti et al., 2009). In addition to organic salt formation, field studies have observed that a significant portion of new particle growth is due to oxidized organic amine aerosol (Silva et al., 2008; Smith et al., 2008). The atmospheric reactions of alkyl amines, however, are poorly understood. Previous atmospheric chamber studies have investigated the oxidation of alkyl amines at room temperature (Lee and Wexler, 2013; Malloy et al., 2009a; Price et al., 2014; Tang et al., 2013). Studies on the effect of temperature on amine aerosol are not previously reported. Earlier temperature work has focused on other biogenic and combustion emissions (Qi et al., 2010; Warren et al., 2009). Even scarcer

are atmospheric chamber studies that investigate response of aerosol to changing environmental temperature.

This study examines the influence of temperature on the physical properties and chemical composition of the aerosol produced from radical oxidation of aliphatic amines. The indoor atmospheric chambers at the UC-Riverside College of Engineering – Center for Environmental Research and Technology (UCR/CE-CERT) are ideally suited for this study.

4.2. Methods

A set of well characterized atmospheric chamber experiments were conducted on three aliphatic amines: trimethylamine (TMA, 25 wt.% solution in water, Sigma-Aldrich), diethylamine (DEA, >99.5%, Sigma-Aldrich), and butylamine (BA, 99.5%, Sigma-Aldrich). All experiments were conducted in the atmospheric chambers located at UCR/CE-CERT. The chamber facility has been described in detail previously (Carter et al., 2005). The amines were reacted in dual 90 m3 volume Teflon® film (50.8 μm) chambers with either hydroxyl radical (OH) or nitrate radical (NO3). The environmental chambers are housed in a 6 m x 6 m x 12 m thermally insulated enclosure.

Photooxidation, when desired, was driven by a bank of 115W black lights with peak intensity of 350 nm (350 BL, Sylvania). The interior of the enclosure is lined with reflective aluminum sheeting to ensure maximum intensity and even distribution of light. Prior to each experiment, the chambers were flushed with purified air (Aadco 737 air purification system) so that background particle concentration, NO_x, and hydrocarbon

concentrations were below the detection limits of the instruments used. There were no seed aerosols injected. Experiments were conducted at various temperatures (10°C - 40°C) and then temperature ramped between 10 and 40°C (Table 4.1). Amine concentrations were allowed to stabilize in the Teflon chambers before radical injection. Hydroxyl radicals (no NO_x experiments) were produced from direct photolysis of hydrogen peroxide (H_2O_2). The nitrate radical was formed from thermal decomposition of dinitrogen pentoxide (N_2O_5). OH experiments were designed to represent daytime chemistry while the NO_3 experiments represented nighttime chemistry.

The chemical composition of the aerosol products was measured by a High Resolution Time of Flight Aerosol Mass Spectrometer (HR-ToF-AMS; Aerodyne Research Inc.) (DeCarlo et al., 2006; Jayne et al., 2000). Briefly, an aerosol sample was drawn through a time-of-flight region where the particles were separated based on their vacuum aerodynamic diameter. The sample was vaporized by a 600°C oven followed by 70 eV electron impact ionization. The resulting ions pass through another time-of-flight section which can be operated in two flight path configurations, V and W. The shorter flight path (V-mode) provides better sensitivity at unit mass resolution. The longer flight path (W-mode) provides sufficient mass spectral resolution (4300 at *m/z* 200) to separate isobaric compounds and determine empirical formulas.

A custom built scanning mobility particle sizer (SMPS) (Cocker et al., 2001), was used to measure the concentration and size distribution (27 - 712 nm) of the aerosol formed during the experiments. The SMPS also communicates size distribution values in

real-time to a pair of custom built instruments designed to measure particle density and volatility.

Particle density was measured by an Aerosol Particle Mass Analyzer (APM, Kanomax model 3600) in series with an SMPS. Details of the instrument are described previously (Ehara et al., 1996; Malloy et al., 2009b). Briefly, the mass of the particle is selected by the APM based on the peak number electrical mobility diameter identified by the independent SMPS. The mass selected particles are then measured by an in-series SMPS to obtain the peak number electrical mobility diameter transmitted by the APM. Density measurements were taken every 85 seconds.

Particle volatility was measured by a custom built Volatility Tandem Differential Mobility Analyzer (VTDMA). The particles entering the first DMA column are size selected based on the peak number electrical mobility diameter provided by the independent SMPS. The resultant monodisperse aerosol is then sent through a Dekati® Thermodenuder (TD, 40°C, residence time: ~17 s). The second DMA column scans the size distribution of the particles exiting the TD to determine the final diameter (D_f). Particle volatility can then be expressed as the volume ratio before and after the TD or Volume Fraction Remaining [VFR, $(D_f/D_i)^3$]. Volatility measurements were taken every 85 seconds.

4.3. Results and Discussion

4.3.1. Trimethylamine aerosol – physical properties

Particle formation (not wall loss corrected) along with temperature profiles for the trimethylamine (TMA) experiments are shown (Figure 4.1). Aerosol formation is greater starting at cold temperature (100 $\mu g/m^3$) then it is at hot temperature (60 $\mu g/m^3$) in the OH oxidation experiments. Particle concentration drops with increasing temperature for both OH experiments. The particles lost with heating return after cooling.

A large particle nucleation event occurred in the cold start NO_3 oxidation experiment (719,000 cm^{-3} within 2 min of oxidation) compared to the cold start OH oxidation experiment (30,000 cm^{-3} within 20 min of oxidation). These particles completely partition to the gas phase with increasing temperature. This is consistent with the formation of volatile amine nitrate salts. Unlike the OH experiments, the particles lost at higher temperatures do not return after cooling. This suggests that one or more of the amine oxidation products may be lost in the gas phase. Particles had difficulty forming at 40°C initial temperature for the NO_3 oxidation experiment and quickly partitioned to the gas phase. There was no subsequent particle formation after cooling. Aerosol formation was greater at cold temperature (110 $\mu g/m^3$) than at hot temperature (37 $\mu g/m^3$) in the NO_3 oxidation experiments.

There is a general decrease in density to 1.45 g/cm^3 for the TMA experiments, while density appears to be largely indifferent to temperature change (Figure 4.2). Density values are not shown above 33°C for the NO_3 oxidation experiments due to the

loss of particles after heating. The artificially large density values observed at the start of particle nucleation in the cold start experiments are due to the evaporation of particles in the line between the APM and in-series SMPS. This instrument is located outside of the enclosure (room temperature). While the line from the chamber to the APM is insulated, the line between the APM and SMPS is not. Therefore, the particle diameter measured by the in-series SMPS is smaller than expected for the selected APM particle mass, translating to a smaller particle volume bias and larger measured density. The significant bias is consistent with the observation of a volatile salt aerosol.

The aerosol produced in the OH oxidation experiments increases in VFR (decreasing volatility) over the course of the experiment (Figure 4.3) suggesting the formation of less volatile aerosol as the experiment progresses. As expected, the VFR increases to nearly 1.0 as the chamber temperature matches the thermodenuder temperature (40°C). The VFR levels off to around 0.8 after cooling the chamber back to 5°C. Highly volatile aerosol formed in the cold start NO_3 experiment with particles completely partitioning to gas phase after heating to 40°C in the thermodenuder, consistent with observed particle loss at chamber temperatures of 40°C and indicative of amine salt aerosol.

4.3.2. Trimethylamine aerosol – chemical composition

The HR-ToF-AMS mass spectra for the TMA + H_2O_2 experiments are presented (Figures 4.4 and 4.5). The mass spectra for the TMA experiments are shown in logarithmic scale to highlight the higher *m/z* peaks, i.e., *m/z* peaks greater than that of the

amine precursor (TMA = 59 amu). The higher *m/z* peaks at 73 ($C_2H_3NO_2^+$), 88 ($C_3H_6NO_2^+$), 104 ($C_3H_6NO_3^+$), 145 ($C_5H_9N_2O_3^+$), 161 ($C_5H_9N_2O_4^+$), and 191 ($C_6H_{11}N_2O_5^+$) are fragment ions indicative of oligomer compounds. The mechanism describing the formation of these oligomer compounds is discussed in detail in Price et al. (2014). Briefly, oligomers are produced through peroxy radical chemistry ($RO_2\cdot$ + $RO_2\cdot$). The lower *m/z* peaks (< 59) at 29 (CHO^+), 30 (CH_2O^+, CH_4N^+), 44 (CO_2^+, CH_2NO^+), 45 (CH_3NO^+), and 58 ($C_2H_4NO^+$, $C_3H_8N^+$) are smaller aldehyde and amide fragment ions also expected from the oligomer compounds. Figure 4.6 shows one of the proposed oligomer compounds and possible fragmentation sites that explain the peaks observed in the mass spectra.

The organic mass spectrum at 10°C was plotted against the organic mass spectrum at 40°C to highlight the differences in the particle composition (Figure 4.7). The higher *m/z* fragments from the oligomer compounds are observed to have a slight temperature dependence. Oligomer formation increases after heating due to an increased availability of gas phase peroxy radical reactions. The *m/z* 76 ($C_2H_6NO_2^+$) and 122 ($C_3H_8NO_4^+$) peaks are significantly reduced by increasing temperature and return after cooling (Figure 4.8). A possible mechanism consistent with these two peaks is shown (Figure 4.9). The OH attack commences with a hydrogen abstraction from TMA to produce an alkyl radical followed by addition of molecular oxygen to form a peroxy radical. A 1,5 hydrogen rearrangement subsequently produces a hydroperoxide alkyl radical, which adds a molecular oxygen to form a hydroperoxide peroxy radical followed by another 1,5 hydrogen rearrangement to produce a di-hydroperoxide alkyl radical.

Addition of molecular oxygen forms the di-hydroperoxide peroxy radical that reacts with hydroperoxy radical to form a tri-hydroperoxide amine molecule. Electron impact ionization in the HR-ToF-MS provides the fragment ion at observed at *m/z* 122. A 1,4 hydrogen rearrangement with the loss of CH_2O_2 yields *m/z* 76. An additional 1,4 hydrogen rearrangement with the loss of CH_2O_2 yields *m/z* 30.

The HR-ToF-AMS mass spectra for the TMA + N_2O_5 experiments are presented (Figures 4.10 and 4.11). The lower *m/z* peaks (< 59) at 29 (CHO^+), 30 (CH_4N^+), 42 ($C_2H_4N^+$), 44 ($C_2H_6N^+$), and 58 ($C_3H_8N^+$) are fragments of the unoxidized parent amine. This is consistent with the fragmentation of trimethylammonium nitrate salt ($TMA{\cdot}HNO_3$). The significant nitrate peaks at m/z 30 (NO^+) and 46 (NO_2^+) also point to $TMA{\cdot}HNO_3$ formation. The higher *m/z* peaks (> 59) at 73 ($C_4H_{11}N^+$), 86 ($C_5H_{12}N^+$), 100 ($C_5H_8O_2^+$), 119 ($C_6HNO_2^+$), 133 ($C_4H_7NO_4^+$), 147 ($C_5H_9NO_4^+$), and 169 ($C_5HN_2O_5^+$) indicate that some additional oligomer chemistry is occurring. Both the salt and oligomers are volatile based on loss at 40°C.

The elemental analyses for the TMA experiments are shown (Figure 4.12). Highly oxidized aerosol is formed in the TMA + H_2O_2 experiments (oxygen to carbon, O/C > 0.5) with greater oxidation at higher temperatures. The hydrogen to carbon (H/C) ratio decreases at higher temperatures (2.0 → 1.8) as the O/C ratio increases (0.55 → 0.75), suggesting an increase in the number of carbonyl functional groups. The organic mass to organic carbon (OM/OC) ratio also increases at higher temperatures. The OM/OC ratio is very high (OM/OC up to 2.5), consistent with the formation of large oligomer compounds. Reduced amine aerosols are formed in the TMA + N_2O_5

experiments (O/C = 0, H/C = 2.7), consistent with the formation of $TMA \cdot HNO_3$, as elemental ratios are determined from only the organic portion of the aerosol.

4.3.3. Diethylamine aerosol – physical properties

Particle formation (not wall loss corrected) along with temperature profiles for the diethylamine (DEA) experiments are shown (Figure 4.13). The mass concentration drops for the two OH experiments when the environmental chamber temperature is warmed from 10°C to 40°C. The particles lost as the environmental chamber is warmed return after cooling the chamber back to its original temperature. Condensational particle growth and a secondary nucleation event occurred after cooling down the chamber to the original temperature in the cold start OH oxidation experiment. Particle nucleation only occurs in the hot start (~40°C) OH oxidation experiment after cooling down the chamber. The amount of aerosol produced after cooling down the chamber in the two OH oxidation experiments are similar (6 and 5 $\mu g/m^3$, respectively). No oligomerization was observed.

Large particle nucleation occurs in the cold start NO_3 oxidation experiment (Figure 4.13). However, these particles, unlike the TMA + NO_3 oxidation generated particles, are not completely lost with increasing temperature. A slight increase in mass concentration occurs after cooling the chamber back to the original temperature. This suggests the formation of an amine nitrate aerosol with a lower volatility than for the TMA + NO_3 or DEA + OH experiments. The particles had difficulty forming at the beginning of the hot start NO_3 oxidation experiment relative to the cold start experiment. Particle mass concentration increased due to condensational growth after cooling the

chamber. The aerosol formation was much higher in the NO_3 than the OH oxidation experiments. The overall aerosol formation was greatest in the cold start experiments.

The density profiles for the DEA experiments are shown (Figure 4.14). Density decreases during increasing temperature for the OH experiments and conversely increases as the temperature decreases. The density increases as the temperature decreases. The high density and extent of temperature change suggests an instrumental bias due to heating of the cold air as it travels between the APM and SMPS leading to smaller diameter particles than present during particle mass selection. This is consistent with an aerosol with high volatility consistent with VTDMA measurements. The first few hours of volatility measurements in the hot start OH experiment were not available due to an instrument issue. There does not appear to be a change in density with temperature change in the NO_3 experiments. However, the density is slightly lower for the hot start NO_3 oxidation aerosol than for the cold start aerosol (1.1 vs. 1.3 g/cm^3). Overall, the density is higher in the OH experiments.

The volatility profiles for the DEA experiments are shown (Figure 4.15). Overall, the volatility behavior at 40°C is comparable to that of the TMA experiments. In the OH experiments, VFR increases as expected to near unity as the enclosure temperature approaches that of the thermodenuder temperature. The VFR returns to around 0.7 after cooling the chamber again. The first few hours of volatility measurements in the hot start OH experiment were not available due to an instrument issue. Highly volatile aerosol formed in the cold start NO_3 experiment consistent with the formation of amine salt

aerosol. The instrument was not available for the hot start NO_3 experiment. There appears to be no change in volatility with changing temperature.

4.3.4. Diethylamine aerosol – chemical composition

The HR-ToF-AMS mass spectra (linear scale) for the DEA + OH experiments are presented (Figures 4.16 and 4.17). The vast majority of ionized fragments from the volatilized (600°C) aerosol was in the lower *m/z* range (< *m/z* of the precursor amine, DEA = 73 amu). The lower *m/z* peaks (≤ 73) at 30 (CH_4N^+, CH_2O^+), 44 (CO_2^+, $C_2H_6N^+$), 58 ($C_3H_8N^+$, $C_3H_6O^+$), and 73 ($C_3H_5O_2^+$, $C_4H_{11}N^+$) are a mixture of fragments from amine and oxidized hydrocarbon aerosol. The lower *m/z* peaks (< 73) at 15 (CH_3^+), 29 (CHO^+, $C_2H_5^+$), 43 ($C_2H_3O^+$, $C_3H_7^+$), 55 ($C_3H_3O^+$, $C_4H_7^+$), and 69 ($C_4H_5O^+$, $C_5H_9^+$) are fragments of hydrocarbon aerosol. The higher *m/z* peak (> 73) at 86 ($C_4H_8NO^+$) is the fragment of an oxidized parent amine molecule. The C3 – C5 hydrocarbon fragments suggest that some type of addition chemistry is occurring, as C2 is the largest hydrocarbon chain on DEA. Amine type peaks (e.g., *m/z* 58) dominate during cold temperatures (10°C) while hydrocarbon peaks (e.g., *m/z* 55 and 69) are the more significant peaks at the hot temperatures (40°C). Both amine and hydrocarbon peaks are observed after the chamber returns to the original temperature.

The HR-ToF-AMS mass spectra (linear scale) for the DEA + NO_3 experiments are presented (Figures 4.18 and 4.19). The lower *m/z* peaks (≤ 73) at 15 (CH_3^+), 30 (CH_4N^+), 44 ($C_2H_6N^+$), 58 ($C_3H_8N^+$), and 73 ($C_4H_{11}N^+$) are fragments of the unoxidized parent amine, consistent with the fragmentation of diethylammonium nitrate salt

($DEA \cdot HNO_3$). The significant nitrate peaks at m/z 30 (NO^+) and 46 (NO_2^+) also support $DEA \cdot HNO_3$ formation. No oligomer formation is observed in the mass spectra for the DEA + NO_3 experiments. Nor does chemical composition change with temperature, consistent with the observations for aerosol density and volatility.

The elemental analyses for the DEA experiments are shown (Figure 4.20). Oxidized aerosol is formed in the DEA + OH experiments (O/C = 0.30) with slightly higher oxidation at the highest chamber temperatures. Reduced aerosol was formed in the DEA + NO_3 experiments (O/C = 0.03, H/C = 2.90, N/C = 0.48), consistent with the formation of $DEA \cdot HNO_3$. No change in elemental ratio is observed with changes in temperature.

4.3.5. Butylamine aerosol – physical properties

Particle formation (not wall loss corrected) along with temperature profiles for the butylamine (BA) experiments are shown (Figure 4.21). Unlike the TMA and DEA plus OH oxidation experiments, particle concentration increases with increasing temperature in the cold start OH oxidation experiment. Particle condensation occurred after cooling the chamber back to the original temperature. Particle nucleation occurred before the start of photooxidation in the hot start OH oxidation experiment. Particle mass concentration increased due to condensational growth after cooling down the chamber. The amount of aerosol produced after cooling down the chamber in the two OH oxidation experiments are similar (7 and 11 $\mu g/m^3$, respectively). No oligomerization was observed.

The overall trends in the BA + NO_3 oxidation experiments were similar to those observed in the TMA and DEA + NO_3 oxidation experiments. Rapid particle growth occurs in the cold start NO_3 oxidation experiment. These particles completely partition to the gas phase as temperature increases past 35°C, consistent with the formation of amine nitrate salts. The particles lost after heating the chamber do not return after cooling. The particles had difficulty forming in the hot start NO_3 oxidation experiment relative to the cold start experiment. Particle mass concentration increased due to condensational growth after cooling the chamber. Aerosol formation was much higher in the NO_3 oxidation experiments. About 30-50% less BA and oxidant were injected in the cold start NO_3 oxidation experiment due to an issue with the injection system. Therefore, the aerosol formation was lower than in the hot start NO_3 experiment.

The density profiles for the BA experiments are shown in (Figure 4.22). A gradual decrease in aerosol density is observed over the course of the cold start OH experiment. A slight drop in density is observed after cooling the chamber in the hot start OH experiment. Further, a slight drop in density occurs as temperature increases in the cold start NO_3 experiment. Most of the BA + NO_3 particles are lost at high temperatures, resulting in the greater scatter in density values (Figure 4.22). The spike in density after cooling the chamber is due to the instrumentation bias discussed in the DEA density section. There is no change in density during temperature change for the aerosol formed in the hot start NO_3 experiment.

Overall, the volatility behavior is comparable to that of the TMA and DEA experiments (Figure 4.23). Measured VFR increases toward unity as expected as the

enclosure temperature approaches the thermodenuder temperature. A slight decrease in VFR to 0.73 is observed after cooling the chamber. Overall, the trend shows increasing VFR (decreasing volatility) over time. Highly volatile aerosol (VFR < 0.20) formed during the cold start NO_3 experiment, consistent with the formation of amine salt aerosol. The chamber particles were lost at higher temperatures. The VFR did not increase after heating the chamber, suggesting that the aerosol was mainly composed of amine salts. Less volatile aerosol was produced in the hot start NO_3 experiment. Volatility gradually decreases over the course of the hot start NO_3 experiment.

4.3.6. Butylamine aerosol – chemical composition

The HR-ToF-AMS mass spectra (linear scale) for the BA + OH experiments are presented (Figures 4.24 and 4.25). Most of the *m/z* fragments from the vaporized and ionized aerosol are in the lower *m/z* range (< *m/z* of the precursor amine, BA = 73 amu). The lower *m/z* peaks (< 73) at 30 (CH_4N^+, CH_2O^+), 44 (CO_2^+, $C_2H_6N^+$), 58 ($C_3H_8N^+$, $C_3H_6O^+$), and 72 ($C_4H_{10}N^+$, $C_4H_8O^+$) are a mixture of fragments from amine and oxidized hydrocarbon aerosol. The lower *m/z* peaks (< 73) at 15 (CH_3^+), 29 (CHO^+, $C_2H_5^+$), 41 ($C_3H_5^+$), 43 ($C_2H_3O^+$, $C_3H_7^+$), and 55 ($C_3H_3O^+$, $C_4H_7^+$) are fragments of hydrocarbon aerosol. There were no significant higher mass peaks, suggesting no oligomer formation. All of the lower mass peaks can be explained through fragmentation of the oxidized products of the precursor amine. There was little to no change in composition with temperature change.

Because of the large particle nucleation that occurred before the start of photooxidation in the hot start OH experiment, the initial aerosol was highly reduced. Significant nitrate peak signal (30, 46) indicates the formation of amine salts. The lower *m/z* peaks (≤ 73) at 30 (CH_4N^+), 44 ($C_2H_6N^+$), 58 ($C_3H_8N^+$), and 73 ($C_4H_{11}N^+$) are consistent with the fragmentation of butylammonium nitrate salt ($BA{\cdot}HNO_3$). This could possibly be due to a small HNO_3 background at the start of the experiment. The aerosol formed after cooling the chamber is more oxidized than the aerosol formed at 40°C.

The HR-ToF-AMS mass spectra (linear scale) for the BA + NO_3 experiments are presented (Figures 4.26 and 4.27). The lower *m/z* peaks (≤ 73) at 15 (CH_3^+), 30 (CH_4N^+), 44 ($C_2H_6N^+$), 58 ($C_3H_8N^+$), and 73 ($C_4H_{11}N^+$) are fragments of the unoxidized parent amine. This is consistent with the fragmentation of butylammonium nitrate salt ($BA{\cdot}HNO_3$). The significant nitrate peaks at *m/z* 30 (NO^+) and 46 (NO_2^+) also support $BA{\cdot}HNO_3$ formation. No oligomer formation is observed for the BA + NO_3 experiments. Further, no change in composition is observed with temperature change. Though the particles completely partition to the gas phase after heating the chamber in the cold start NO_3 experiment, the mass spectra suggests that a very small amount of particles return after cooling the chamber.

The elemental analyses for the BA experiments are shown (Figure 4.28). Oxidized aerosol is formed in the BA + OH experiments (O/C = 0.30). The elemental ratios further confirm that $BA{\cdot}HNO_3$ was formed at the beginning of the hot start OH experiment due to reaction with trace HNO_3 contamination. It appears that the amine salt aerosol is lost at the high temperature and the aerosol becomes more oxidized after

cooling the chamber. Reduced aerosol was formed in the BA + NO_3 experiments (O/C = 0.02, H/C = 3.00, N/C = 0.55), consistent with the formation of BA·HNO_3. Most of the particles are lost with increasing temperature in the cold start NO_3 experiment. However, a small amount of less volatile, and slightly more oxidized aerosol remains. No change in elemental ratio with temperature change is observed in the hot start NO_3 experiment. The N/C ratio is higher in the BA + NO_3 experiments compared to the other amines (BA = 0.55, DEA = 0.45, TMA = 0.35). This could be due to the formation of ammonium nitrate, which has been observed in previous studies (Tang et al., 2013).

4.4. Conclusion

Temperature had a significant effect on aerosol formed from aliphatic amine precursors. The nucleation temperature is an important factor influencing the overall chemical composition of the aged aerosol, especially as the aerosol experiences temperature gradients. In general, more aerosol is formed at colder temperatures. This has important implications for locations influenced by amine emissions during the winter months. The aerosol formed in the TMA + OH oxidation experiments supports the oligomer mechanism discussed in previous work (Price et al., 2014). The formation of highly temperature dependent hydroperoxide amine compounds at cold temperatures confirms that $RO_2\cdot$ + $HO_2\cdot$ chemistry occurs significantly in addition to the $RO_2\cdot$ + $RO_2\cdot$ chemistry that leads to oligomer aerosol. Peroxy radical chemistry is an important contributor to aerosol formation during the daylight hours. The aerosol formed in the NO_3 oxidation experiments consists mainly of amine nitrate salts. The extent of amine

salt formation is highly dependent on temperature. Amine nitrate salts are an important contributor to aerosol formation during the nighttime hours, when temperatures tend to be cooler.

4.5. References

Barsanti, K.C., McMurry, P.H., Smith, J.N., 2009. The potential contribution of organic salts to new particle growth. Atmos Chem Phys 9, 2949-2957.

Borduas, N., Abbatt, J.P.D., Murphy, J.G., 2013. Gas Phase Oxidation of Monoethanolamine (MEA) with OH Radical and Ozone: Kinetics, Products, and Particles. Environ Sci Technol 47, 6377-6383.

Cadle, S.H., Mulawa, P.A., 1980. Low-Molecular Weight Aliphatic-Amines in Exhaust from Catalyst-Equipped Cars. Environ Sci Technol 14, 718-723.

Carter, W.P.L., Cocker, D.R., III, Fitz, D.R., Malkina, I.L., Bumiller, K., Sauer, C.G., Pisano, J.T., Bufalino, C., Song, C., 2005. A new environmental chamber for evaluation of gas-phase chemical mechanisms and secondary aerosol formation. Atmos Environ 39, 7768-7788.

Cocker, D.R., Flagan, R.C., Seinfeld, J.H., 2001. State-of-the-art chamber facility for studying atmospheric aerosol chemistry. Environ Sci Technol 35, 2594-2601.

DeCarlo, P.F., Kimmel, J.R., Trimborn, A., Northway, M.J., Jayne, J.T., Aiken, A.C., Gonin, M., Fuhrer, K., Horvath, T., Docherty, K.S., Worsnop, D.R., Jimenez, J.L., 2006. Field-deployable, high-resolution, time-of-flight aerosol mass spectrometer. Analytical Chemistry 78, 8281-8289.

Dockery, D.W., 2009. Health Effects of Particulate Air Pollution. Annals of Epidemiology 19, 257-263.

Ehara, K., Hagwood, C., Coakley, K.J., 1996. Novel method to classify aerosol particles according to their mass-to-charge ratio - Aerosol particle mass analyser. J Aerosol Sci 27, 217-234.

Ge, X., Wexler, A.S., Clegg, S.L., 2011. Atmospheric Amines – Part I, A Review. Atmos Environ 45, 524-546.

IPCC, 2013. Climate change 2013: The physical science basis. Contribution of working group I to the fifth assessment report of the Intergovernmental Panel on Climate Change [Stocker, T.F., D. Qin, G.-K. Plattner, M. Tignor, S.K. Allen, J. Boschung, A. Nauels, Y. Xia, V. Bex and P.M. Midgley (eds.)]. Cambridge University Press, Cambridge, United Kingdom and New York, NY, USA, p. 1535 pp.

Jayne, J.T., Leard, D.C., Zhang, X.F., Davidovits, P., Smith, K.A., Kolb, C.E., Worsnop, D.R., 2000. Development of an aerosol mass spectrometer for size and composition analysis of submicron particles. Aerosol Sci Tech 33, 49-70.

Lee, D., Wexler, A.S., 2013. Atmospheric amines - Part III: Photochemistry and toxicity. Atmos Environ 71, 95-103.

Malloy, Q.G.J., Li, Q., Warren, B., Cocker, D.R., III, Erupe, M.E., Silva, P.J., 2009a. Secondary organic aerosol formation from primary aliphatic amines with NO3 radical. Atmos Chem Phys 9, 2051-2060.

Malloy, Q.G.J., Nakao, S., Qi, L., Austin, R., Stothers, C., Hagino, H., Cocker, D.R., 2009b. Real-Time Aerosol Density Determination Utilizing a Modified Scanning Mobility Particle SizerAerosol Particle Mass Analyzer System. Aerosol Sci Tech 43, 673-678.

Mosier, A.R., Andre, C.E., Viets, F.G., Jr., 1973. Identification of Aliphatic Amines Volatilized from Cattle Feedyard. Environ Sci Technol 7, 642-644.

Pope, C.A., Thun, M.J., Namboodiri, M.M., Dockery, D.W., Evans, J.S., Speizer, F.E., Heath, C.W., 1995. Particulate Air-Pollution as a Predictor of Mortality in a Prospective-Study of Us Adults. American Journal of Respiratory and Critical Care Medicine 151, 669-674.

Price, D.J., Clark, C.H., Tang, X.C., Cocker, D.R., Purvis-Roberts, K.L., Silva, P.J., 2014. Proposed chemical mechanisms leading to secondary organic aerosol in the reactions of aliphatic amines with hydroxyl and nitrate radicals. Atmos Environ 96, 135-144.

Qi, L., Nakao, S., Tang, P., Cocker, D.R., 2010. Temperature effect on physical and chemical properties of secondary organic aerosol from m-xylene photooxidation. Atmos Chem Phys 10, 3847-3854.

Silva, P.J., Erupe, M.E., Price, D.J., Elias, J., Malloy, Q.G.J., Li, Q., Warren, B., Cocker, D.R., III, 2008. Trimethylamine as precursor to secondary organic aerosol formation via nitrate radical reaction in the atmosphere. Environ Sci Technol 42, 4689-4696.

Smith, J.N., Dunn, M.J., VanReken, T.M., Iida, K., Stolzenburg, M.R., McMurry, P.H., Huey, L.G., 2008. Chemical composition of atmospheric nanoparticles formed from nucleation in Tecamac, Mexico: Evidence for an important role for organic species in nanoparticle growth. Geophys Res Lett 35.

Tang, X.C., Price, D., Praske, E., Lee, S.A., Shattuck, M.A., Purvis-Roberts, K., Silva, P.J., Asa-Awuku, A., Cocker, D.R., 2013. NO3 radical, OH radical and O-3-initiated secondary aerosol formation from aliphatic amines. Atmos Environ 72, 105-112.

Warren, B., Austin, R.L., Cocker, D.R., 2009. Temperature dependence of secondary organic aerosol. Atmos Environ 43, 3548-3555.

Watson, J.G., 2002. Visibility: Science and regulation. J Air Waste Manage 52, 628-713.

Westerholm, R., Li, H., Almen, J., 1993. Estimation of Aliphatic Amine Emissions in Automobile Exhausts. Chemosphere 27, 1381-1384.

4.6 Tables

Table 4.1. Environmental chamber experiments.

Amine	Structure	Temperature gradient	[Amine] ppb	Oxidant	[Oxidant] ppb
TMA	$(CH_3)_3N$	10°C - 40°C - 10°C	100	H_2O_2 (OH)	1000
TMA	$(CH_3)_3N$	40°C - 10°C -40°C	100	H_2O_2 (OH)	1000
TMA	$(CH_3)_3N$	10°C - 40°C - 10°C	100	N_2O_5 (NO_3)	215
TMA	$(CH_3)_3N$	40°C - 10°C -40°C	100	N_2O_5 (NO_3)	400
DEA	$(CH_3CH_2)_2NH$	10°C - 40°C - 10°C	100	H_2O_2 (OH)	1000
DEA	$(CH_3CH_2)_2NH$	40°C - 10°C -40°C	100	H_2O_2 (OH)	1000
DEA	$(CH_3CH_2)_2NH$	10°C - 40°C - 10°C	100	N_2O_5 (NO_3)	140
DEA	$(CH_3CH_2)_2NH$	40°C - 10°C -40°C	100	N_2O_5 (NO_3)	350
BA	$CH_3(CH_2)_3NH_2$	10°C - 40°C - 10°C	100	H_2O_2 (OH)	1000
BA	$CH_3(CH_2)_3NH_2$	40°C - 10°C -40°C	100	H_2O_2 (OH)	1000
BA	$CH_3(CH_2)_3NH_2$	10°C - 40°C - 10°C	<100	N_2O_5 (NO_3)	<345
BA	$CH_3(CH_2)_3NH_2$	40°C - 10°C -40°C	100	N_2O_5 (NO_3)	345

4.7 Figures

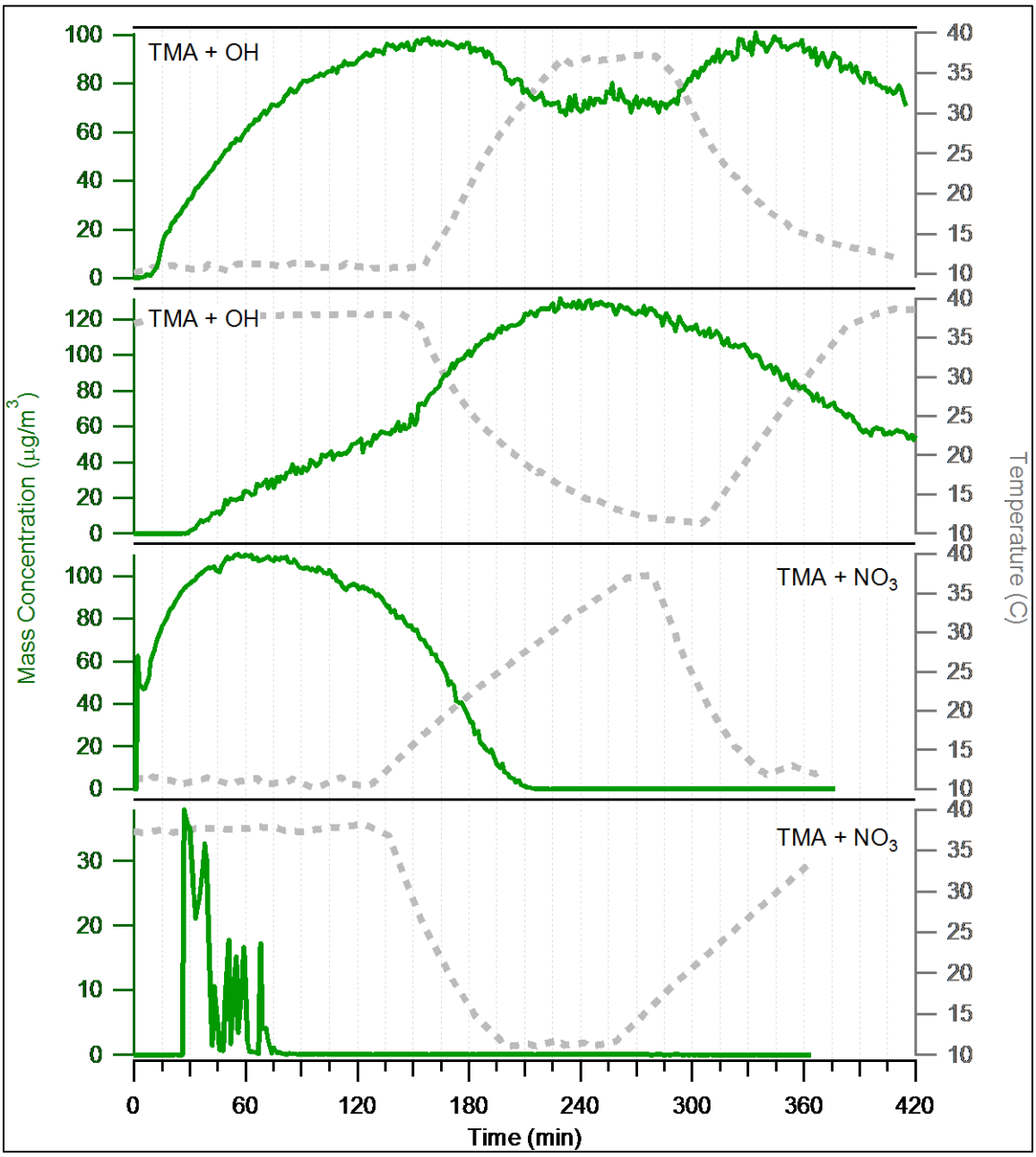

Figure 4.1. Mass concentration and temperature profiles for the trimethylamine oxidation experiments.

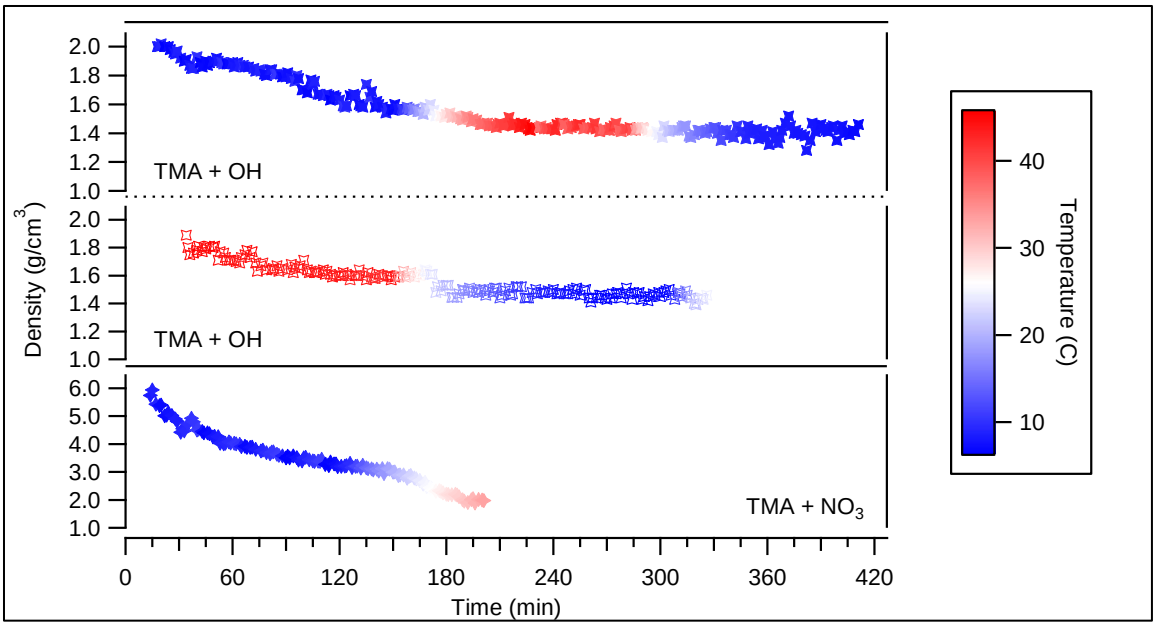

Figure 4.2. Density profiles for the aerosol produced in the trimethylamine oxidation experiments.

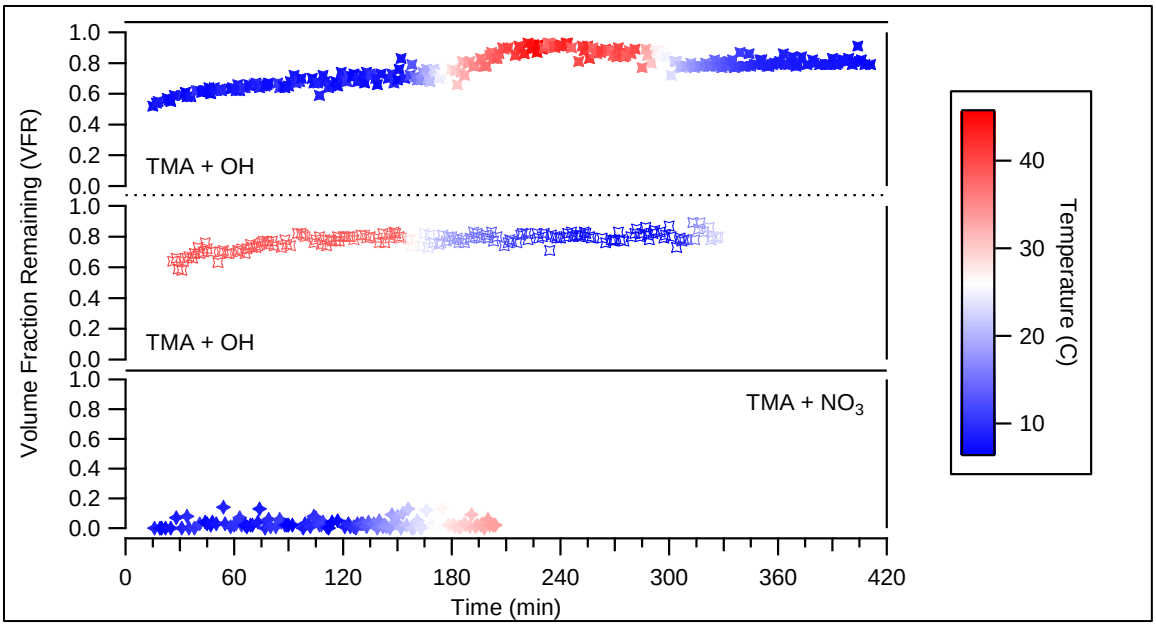

Figure 4.3. The volatility profiles for the aerosol produced in the trimethylamine oxidation experiments.

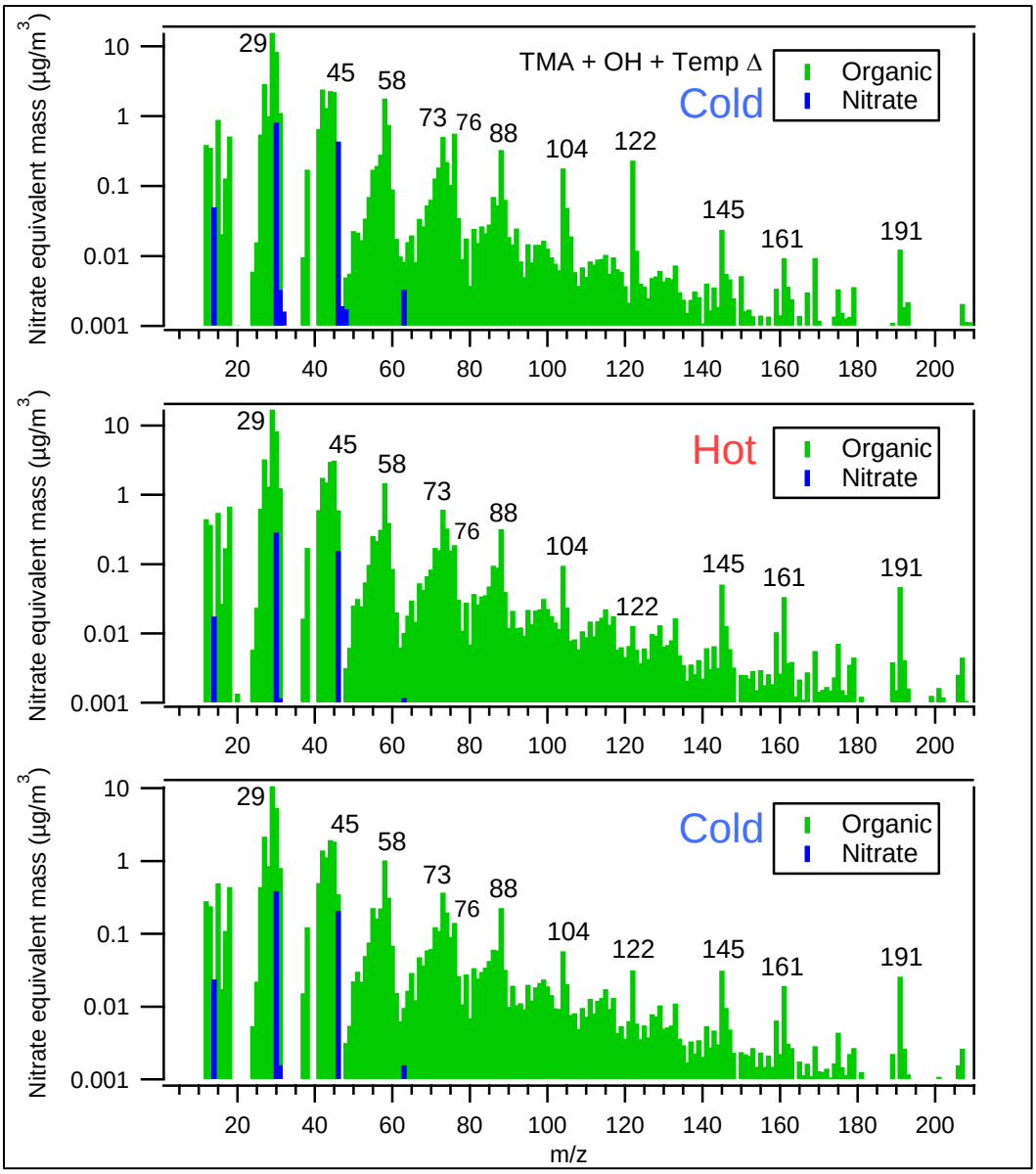

Figure 4.4. HR-ToF-AMS mass spectra from the cold start trimethylamine with OH oxidation experiment.

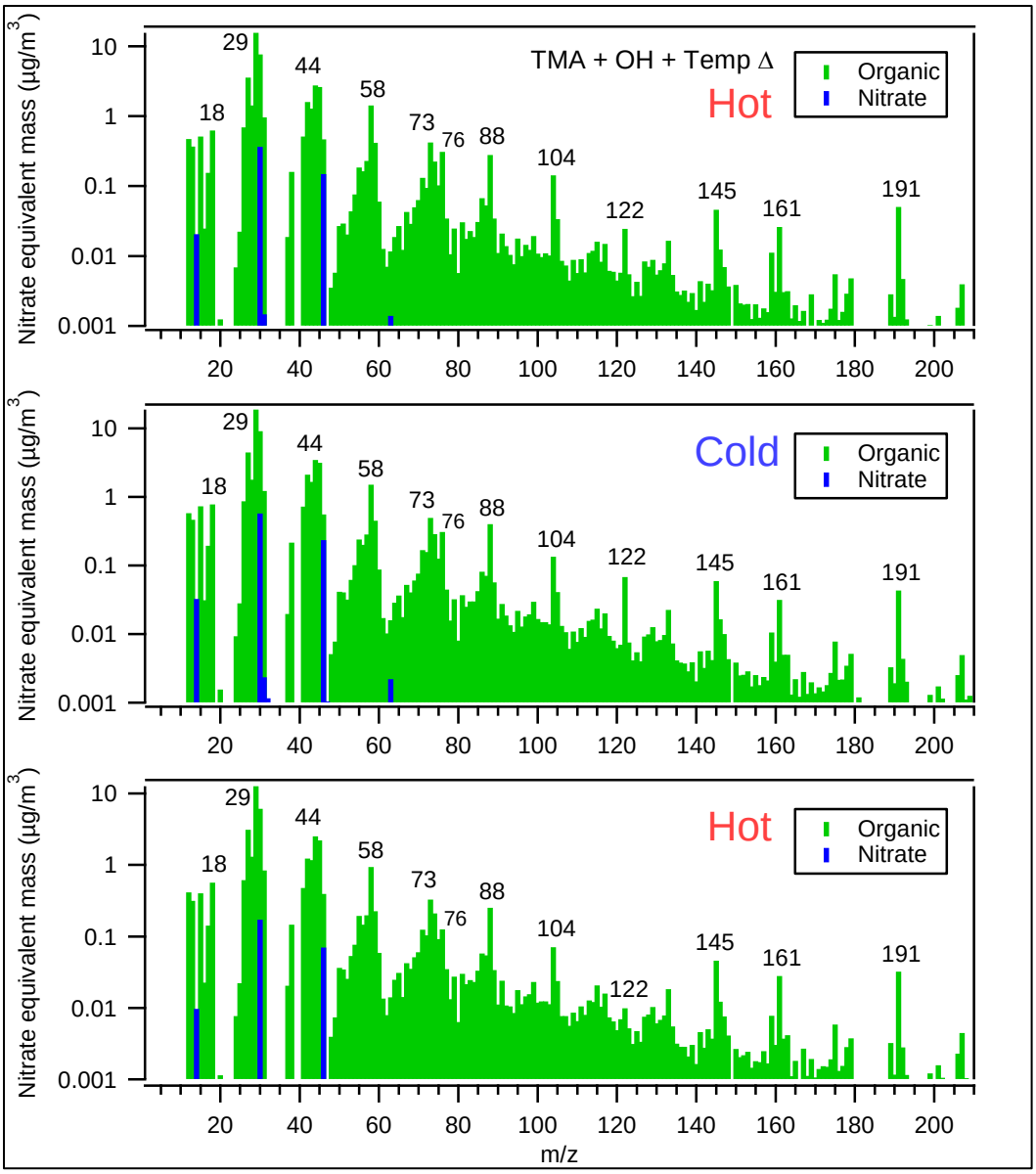

Figure 4.5. HR-ToF-AMS mass spectra from the hot start trimethylamine with OH oxidation experiment.

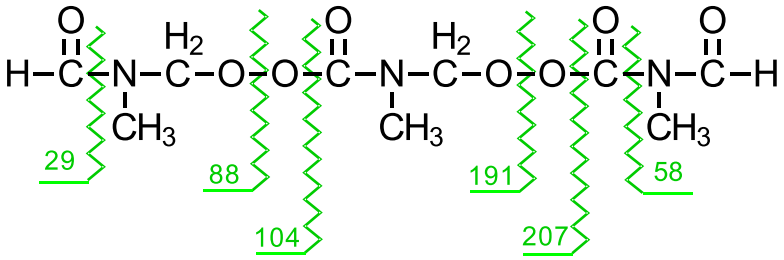

Figure 4.6. Proposed oligomer compound with possible ion fragmentation sites.

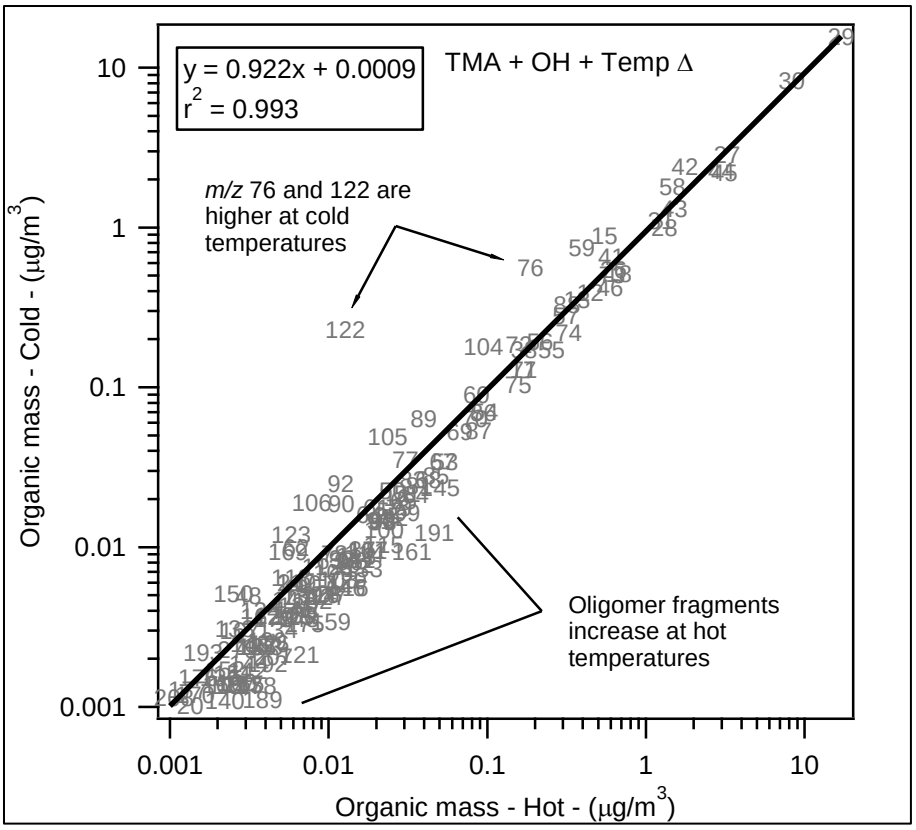

Figure 4.7. Correlation plot of the organic mass spectra (cold vs hot) from the TMA + OH oxidation experiment.

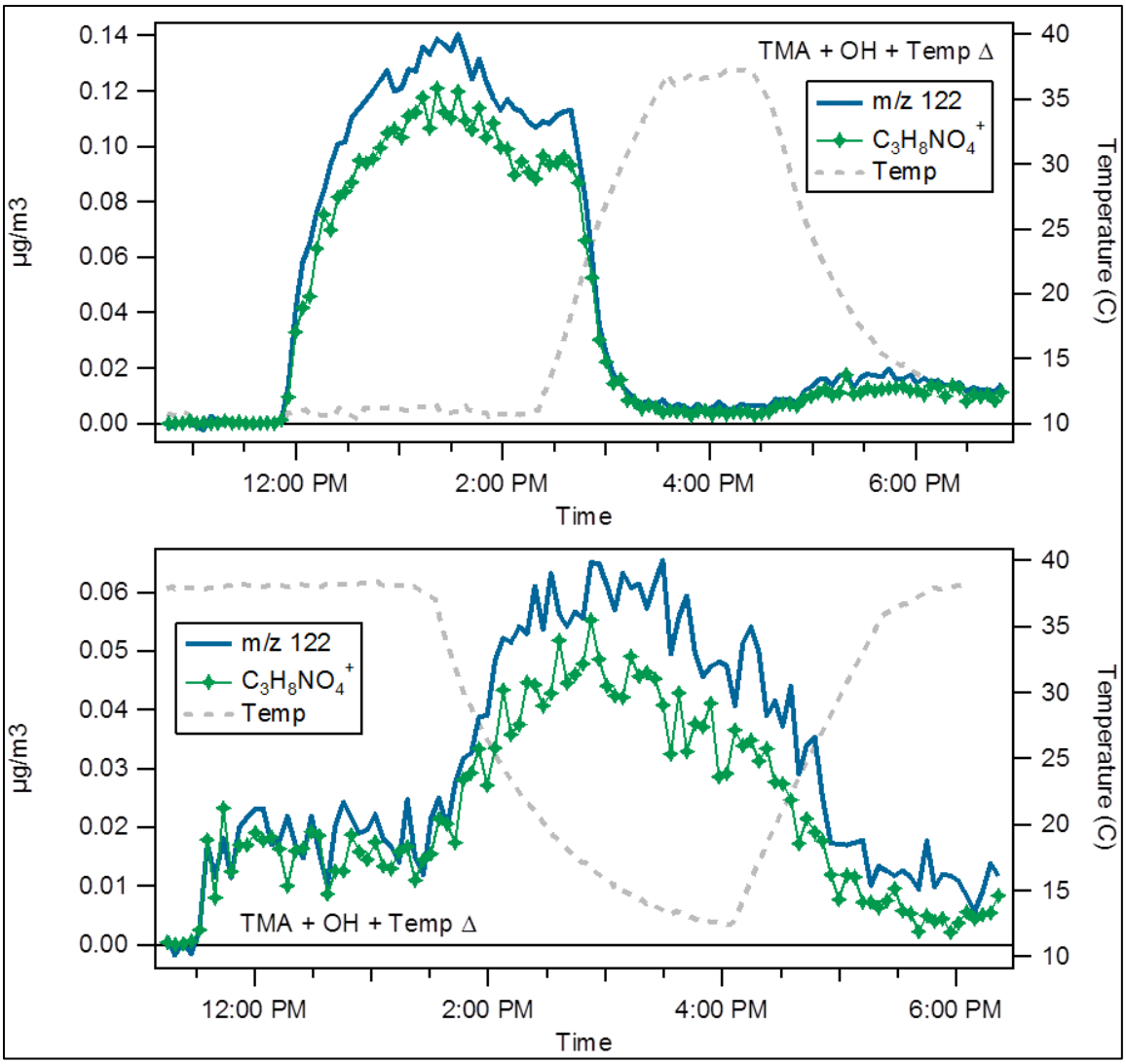

Figure 4.8. Time profiles for *m/z* 122 in the cold start (top) and hot start (bottom) trimethylamine with OH oxidation experiments.

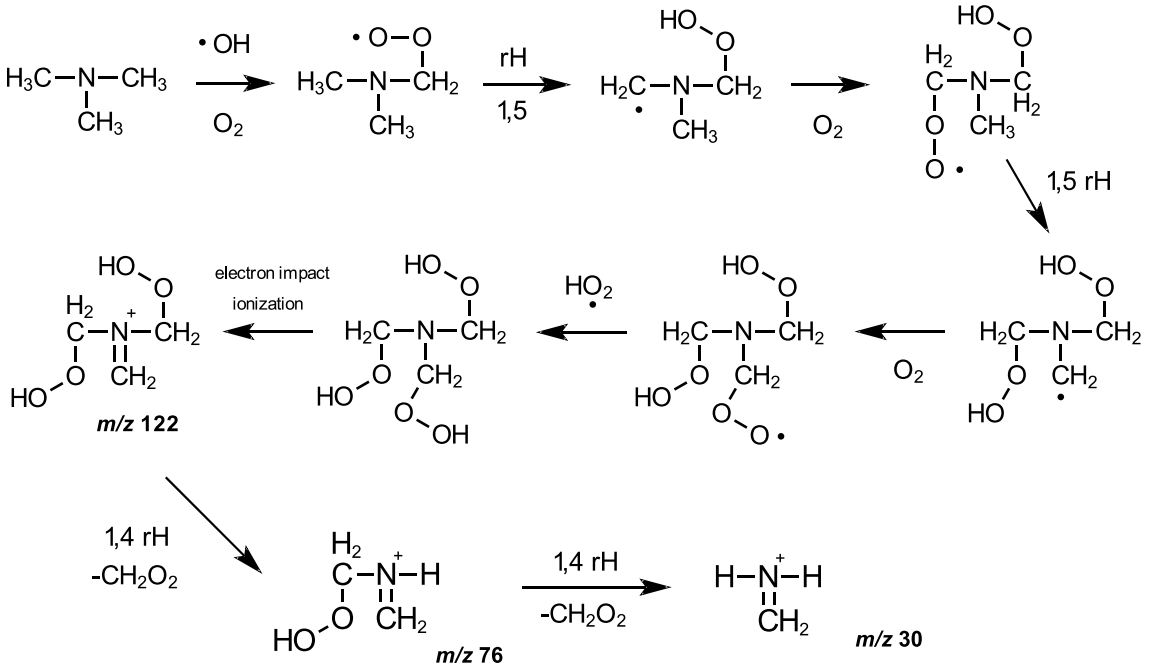

Figure 4.9. Proposed mechanism for the formation of temperature dependent aerosol with *m/z* 76 and *m/z* 122 observed by the HR-ToF-AMS.

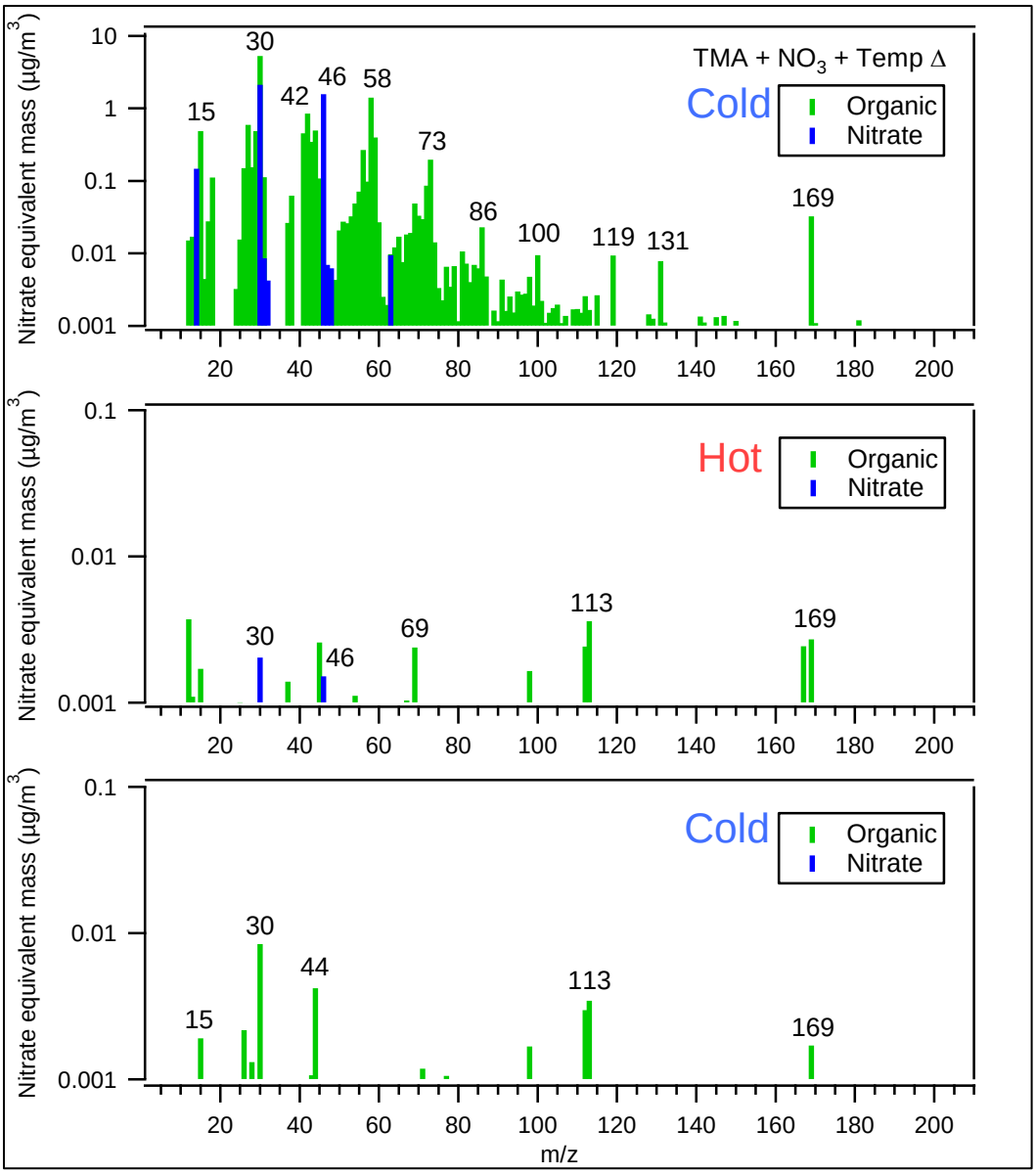

Figure 4.10. HR-ToF-AMS mass spectra from the cold start trimethylamine with NO_3 oxidation experiment.

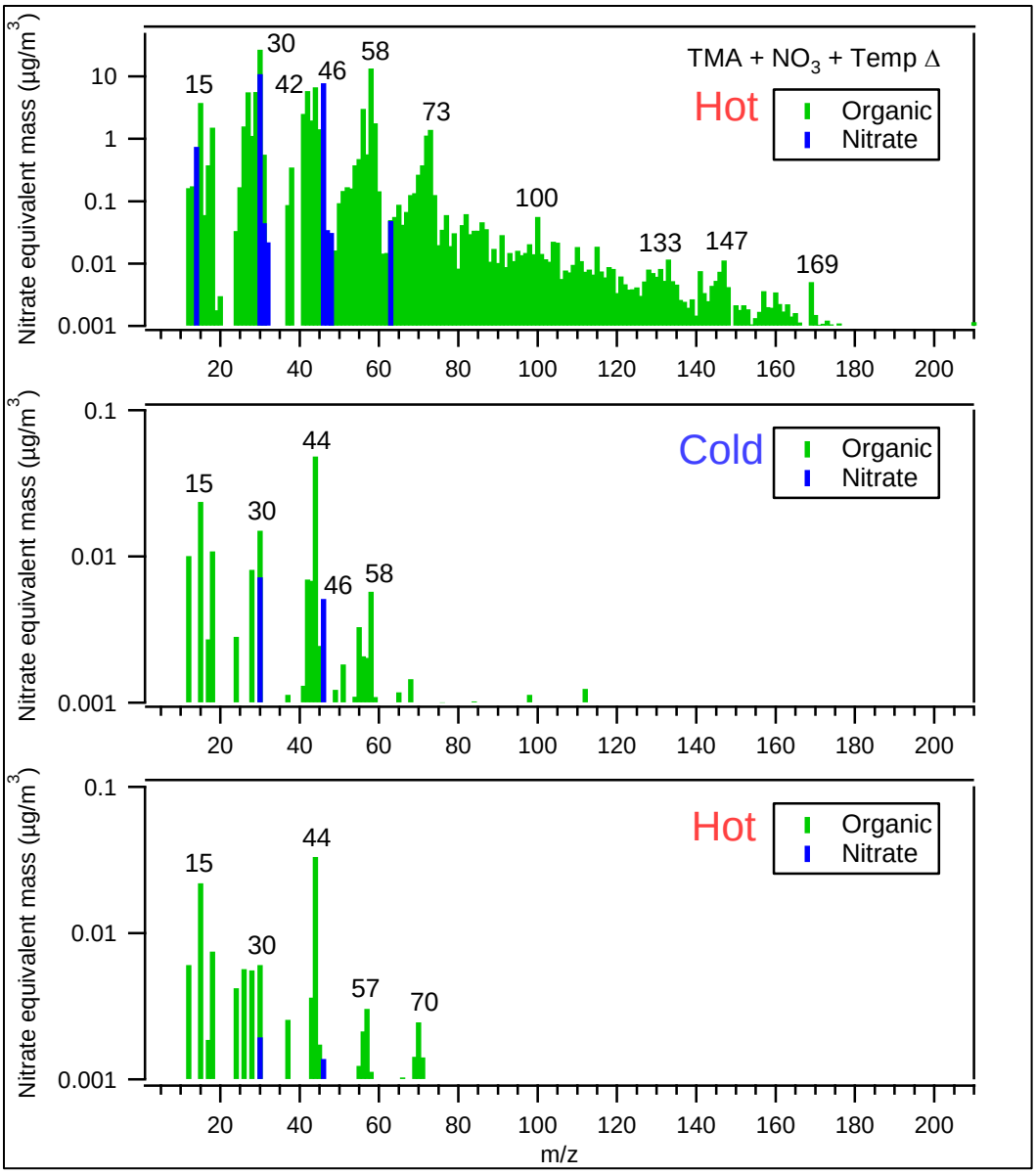

Figure 4.11. HR-ToF-AMS mass spectra from the hot start trimethylamine with NO_3 oxidation experiment.

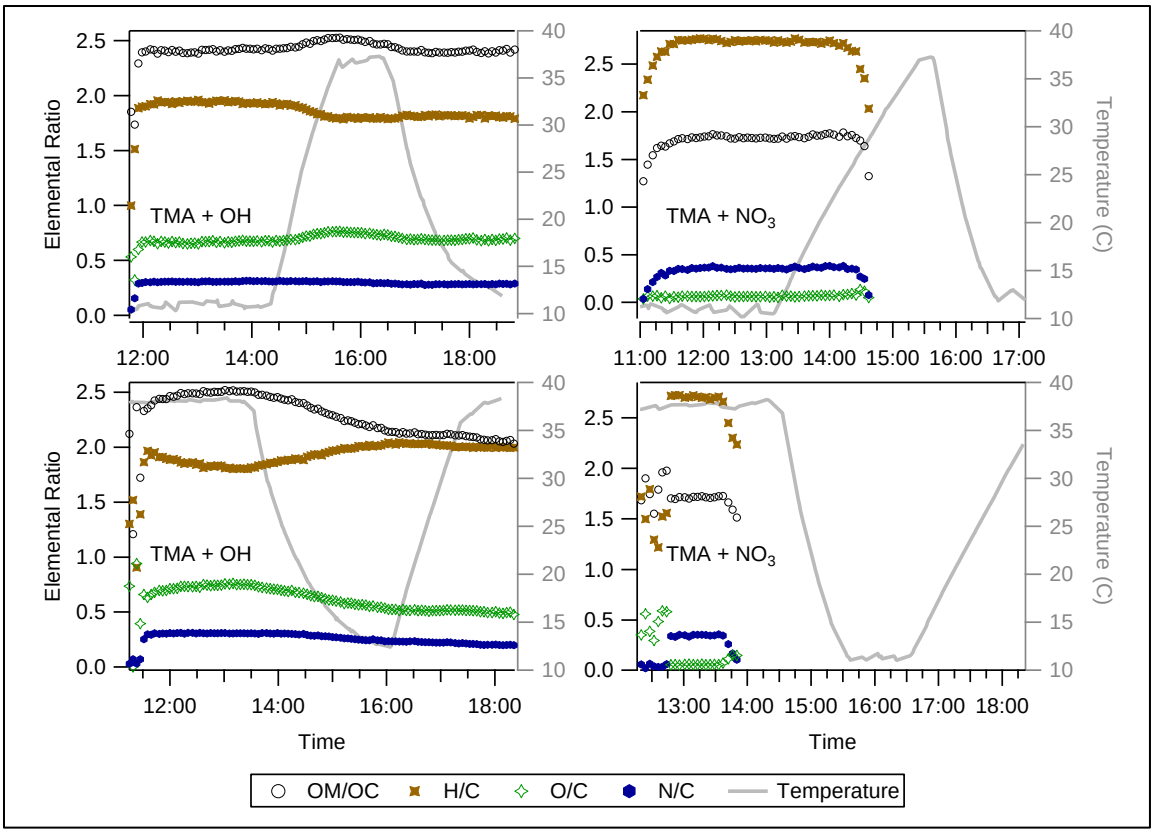

Figure 4.12. The elemental analysis for the aerosol formed in the trimethylamine oxidation experiments.

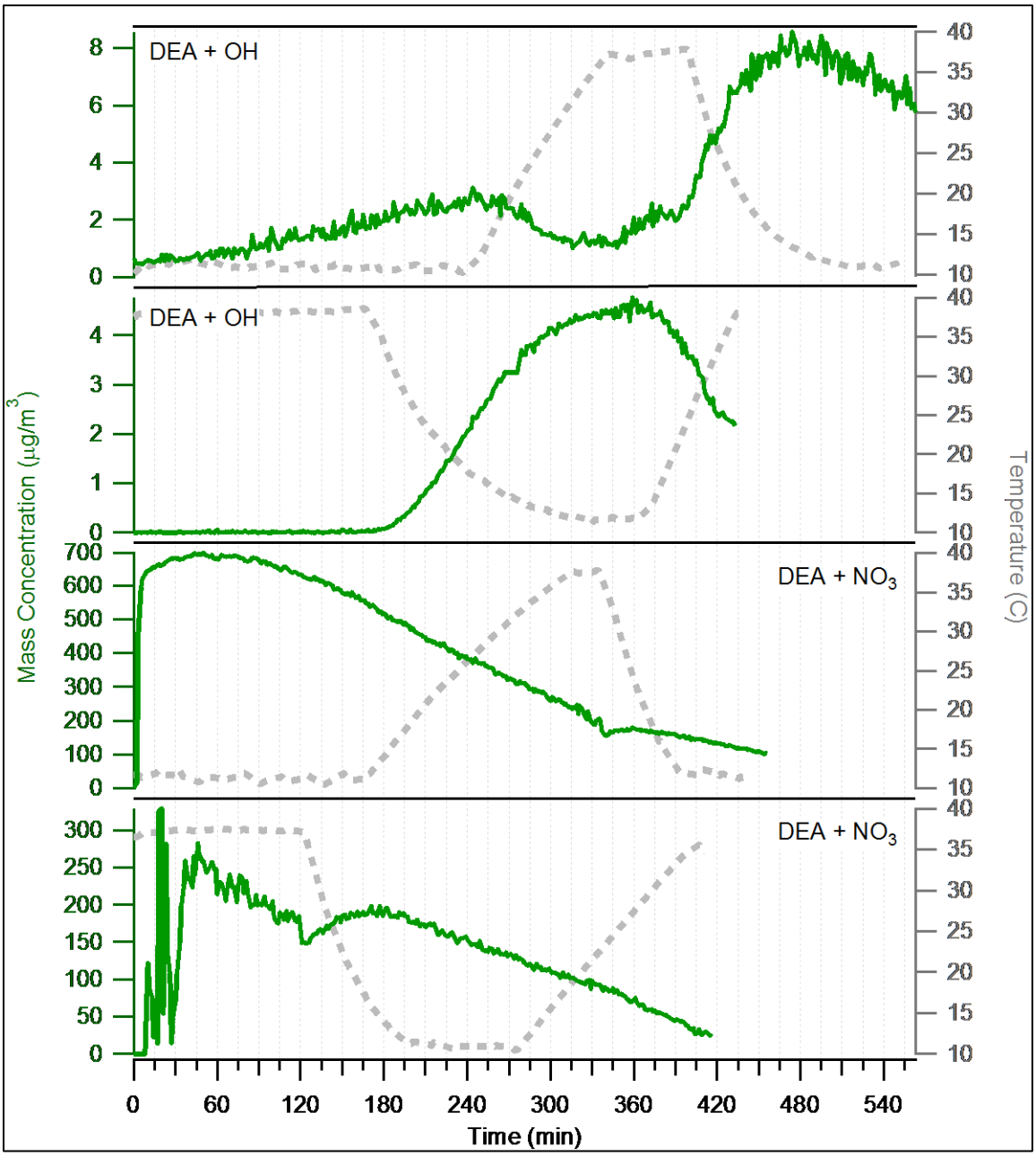

Figure 4.13. Mass concentration and temperature profiles for the diethylamine oxidation experiments.

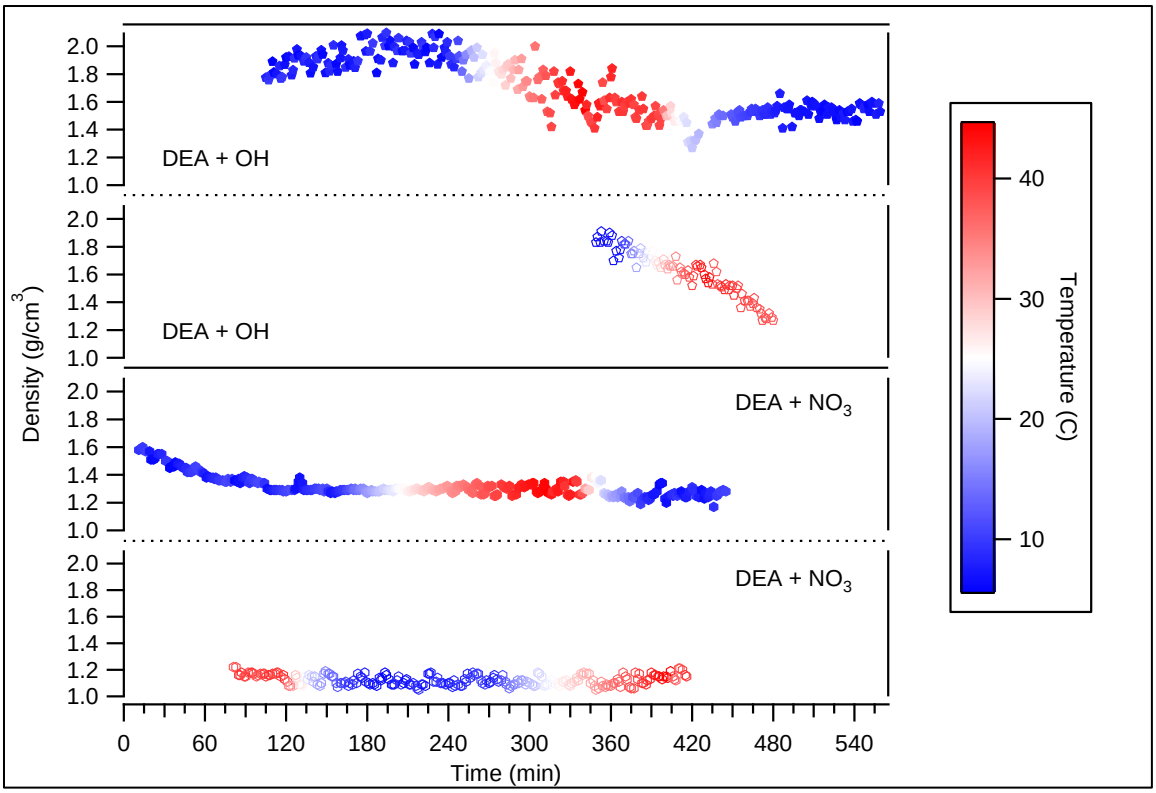

Figure 4.14. Density profiles for the aerosol produced in the diethylamine oxidation experiments.

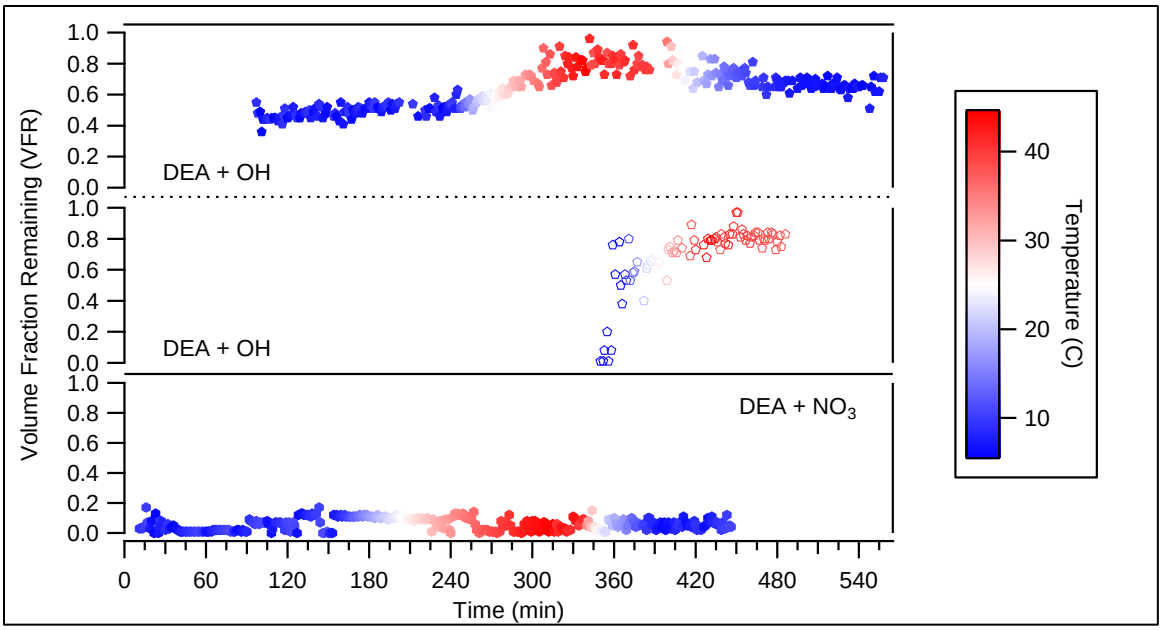

Figure 4.15. The volatility profiles for the aerosol produced in the diethylamine oxidation experiments.

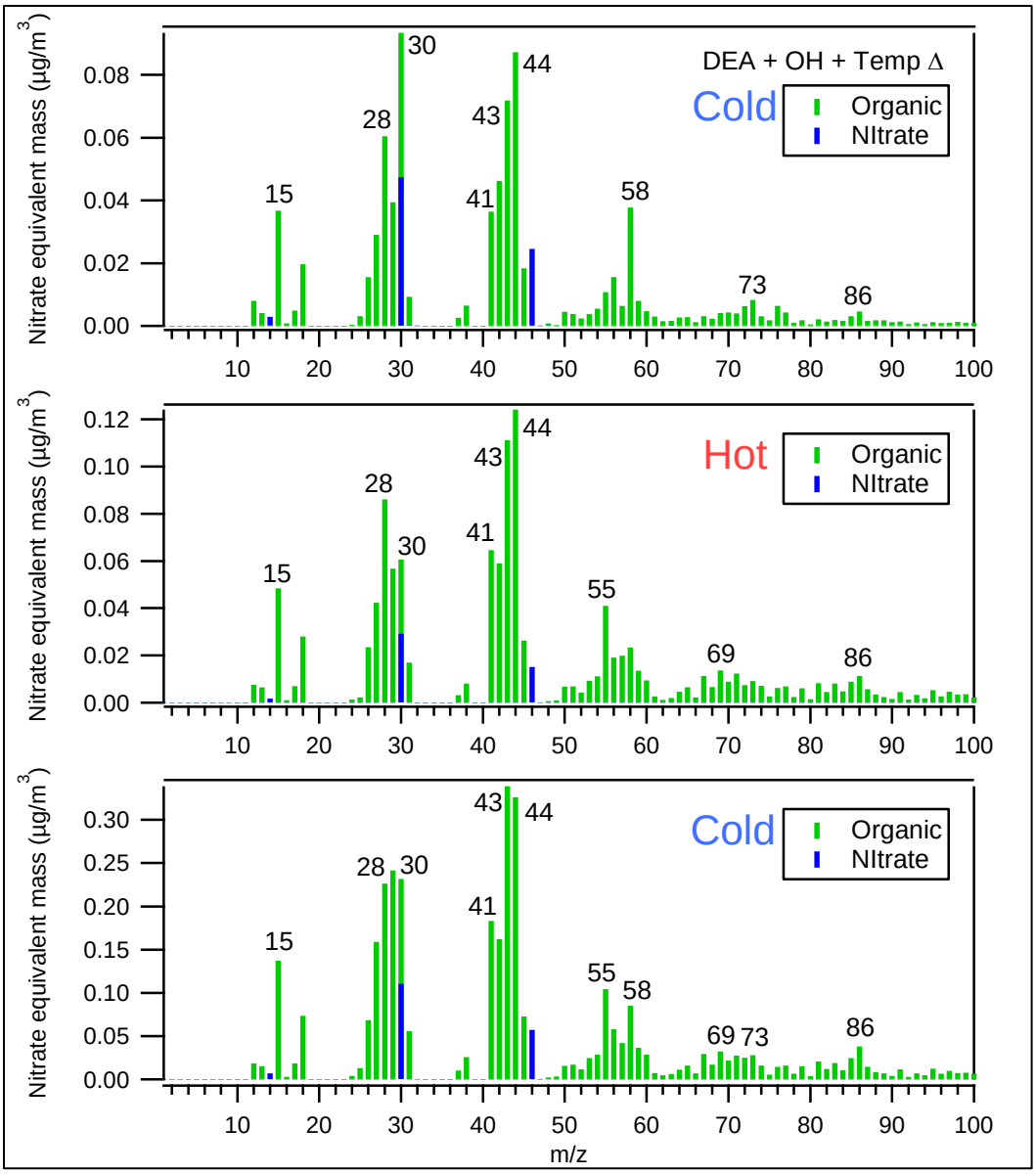

Figure 4.16. HR-ToF-AMS mass spectra from the cold start diethylamine with OH oxidation experiment.

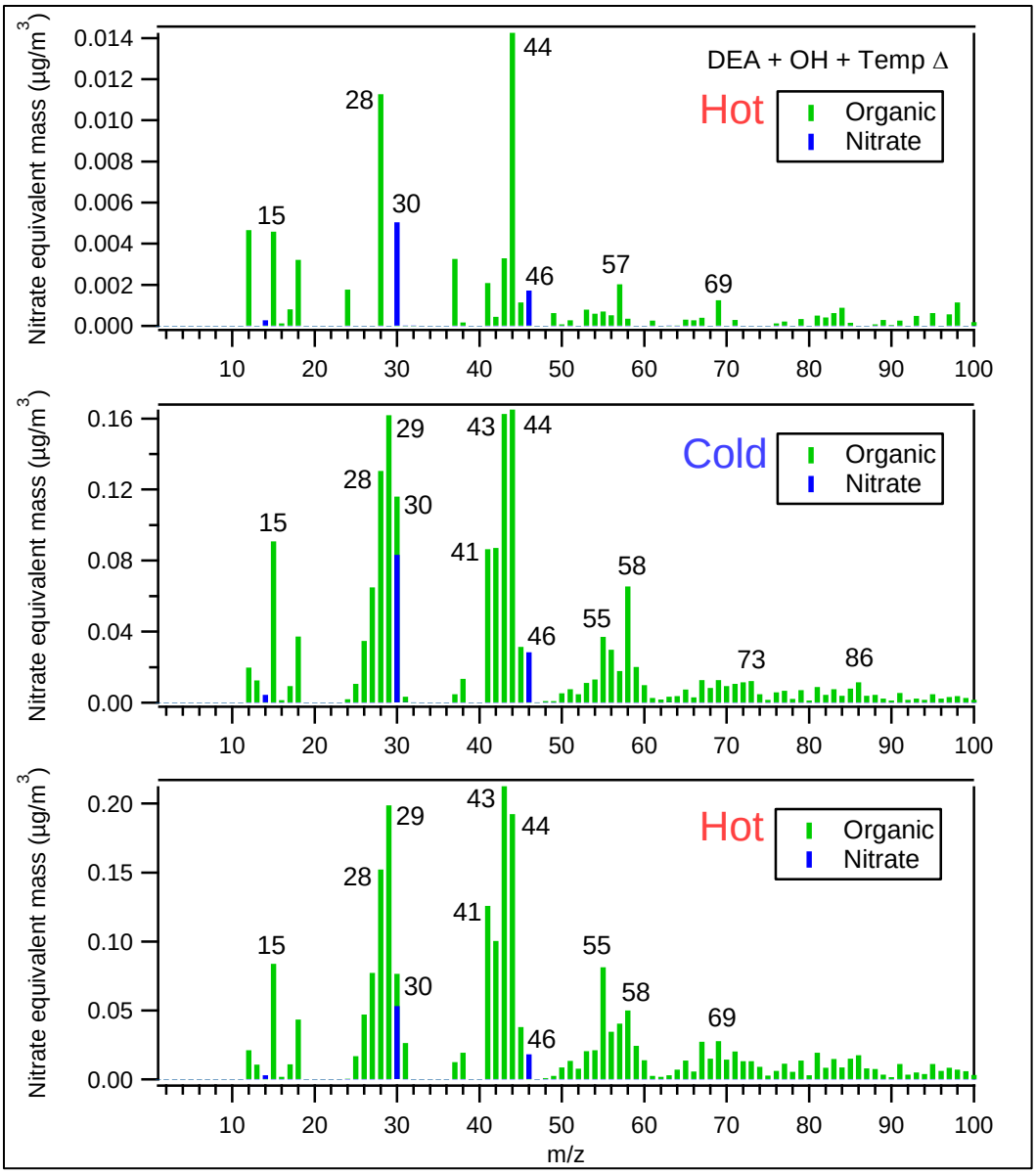

Figure 4.17. HR-ToF-AMS mass spectra from the hot start diethylamine with OH oxidation experiment.

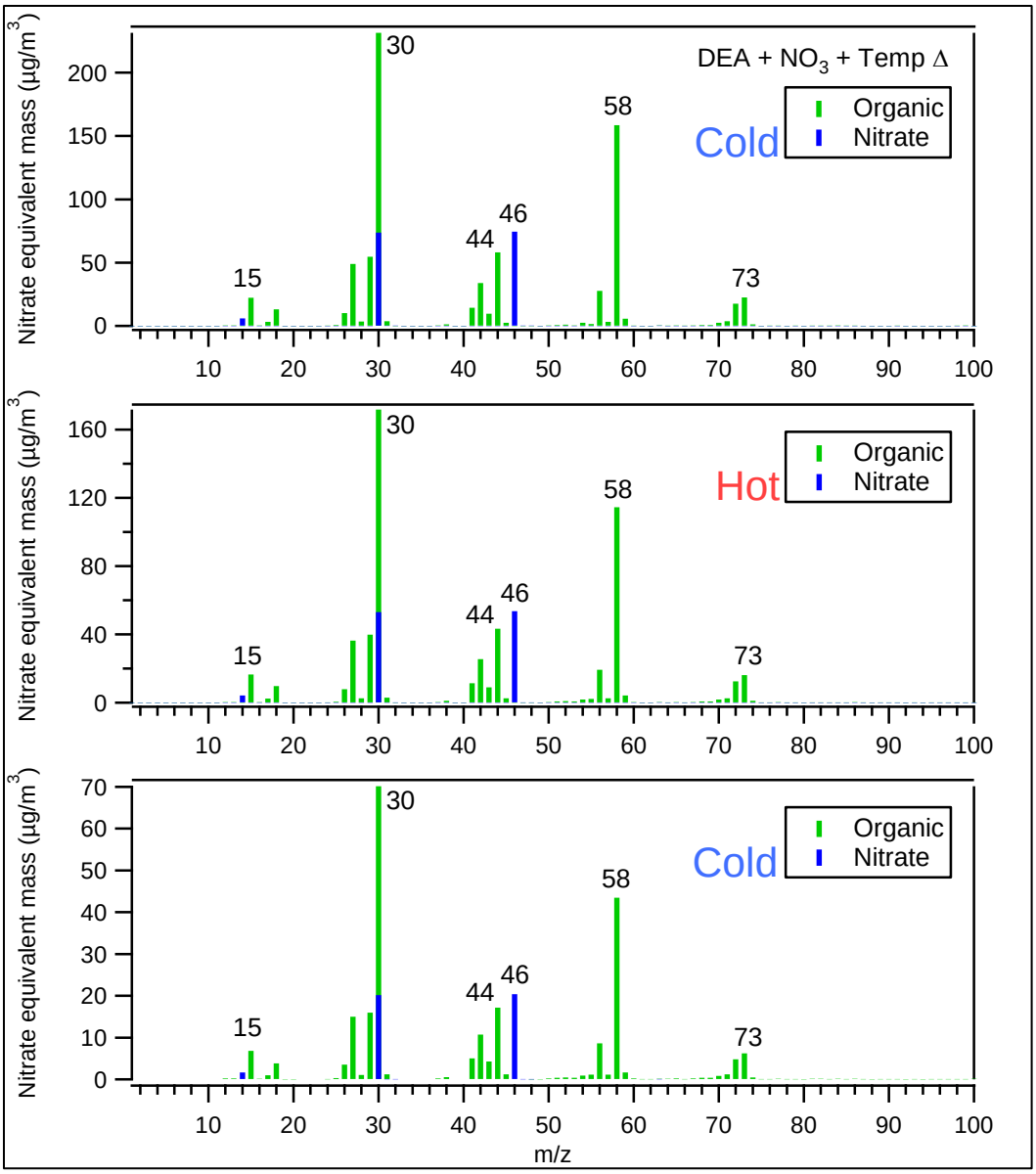

Figure 4.18. HR-ToF-AMS mass spectra from the cold start diethylamine with NO_3 oxidation experiment.

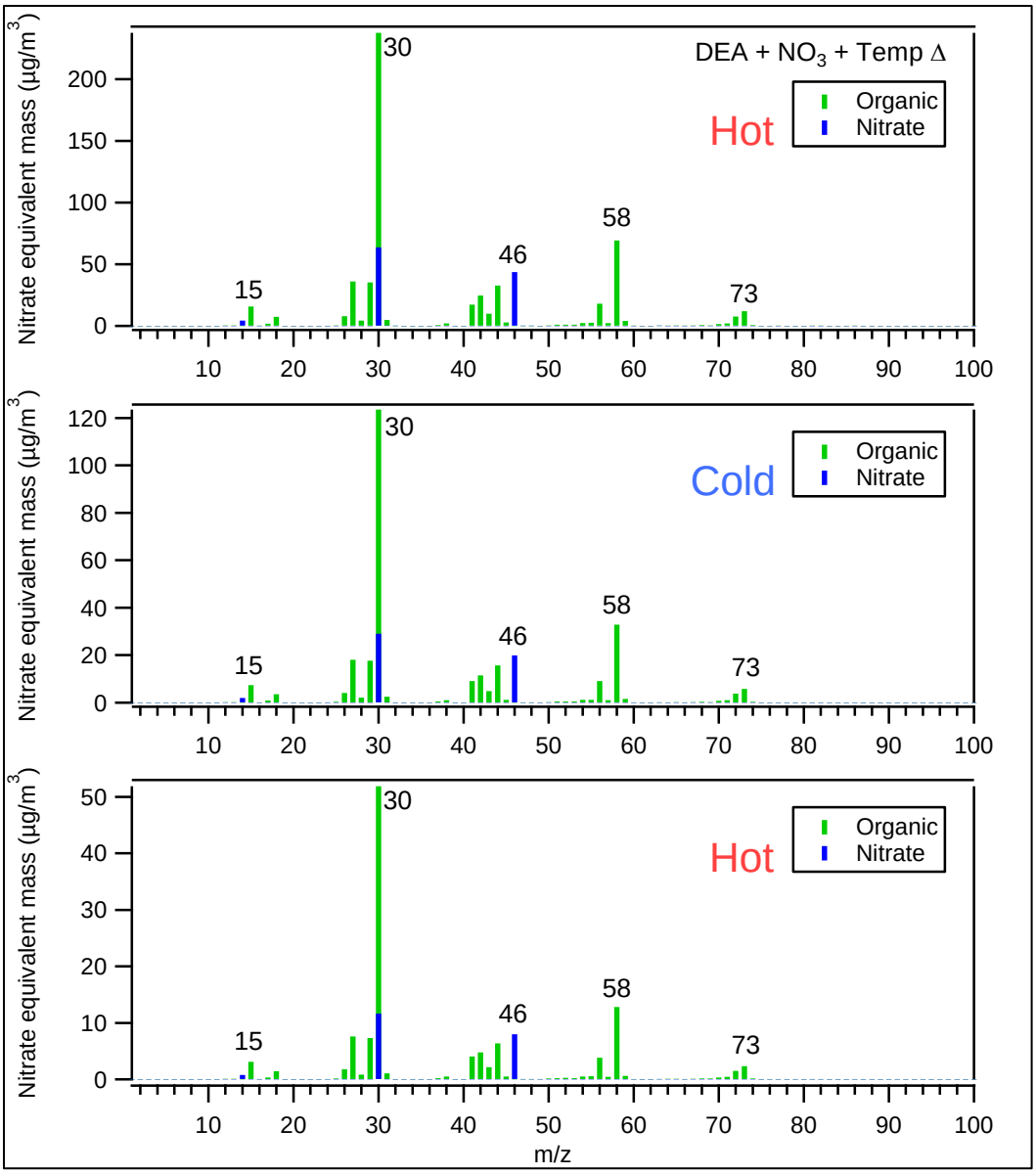

Figure 4.19. HR-ToF-AMS mass spectra from the hot start diethylamine with NO_3 oxidation experiment.

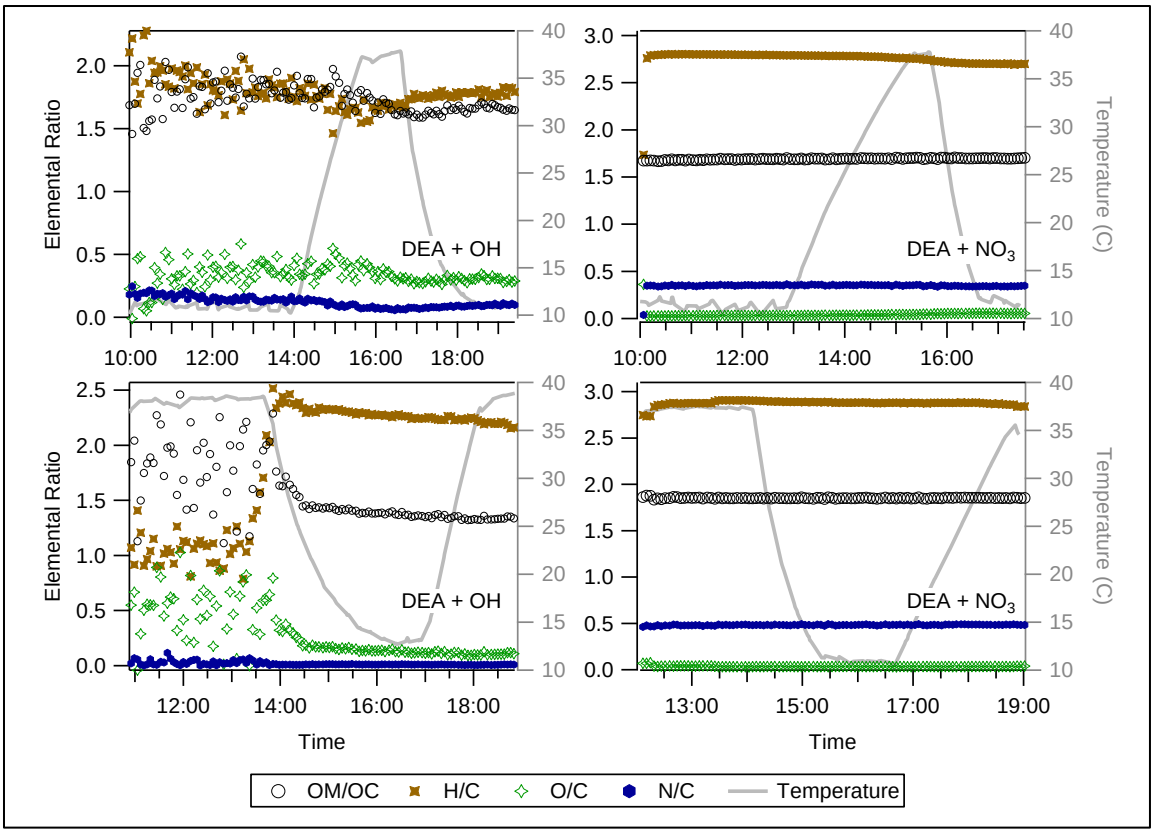

Figure 4.20. The elemental analysis for the aerosol formed in the diethylamine oxidation experiments.

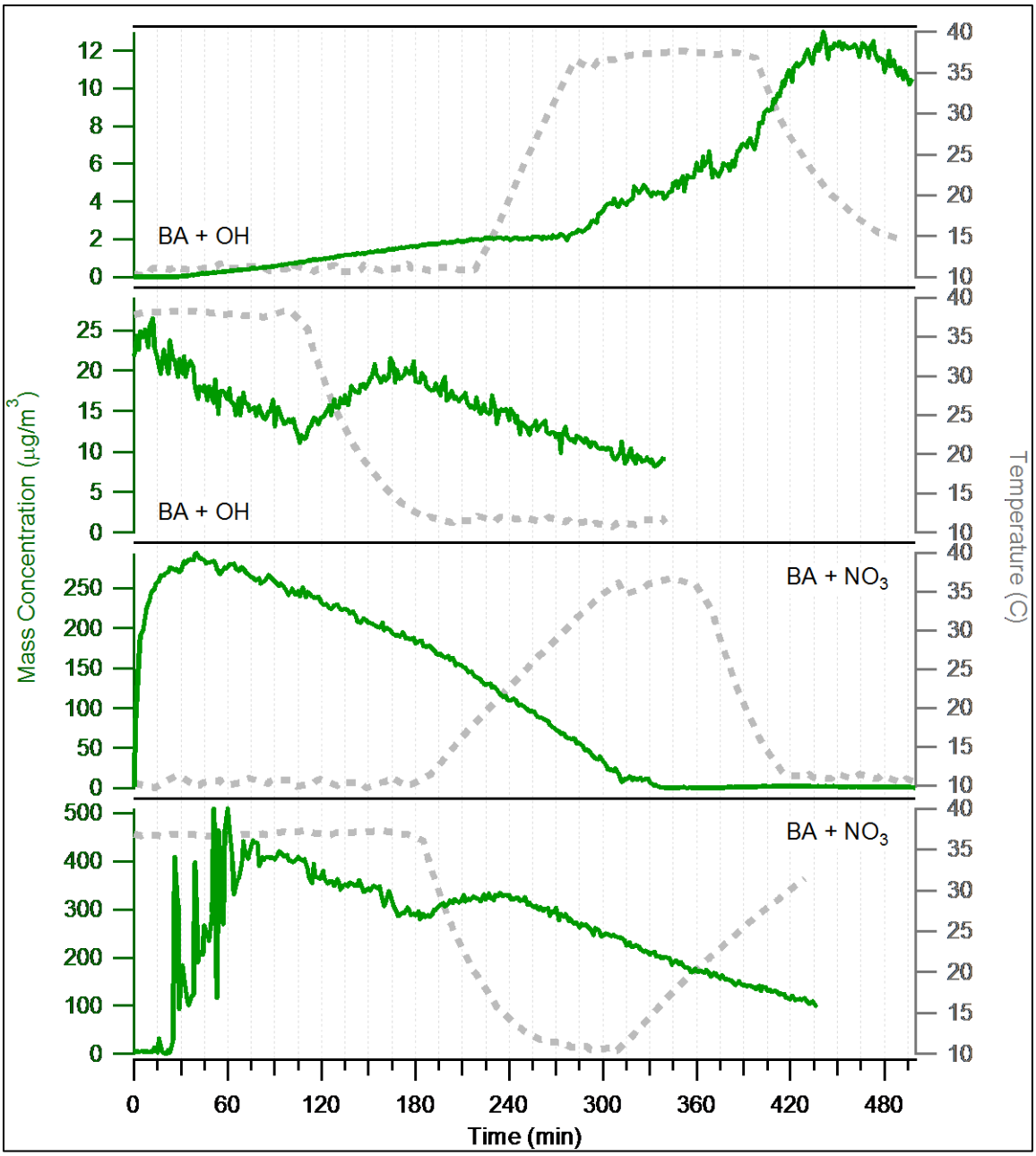

Figure 4.21. Mass concentration and temperature profiles for the butylamine oxidation experiments.

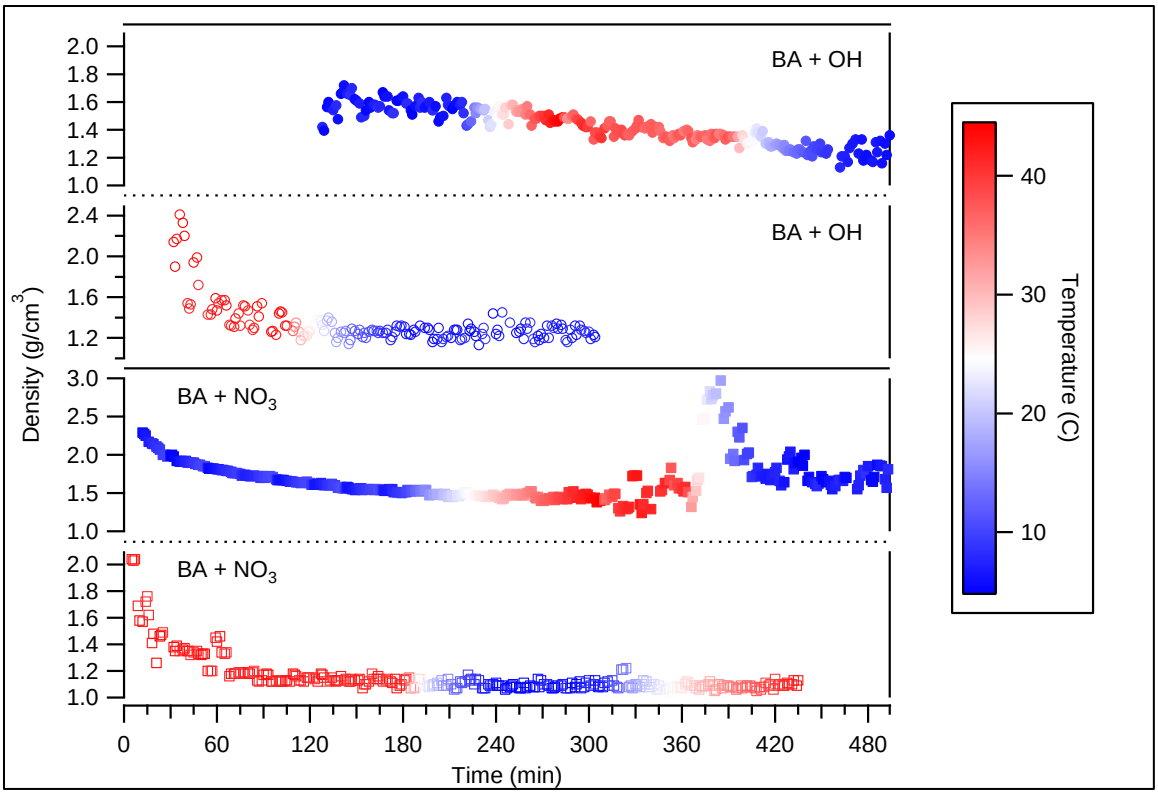

Figure 4.22. Density profiles for the aerosol produced in the butylamine oxidation experiments.

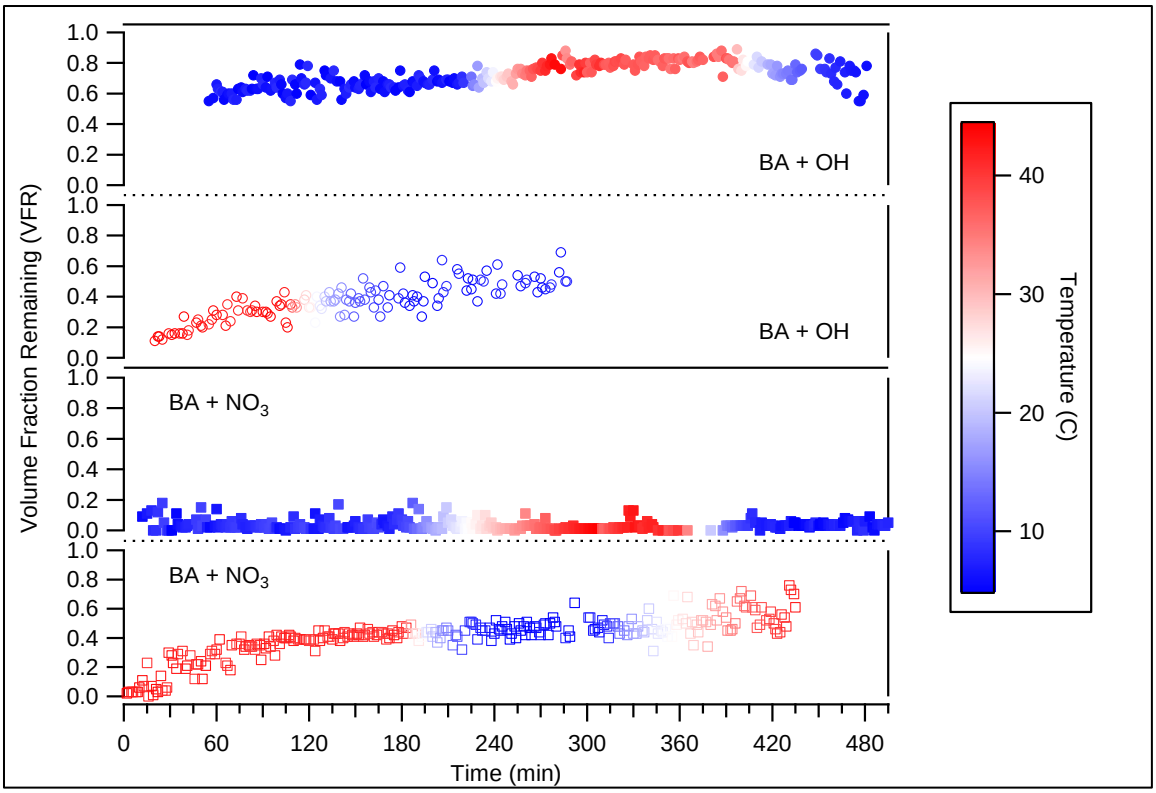

Figure 4.23. The volatility profiles for the aerosol produced in the butylamine oxidation experiments.

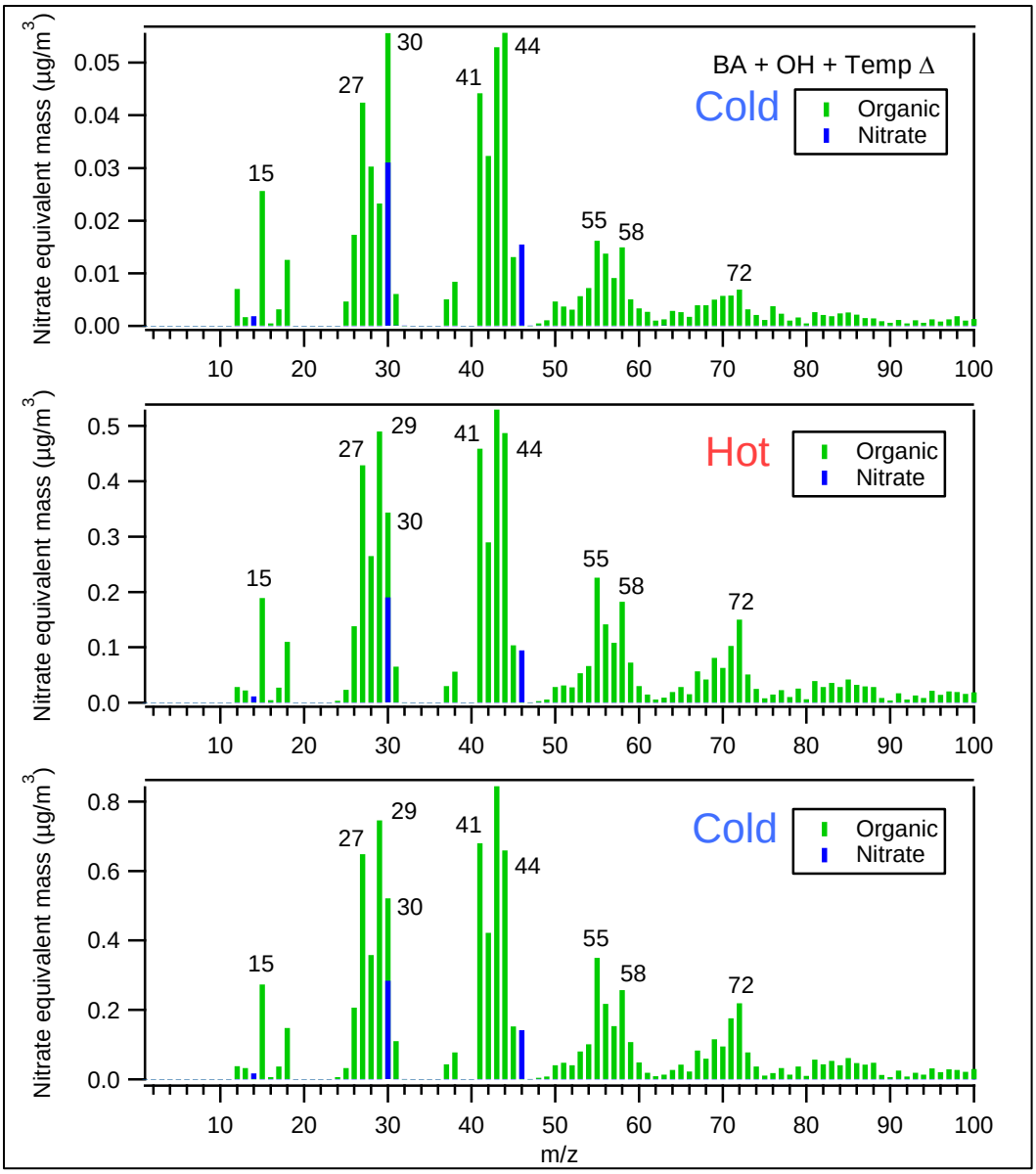

Figure 4.24. HR-ToF-AMS mass spectra from the cold start butylamine with OH oxidation experiment.

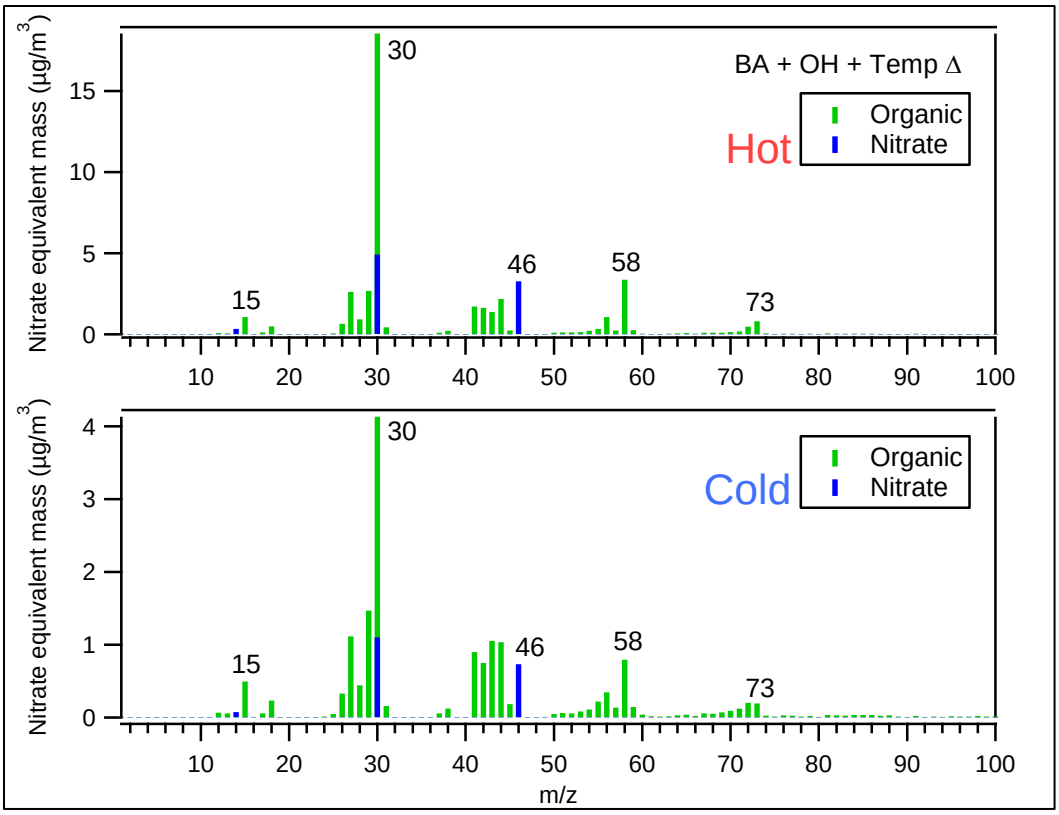

Figure 4.25. HR-ToF-AMS mass spectra from the hot start butylamine with OH oxidation experiment.

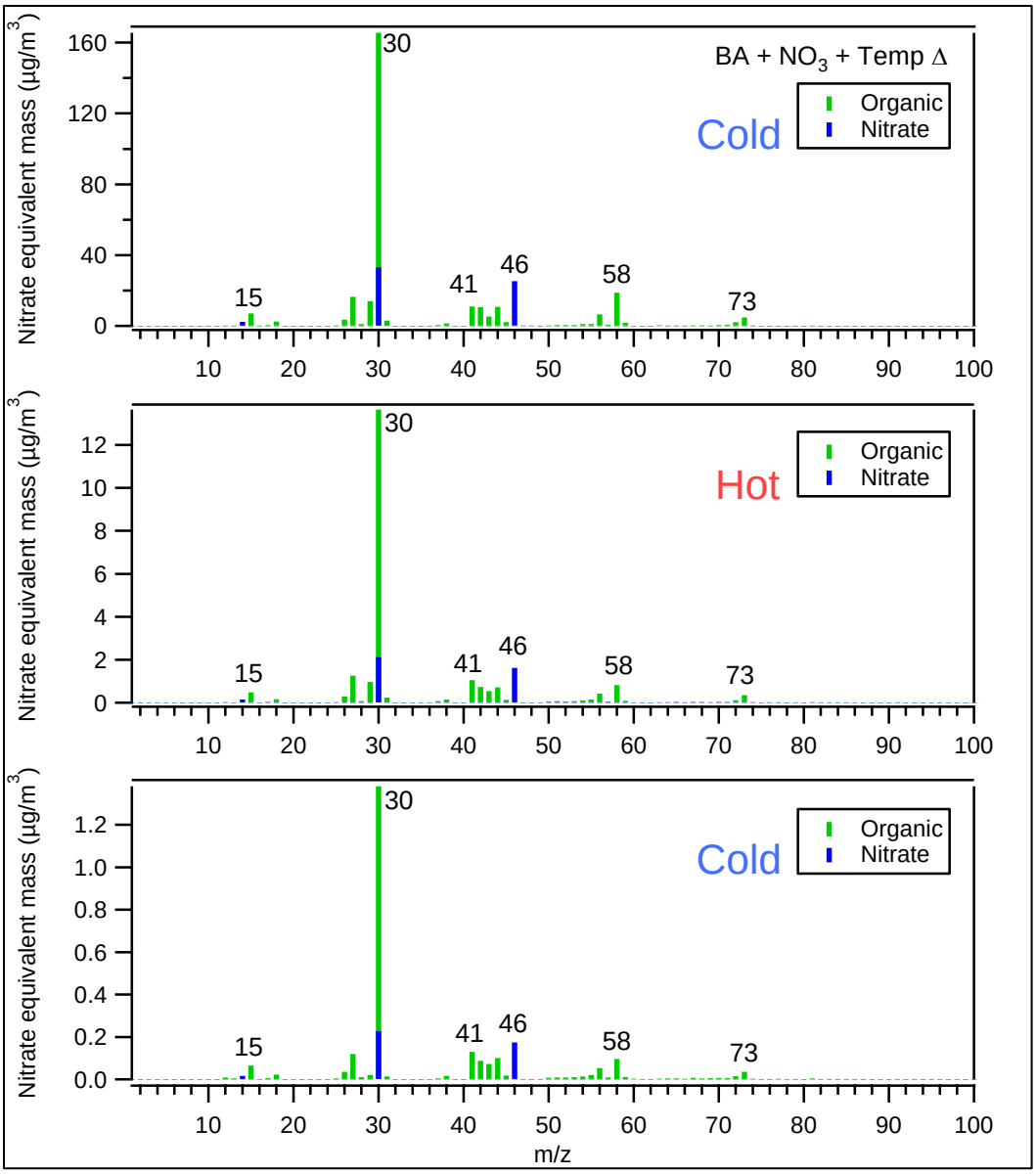

Figure 4.26. HR-ToF-AMS mass spectra from the cold start butylamine with NO_3 oxidation experiment.

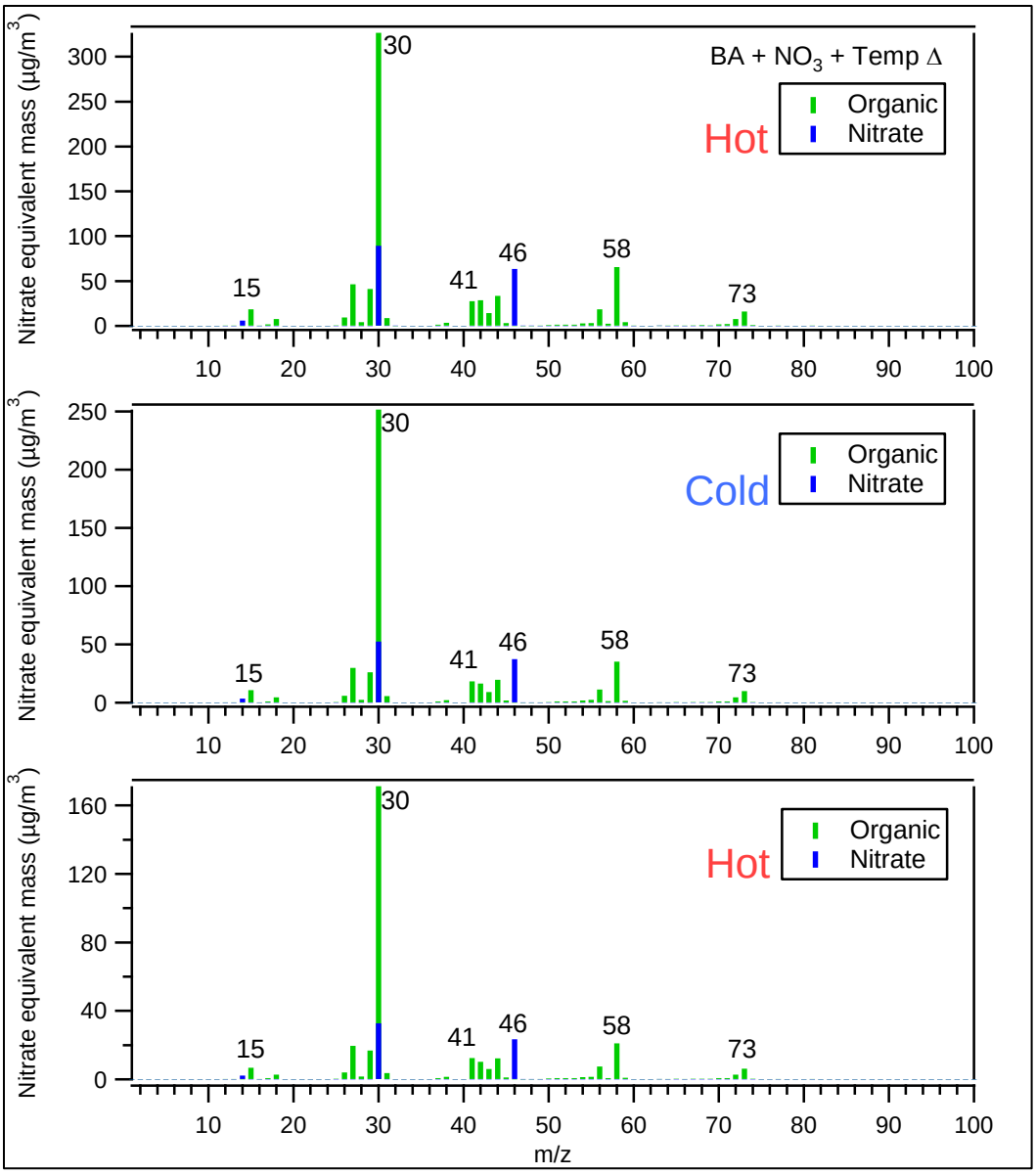

Figure 4.27. HR-ToF-AMS mass spectra from the hot start butylamine with NO_3 oxidation experiment.

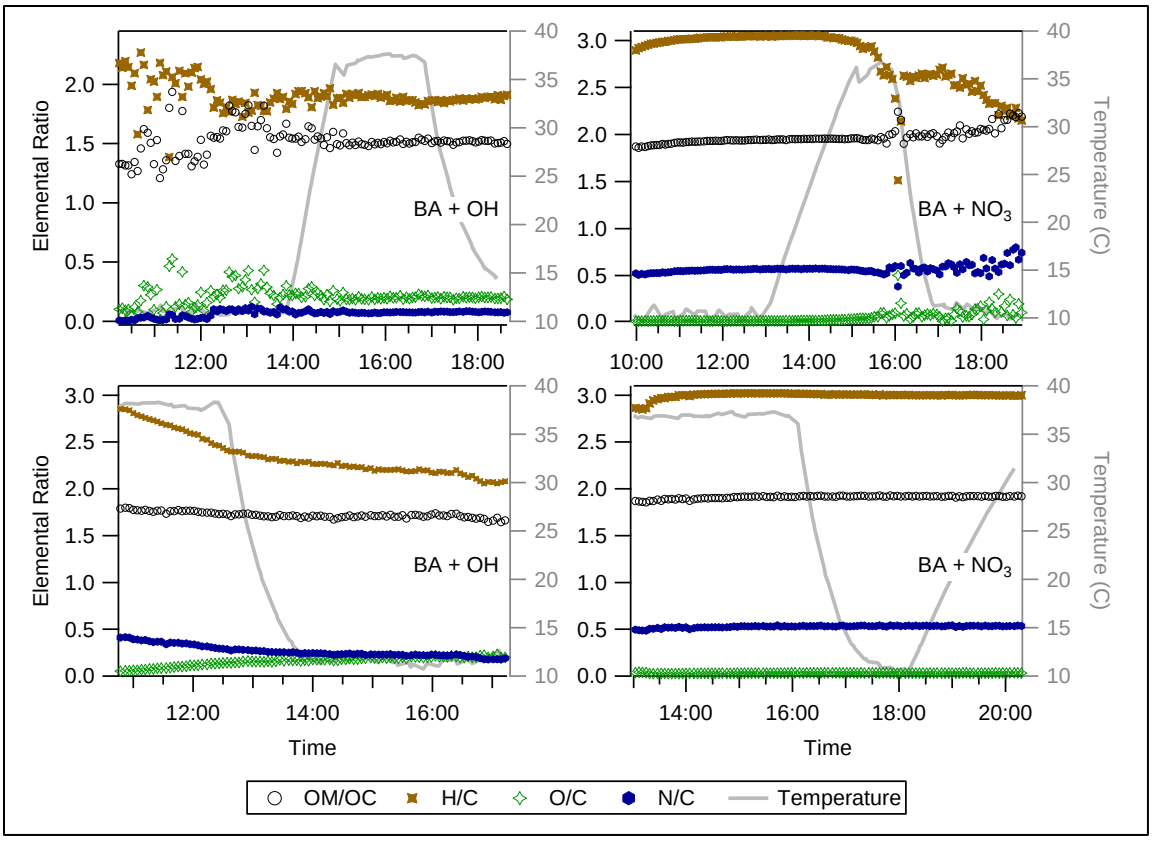

Figure 4.28. The elemental analysis for the aerosol formed in the butylamine oxidation experiments.

Chapter 5: Secondary Organic Aerosol Formation from Amino Alcohols used in Carbon Capture and Sequestration Control Technologies

5.1. Introduction

Secondary organic aerosol (SOA) and fine particulate matter negatively impact human health, air quality, visibility, and plays a role in direct and indirect climate forcing (Dockery, 2009; IPCC, 2013; Pope et al., 1995; Watson, 2002). Significant precursors to atmospheric aerosol formation are reduced nitrogen compounds including ammonia and amines (Ge et al., 2011). Anthropogenic and biogenic sources of amines include agricultural emissions, selective catalytic reduction and carbon capture control technologies by-products, and biomass burning (Borduas et al., 2013; Cadle and Mulawa, 1980; Ge et al., 2011; Mosier et al., 1973; Westerholm et al., 1993).

Amino alcohols, such as 2-aminoethanol, are used in control technologies designed to capture CO_2 from the flue gas of power plants (Reynolds et al., 2012; Veltman et al., 2010). Amino alcohols used in carbon capture and sequestration control technologies are volatile compounds that can escape into the atmosphere. Emissions of amino alcohols from CO_2 capture facilities are estimated to be 40 - 160 tons/year depending on process conditions (Karl et al., 2011). Once emitted to the atmosphere, amino alcohols can react with atmospheric oxidants to form secondary aerosol.

The importance of amines in new particle formation is gaining attention. Previous studies have investigated the formation of organic salt aerosol through the reactions of atmospherically relevant acids (HNO_3, H_2SO_4) with alkyl amines (Barsanti et

al., 2009). In addition to organic salt formation, field studies have observed that a significant portion of new particle growth is due to oxidized organic amine aerosol (Silva et al., 2008; Smith et al., 2008) from reactions with atmospheric radicals. The atmospheric reactivity of amino alcohols, however, is poorly understood. Previous studies have examined the reactions of 2-aminoethanol with hydroxyl radical (OH) or ozone (Borduas et al., 2013; Karl et al., 2012). The oxidation of amino alcohols with nitrate radical (NO_3) has not been previously reported. This study investigates the SOA formation from the atmospheric oxidation of three amino alcohols with OH and NO_3 radicals. The effect of humidity on the physical properties and chemical composition of the aerosol is also investigated.

5.2. Methods

A set of three amino alcohols were chosen for this study: 2-aminoethanol (AE, >99.0%, Sigma-Aldrich), 2-methylaminoethanol (MAE, >99%, Matrix Scientific), and 2-dimethylaminoethanol (DMAE, >99.5%, Sigma-Aldrich). All experiments were conducted in an environmental chamber located at the College of Engineering - Center for Environmental Research and Technology, University of California - Riverside (CE-CERT/UCR). The amines were reacted in a 37.5 m^3 volume Teflon® film (50.8 μm) chamber with hydroxyl radical (OH) and nitrate radical (NO_3). The environmental chamber is housed in a 2.5m x 3m x 7.8m reflective aluminum enclosure.

Photooxidation, when desired, was driven by 170 40W black lights with peak intensity of 350 nm (350 BL, Sylvania) mounted to two of the enclosure walls. Excess

ozone was injected into the chamber with black lights on to purge the chamber of any background hydrocarbons to ensure a clean chamber for each experiment. Additionally, the injection glassware was washed with methanol to remove any residual amine from previous experiments. Prior to each experiment, the chamber was flushed with purified air (Aadco 737 air purification system) so that background particle concentration, NO_x, and hydrocarbon concentrations were below the detection limits of the instruments used. No seed aerosols were injected. All experiments were conducted at room temperature (~295 K). The experiments were run under dry conditions (RH < 0.001%) and then repeated with humidity (RH ~ 30%). An experimental summary is provided (Table 5.1). Amines injected into the chamber were allowed to mix and stabilize in the Teflon chambers before radical injection. Hydroxyl radicals (no NO_x experiments) were produced from direct photolysis of hydrogen peroxide (H_2O_2) in the chamber. The nitrate radical was formed from thermal decomposition of dinitrogen pentoxide (N_2O_5) in the chamber. OH and NO_3 experiments were designed to represent daytime and nighttime chemistry, respectively.

The chemical composition of the aerosol products was measured by a High Resolution Time of Flight Aerosol Mass Spectrometer (HR-ToF-AMS; Aerodyne Research Inc.) (DeCarlo et al., 2006; Jayne et al., 2000). Briefly, an aerosol sample was drawn through a time-of-flight region where the particles were separated based on their vacuum aerodynamic diameter. The sample was vaporized by a 600°C oven followed by 70 eV electron impact ionization. The resulting ions pass through another time-of-flight section which can be operated in two flight path configurations, V and W. The shorter

flight path (V-mode) provides better sensitivity at unit mass resolution. The longer flight path (W-mode) provides sufficient mass spectral resolution (4300 at *m/z* 200) to separate isobaric compounds and determine empirical formulas.

A custom built scanning mobility particle sizer (SMPS) (Cocker et al., 2001) was used to measure the concentration and size distribution (27 - 712 nm) of the aerosol formed during the experiments. The SMPS also communicates size distribution values in real-time to an Aerosol Particle Mass Analyzer (APM, Kanomax model 3600) in series with an SMPS used to measure effective density (Ehara et al., 1996; Malloy et al., 2009). Briefly, the mass of the particle is selected by the APM based on the peak number electrical mobility diameter identified by the independent SMPS. The mass selected particles are then measured by an in-series SMPS to obtain the peak number electrical mobility diameter transmitted by the APM. Density measurements were taken every 85 seconds.

5.3. Results and Discussion

5.3.1. Particle Phase - Density

Density traces for AE, MAE, and DMAE aerosol produced from OH and NO_3 oxidation experiments for dry and humid conditions are located in Figure 5.1. There is an overall trend of lower aerosol density with the addition of humidity in the OH and NO_3 oxidation experiments. The aerosol densities for the OH oxidation experiments for the three amino alcohols ranged between 1.4 - 1.65 g/cm^3 (dry) and between 1.25 -1.5 g/cm^3 (humid). DMAE aerosol had the highest density (1.65 g/cm^3 dry, 1.5 g/cm^3 humid) in

both OH experiments compared to the other amino alcohols. Humidity had the most significant effect on the density for aerosol produced in the AE + NO_3 oxidation experiments (1.8 g/cm^3 dry, 1.25 g/cm^3 humid).

5.3.2. 2-aminoethanol Experiments

Particle formation from AE oxidation, with and without wall loss correction (WLC), is shown in Figure 5.2. An overall mass-based aerosol yield was calculated for each experiment assuming complete consumption of the gas-phase precursor amine (Table 5.2). Far more aerosol formed in the humid OH oxidation experiment compared to the dry experiment (yield of 26.3% and 0.5%, respectively). Far more aerosol formed in the NO_3 experiments than in the OH experiments (>> 100% and <30%, respectively). As with the OH oxidation experiments, far greater aerosol formation is observed in the humid NO_3 oxidation experiment than in the dry experiment (~2.4 times). It is possible to have a mass-based yield over 100% (through the addition of oxygen, nitric acid, or oligomerization). The maximum possible yield was calculated for each experiment to constrain the maximum observable aerosol yields (Table 5.2). For example, in the NO_3 oxidation experiments, it was assumed that amine nitrate salts were the dominant component of the aerosol. Therefore, the maximum possible yield for the AE + NO_3 oxidation experiments, assuming complete consumption of gas-phase AE to 2-aminoethanol nitrate salt ($AE{\cdot}HNO_3$), is $MW_{AE{\cdot}HNO3}/MW_{AE}$ or 203.3%.

The observed aerosol yields for the AE + NO_3 experiment are both above the yield maximum estimated based on the final MW of the products. Further investigation

revealed some interesting trends in the aerosol produced from the NO_3 oxidation experiments. Little to no particle wall loss is observed in the non-wall loss corrected (NWLC) concentration profiles for the AE + NO_3 oxidation experiments (Figure 5.2). The suspended aerosol concentration plateaus quickly with little to no decay of suspended aerosol over time. This trend is highly unusual as wall loss to Teflon chambers typically range from 0.0015-0.01 min^{-1}. A possible explanation is that the amine salt aerosol is not stable on the Teflon surface of the chamber resulting in partitioning of the aerosol back to the gas phase components (AE + HNO_3), which then quickly partition back to suspended amine salt aerosol. The normally robust wall loss correction, therefore, over-predicts the aerosol formation in the NO_3 oxidation experiments. The overall NWLC mass-based aerosol yields are also reported (Table 5.2). The NWLC aerosol yield for the humid NO_3 experiment (322.7% at particle nucleation, 276.0% at end of experiment) is still over the maximum predicted yield. In order for this yield to be achieved in the humid experiment, an aerosol with MW > 197 g/mol must be formed relative to the gas-phase precursor. The formation of a trimer-amine nitrate salt would have sufficient MW (246 g/mol) to allow a maximum aerosol yield of 403.2%.

The mass concentration profiles of the organic and nitrate components of the aerosol measured by the HR-ToF-AMS (Figure 5.3) confirm the trends observed by the SMPS. Far more aerosol formed in the humid OH experiment than in the dry OH experiment, far more aerosol formed in the NO_3 experiments than in the OH experiments, more aerosol formed in the humid NO_3 experiment than in the dry NO_3 experiment, with little to no wall loss was observed in the NO_3 experiments. The organic to nitrate mass

ratios (Org/NO_3) are reported in Table 5.2. The Org/NO_3 is higher in the humid NO_3 experiment (2.1 humid vs 1.3 dry) indicating the formation of a more organic based aerosol consistent with the formation of dimer and trimer-amine nitrate salts in the humid NO_3 experiment.

The HR-ToF-AMS organic mass spectra for the AE experiments are presented in Figure 5.4. The organic spectra from the dry and humid experiments are plotted together for both OH and NO_3 oxidation. The mass spectra for the secondary amine experiments are shown in logarithmic scale to highlight the higher mass peaks, i.e., peaks greater than that of the amine precursor (AE = 61 amu). To highlight the differences between the two spectra, a correlation plot of the dry organic mass versus the humid organic mass with respect to *m/z* is presented. It is noted that little aerosol was formed in the dry AE + OH experiment, (not much above the typical background chamber SOA formed during photooxidation) leading to the poor observed correlation ($r^2 = 0.426$) between the dry and humid OH oxidation experiments. The slope (0.009) indicates far more organic mass was formed in the humid OH experiment. The fragmentation pattern observed in the mass spectrum for the humid OH experiment is similar to the fragmentation observed with long-chain hydrocarbons. The *m/z* peaks for the humid OH experiment include 41 ($C_2H_3N^+$, $C_3H_5^+$), 55 (C_2HNO^+, $C_3H_5N^+$, $C_4H_7^+$), 69 ($C_3H_3NO^+$, $C_3H_5N_2^+$, $C_5H_9^+$), 81 ($C_4H_5N_2^+$, $C_6H_9^+$), 95 ($C_4H_3N_2O^+$, $C_5H_7N_2^+$, $C_4H_5N_3^+$, $C_7H_{11}^+$), 141 ($C_6H_{11}N_3O^+$, $C_6H_9N_2O_2^+$, $C_6H_7NO_3^+$), and 165 ($C_8H_9N_2O_2^+$, $C_8H_{13}N_4^+$) and are fragment ions indicative of oxidized and reduced amine-oligomer compounds. These oligomer compounds are possibly produced through aqueous-phase nucleophilic addition-

elimination reactions of the primary amine functionality of one AE with the alcohol functionality of another AE (e.g., H_2N-CH_2-CH_2-NH-CH_2-CH_2-OH) or with the carbonyl functionality of an oxidized AE product to form an imine linkage (e.g., H_2N-CH_2-CH=NH-CH_2-CH_2-OH) (Borduas et al., 2013; Bruice, 2004).

Good correlation ($r^2 = 0.983$) is observed between the dry and humid NO_3 oxidation experiments, indicating similar chemical composition between the two experiment types. The slope (0.403) indicates that more organic mass formed in the humid NO_3 experiment compared to the dry experiment. The lower *m/z* peaks (≤ 61) at 30 (CH_4N^+), 42 ($C_2H_4N^+$), 58 ($C_3H_8N^+$), and 61 ($C_2H_7NO^+$) are fragments of the unoxidized parent amine consistent with the fragmentation of 2-aminoethanol nitrate salt ($AE \cdot HNO_3$). The higher *m/z* peaks (> 61) at 72 ($C_4H_{10}N^+$, $C_3H_6NO^+$), 86 ($C_5H_{12}N^+$, $C_3H_6N_2O^+$), and 100 ($C_6H_{14}N^+$, $C_4H_8N_2O^+$, $C_5H_{12}N_2^+$), are fragment ions indicative of amine-oligomer nitrate salts, which explains the high aerosol yields observed in the AE + NO_3 oxidation experiments. Humidity enhances this oligomer mechanism, which explains the formation of more organic mass in the humid experiments. The series of higher *m/z* peaks (> 61) at 97, 101, 109, 111, 121, 123, and 125 in the dry NO_3 experiment are fragments of highly reduced aerosol with three nitrogen and two oxygen separated by CH_2 groups ($CH_{11}N_3O_2^+ - C_3H_{15}N_3O_2^+$). The higher *m/z* peaks at 173 ($C_7H_{13}N_2O_3^+$) and 175 ($C_7H_{15}N_2O_3^+$) indicate the formation of oxidized amine oligomer aerosol in the dry NO_3 experiment.

The elemental analyses for the AE ($H_2NCH_2CH_2OH$; H/C = 3.5, N/C = 0.5, O/C = 0.5) experiments are shown (Figure 5.5). The aerosol produced in the humid OH experiments was oxidized (O/C = 0.23) and consistent with carbonyl functional groups (H/C = 1.95). The aerosol formed in the humid NO_3 experiment has high H/C (2.7) and N/C (0.50) and a low O/C (0.12), suggesting the fragmentation of reduced amine nitrate salts. However, the H/C and O/C are lower than expected for the fragmentation of $AE{\cdot}HNO_3$ ($H_2N^+{=}CHCH_2OH$; H/C = 3, O/C = 0.5) indicating the formation of reduced oligomer salts (e.g., $H_2N^+{=}CHCH_2NHCH_2CH_2NHCH_2CH_2OH$; H/C = 2.67, N/C = 0.5, O/C = 0.167). The H/C ratio is lower and the O/C ratio is higher in the dry NO_3 experiment than in the humid experiment, indicating the formation of more oxidized aerosol in the dry NO_3 experiment.

5.3.3. 2-Methylaminoethanol Experiments

Particle formation, with and without WLC, for the MAE experiments are shown (Figure 5.6). The overall mass-based aerosol yield for each experiment is reported (Table 5.2). Unlike the AE + OH experiments, more aerosol formed in the humid MAE + OH experiment than in the dry experiment (28.6% and 19.2%, respectively). However, the concentration trends observed in the MAE + NO_3 experiments were similar to those observed in the AE experiments. Far more aerosol was produced in the NO_3 experiments than in the OH experiments (> 85% and < 30%, respectively). More aerosol formed in the humid NO_3 oxidation experiment than in the dry experiment (339.7% and 185.4%, respectively). The maximum possible yield for the MAE + NO_3 oxidation experiments,

assuming complete consumption of the gas-phase precursor amine to 2-methylaminoethanol nitrate salt ($MAE \cdot HNO_3$), is 184.0%. The WLC aerosol yields in the NO_3 experiments are greater than the maximum possible yield and, therefore, over-predict the aerosol formation. As in the AE experiment, little to no particle wall loss is observed in the NWLC concentration profiles for the MAE + NO_3 oxidation experiments (Figure 5.6). The NWLC aerosol yields for the humid and dry NO_3 oxidation experiments are 134.6% and 86.6% respectively. The humid NO_3 yield is close to the maximum (184.0%), suggesting that most of the precursor amine reacts to form $MAE \cdot HNO_3$ aerosol.

The mass concentration profiles of the organic and nitrate components of the aerosol measured by HR-ToF-AMS (Figure 5.7) confirm the trends observed by the SMPS in the MAE experiments. More aerosol formed in the dry OH experiment than in the humid OH experiment, far more aerosol formed in the NO_3 experiments than in the OH experiments, more aerosol formed in the humid NO_3 experiment than in the dry NO_3 experiment, and little to no wall loss is observed in the MAE + NO_3 experiments. The Org/NO_3 is higher in the humid NO_3 experiment (2.5 humid vs 1.6 dry), indicating the formation of more organic aerosol and consistent with the formation of oligomer nitrate salts.

The HR-ToF-AMS organic mass spectra and correlation plots for the MAE experiments are presented (Figure 5.8). Good correlation ($r^2 = 0.909$) is observed between the dry and humid OH oxidation experiments. The linear regression slope (m =

1.771) confirms that more organic mass formed in the dry OH experiment. The lower *m/z* peaks (≤ 75) at 30 (CH_4N^+, CH_2O^+), 44 ($C_2H_6N^+$, CO_2^+, CH_2NO^+), 58 ($C_3H_8N^+$, $C_2H_4NO^+$), and 72 ($C_4H_{10}N^+$, $C_3H_6NO^+$) are fragment ions of oxidized amines. Oxidized amine fragment ions (*m/z* 86) and the highly reduced fragmentation series (*m/z* 97, 109, 111, 123, and 125) are also observed in the MAE + OH experiments. The higher *m/z* peaks (> 75) observed in the dry OH oxidation experiment at 133 ($C_4H_{11}N_3O_2^+$), 147 ($C_5H_{13}N_3O_2^+$), 158 ($C_6H_{14}N_4O^+$), and 174 ($C_6H_{14}N_4O_2^+$) are fragment ions indicative of oxidized oligomer compounds.

Poor correlation (Figure 5.8, $r^2 = 0.781$) is observed between the dry and humid NO_3 oxidation experiments, indicating differences in chemical composition between the experiments. The linear regression slope (0.619) confirms that more organic mass was formed in the humid NO_3 experiment. Most of the aerosol in the humid NO_3 experiment is in the lower *m/z* peaks (≤ 75) at 30 (CH_4N^+), 44 ($C_2H_6N^+$), 58 ($C_3H_8N^+$), 72 ($C_4H_{10}N^+$), and 75 ($C_3H_9NO^+$), which is consistent with the fragmentation of 2-methylaminoethanol nitrate salt ($MAE{\cdot}HNO_3$). Oxidized amine fragment ions (*m/z* 86) and the highly reduced fragmentation series (*m/z* 97, 109, 111, 123, 125, 137, 139, 151, 153, 165, 167, 179, and 181) were observed in both the dry and humid NO_3 experiments. The higher *m/z* peaks (> 75) observed in the dry NO_3 oxidation experiment at 148, ($C_4H_{12}N_4O_2^+$), 162 ($C_5H_{14}N_4O_2^+$), and 175 ($C_6H_{15}N_4O_2^+$) are fragment ions indicative of oxidized oligomer compounds. More oxidized amine oligomer / highly-reduced fragment series aerosol formed in the dry NO_3 experiment. More amine nitrate salt formed in the humid NO_3

experiment suggesting that the amine nitrate salt mechanism is enhanced in the humid experiment while there is more time for oxidation in the dry experiment.

The elemental analyses for the MAE ($CH_3NHCH_2CH_2OH$; H/C = 3.00, N/C = 0.33, O/C = 0.33) experiments are shown (Figure 5.9). The aerosol produced in the OH experiments consisted of oxidized amines (O/C = 0.29; N/C = 0.24) with carbonyl functional groups (H/C = 1.97). The aerosol formed in the NO_3 oxidation experiments have high H/C (2.52) and N/C (0.36) and low O/C (0.06) consistent with the vast majority of signal originating from the fragmentation of DEA·HNO_3. The H/C drops (2.26) and the O/C increases (0.11) over the course of the dry NO_3 experiment, indicating the formation of more oxidized aerosol in the dry experiment.

5.3.4. 2-dimethylaminoethanol Experiments

Particle formation, WLC and NWLC, for the DMAE experiments are shown (Figure 5.10). The overall mass-based aerosol yield for each experiment is reported (Table 5.2). The concentration trends observed in the DMAE experiments were similar to those observed in the AE experiments - more aerosol formed in the humid OH experiment than in the dry experiment (26.7% and 5.5%, respectively), far more aerosol formed in the NO_3 experiments than in the OH experiments (> 95% and < 30%, respectively), and more aerosol formed in the humid NO_3 oxidation experiment than in the dry experiment (333.2% and 202.6%, respectively). The maximum possible yield for the DMAE + NO_3 oxidation experiments, assuming complete consumption of the gas-phase precursor amine to 2-dimethylaminoethanol nitrate salt (DMAE·HNO_3), is 170.8%.

As with the previous amino alcohol experiments, the wall loss corrected aerosol yields in the DMAE + NO_3 experiments are greater than the maximum possible yield and over-predict the aerosol formation. As in the previous amine experiments, little to no particle wall loss is observed in the NWLC concentration profiles for the DMAE + NO_3 oxidation experiments (Figure 5.10). The NWLC aerosol yields for the humid and dry NO_3 oxidation experiments are 136.8% and 96.3%, respectively. The humid NO_3 experiment yield is close to the maximum (170.8%), suggesting that most of the precursor amine reacts to form DMAE·HNO_3 aerosol.

The mass concentration profiles of the organic and nitrate components of the aerosol measured by the HR-ToF-AMS (Figure 5.11) confirm the trends observed by the SMPS in the DMAE experiments. More aerosol formed in the humid OH experiment than in the dry OH experiment and far more aerosol formed in the NO_3 experiments than in the OH experiments. However, conflicting with SMPS measurements, more organic aerosol is observed in the dry NO_3 experiment than in the humid NO_3 experiment. A possible explanation for this inconsistency is the significantly large peak at *m/z* 58 in the dry NO_3 oxidation experiment (Figure 5.12). Abnormally large m/z 58 signal intensity has been reported previously (Tang et al., 2013) for trimethylamine (TMA); a compound similar in structure to DMAE. It was proposed in the earlier work that the low ionization potential of the amine nitrate salts allowed surface ionization to occur on the HR-ToF-AMS vaporizer, which lead to the inaccurately high organic aerosol concentrations. Similar to AE and MAE, little to no wall loss is observed in the DMAE + NO_3

experiments. The Org/NO_3 ratio of 2.5 in the humid NO_3 experiment indicates the formation of an amine oligomer aerosol.

The HR-ToF-AMS organic mass spectra and correlation plots for the DMAE experiments are presented (Figure 5.12). Good correlation (r^2 = 0.975) is observed between the dry and humid OH oxidation experiments, indicating similar chemical composition for the two types of experiments. The linear regression slope (m = 0.178) confirms that more organic mass formed in the humid OH experiment. The lower *m/z* peaks (≤ 89) at 29 (CHO^+, CH_3N^+), 44 ($C_2H_6N^+$, CO_2^+, CH_2NO^+), 58 ($C_3H_8N^+$, $C_2H_4NO^+$), 72 ($C_4H_{10}N^+$, $C_3H_6NO^+$), and 86 ($C_5H_{12}N^+$, $C_4H_8NO^+$, $C_3H_4NO_2^+$) are fragment ions of the oxidized amine. The *m/z* peaks observed in the humid OH oxidation experiment at 88 ($C_3H_6NO_2^+$), 104 ($C_3H_6NO_3^+$), 145 ($C_5H_9N_2O_3^+$), 161 ($C_5H_9N_2O_4^+$), and 191 ($C_6H_{11}N_2O_5^+$) are fragment ions indicative of oligomer compounds observed in previous experiments with TMA. The mechanism describing the formation of these oligomer compounds is discussed in detail in Price et al. (2014). Briefly, oligomers are produced through peroxy radical chemistry ($RO_2\cdot$ + $RO_2\cdot$) that creates a peroxide linkage (R-O-O-R).

Poor correlation (r^2 = 0.794) is observed between the dry and humid NO_3 oxidation experiments, indicating differences in chemical composition between these experiments. The linear regression slope (m = 2.062) indicates that more organic mass was formed in the dry NO_3 experiment. However, this is largely due to the abnormally high *m/z* 58 signal intensity caused by surface ionization on the HR-ToF-AMS vaporizer.

Most of the aerosol in the humid NO_3 experiment is with the lower *m/z* peaks ($\leq$ 89) at 30 (CH_4N^+), 44 ($C_2H_6N^+$), 58 ($C_3H_8N^+$), 72 ($C_4H_{10}N^+$), 86 ($C_5H_{12}N^+$), and 89 ($C_4H_{11}NO^+$) which is consistent with the fragmentation of 2-dimethylaminoethanol nitrate salt ($DMAE \cdot HNO_3$). The highly reduced fragmentation series (*m/z* 97, 109, 111, 123, 125, 137, 139, 151, 153, 165, 167, 179, and 181) was observed in both the dry and humid NO_3 experiments. The higher *m/z* peaks (> 89) observed in the dry NO_3 oxidation experiment at 133 ($C_4H_{11}N_3O_2^+$) and 147 ($C_5H_{13}N_3O_2^+$) are fragment ions indicative of oxidized oligomer compounds. Similar to the MAE experiments, more oxidized amine oligomer / highly-reduced fragmentation series aerosol formed in the dry DMAE + NO_3 experiment. More amine nitrate salt formed in the humid DMAE + NO_3 experiment suggesting that the amine nitrate salt mechanism is enhanced in the humid experiment while there is more time for greater oxidation in the dry experiment.

The elemental analyses for the DMAE ($(CH_3)_2NCH_2CH_2OH$; H/C = 2.75, N/C = 0.25, O/C = 0.25) experiments are shown (Figure 5.13). The aerosol produced in the dry OH experiment consists of oxidized amines with carbonyl and alcohol functional groups (H/C = 2.10, N/C = 0.28, O/C = 0.46). The aerosol produced at the beginning of the humid OH experiment consists of highly oxidized amines (O/C = 0.64; N/C = 0.26) with mostly carbonyl and peroxide functional groups (H/C = 1.88). Additionally, the organic mass to organic carbon ratio is larger than in the previous amino alcohol experiments (OM/OC = 2.26). This is consistent with the formation of the highly oxidized peroxide oligomer compounds. Over the course of the experiment, the O/C and OM/OC decrease while the H/C and N/C increase (O/C = 0.37; OM/OC = 2.01; H/C = 2.15; N/C = 0.29)

suggesting the formation of more reduced amine oligomer aerosol. The aerosol formed in the NO_3 oxidation experiments have high H/C (2.55) and N/C (0.34) and low O/C (0.09) suggesting the fragmentation of DMAE·HNO_3 salt.

5.4. Conclusion

Significant aerosol formation was observed in the amino alcohol oxidation experiments. Generally, more aerosol was produced in the humid oxidation experiments than in the dry oxidation experiments. The addition of humidity to the system allowed for uptake of reaction products (amine products, HNO_3, etc.) into water, thereby introducing additional aqueous phase reactions leading to SOA formation under the humid conditions. Also, the reactions with NO_3 produced far more aerosol than the OH reactions. Little to no loss of particles to the chamber walls are observed in the NO_3 oxidation experiments. This is possibly due to the formation of amine nitrate salts not stable on the chamber surface, partitioning back to the gas-phase, and then returning to an aerosol salt once suspended in the chamber.

Different oligomer pathways were observed for the different amino alcohol experiments. A mechanism to form highly reduced oligomers was observed in the humid AE + OH oxidation experiments and was enhanced with humidity. It is proposed that these oligomer compounds are produced through nucleophilic addition-elimination reactions of the primary amine functionality of AE with the alcohol functionality of another AE. An oxidized oligomer pathway was observed in the dry amino alcohol experiments. A highly oxidized peroxide oligomer mechanism was observed in the

humid DMAE + OH oxidation experiment. A highly reduced aerosol containing nitrogen and oxygen was observed in the NO_3 oxidation experiments. In general, the OH oxidation reactions produced highly oxidized organic aerosol while the NO_3 oxidation reactions produced reduced amine nitrate salt aerosol. Humidity enhanced the reduced-amine nitrate salt formation in the NO_3 oxidation reactions.

As the use of amino alcohols becomes increasingly prevalent in carbon capture sequestration and control technologies, it is imperative to understand the atmospheric reactivity of these compounds. The significant aerosol yields observed in the NO_3 oxidation of amino alcohols has important implications for the use of these compounds in carbon capture control devices. Measures to reduce or prevent the release of amino alcohols from the system should be implemented.

5.5. References

Barsanti, K.C., McMurry, P.H., Smith, J.N., 2009. The potential contribution of organic salts to new particle growth. Atmospheric Chemistry and Physics 9, 2949-2957.

Borduas, N., Abbatt, J.P.D., Murphy, J.G., 2013. Gas Phase Oxidation of Monoethanolamine (MEA) with OH Radical and Ozone: Kinetics, Products, and Particles. Environmental Science & Technology 47, 6377-6383.

Bruice, P.Y., 2004. Organic Chemistry, 4th ed. Pearson Prentice Hall, Upper Saddle River.

Cadle, S.H., Mulawa, P.A., 1980. Low-Molecular Weight Aliphatic-Amines in Exhaust from Catalyst-Equipped Cars. Environmental Science & Technology 14, 718-723.

Cocker, D.R., Flagan, R.C., Seinfeld, J.H., 2001. State-of-the-art chamber facility for studying atmospheric aerosol chemistry. Environ Sci Technol 35, 2594-2601.

DeCarlo, P.F., Kimmel, J.R., Trimborn, A., Northway, M.J., Jayne, J.T., Aiken, A.C., Gonin, M., Fuhrer, K., Horvath, T., Docherty, K.S., Worsnop, D.R., Jimenez, J.L., 2006. Field-deployable, high-resolution, time-of-flight aerosol mass spectrometer. Anal. Chem. 78, 8281-8289.

Dockery, D.W., 2009. Health Effects of Particulate Air Pollution. Ann. Epidemiol. 19, 257-263.

Ehara, K., Hagwood, C., Coakley, K.J., 1996. Novel method to classify aerosol particles according to their mass-to-charge ratio - Aerosol particle mass analyser. J Aerosol Sci 27, 217-234.

Ge, X., Wexler, A.S., Clegg, S.L., 2011. Atmospheric Amines – Part I, A Review. Atmospheric Environment 45, 524-546.

IPCC, 2013. Climate change 2013: The physical science basis. Contribution of working group I to the fifth assessment report of the Intergovernmental Panel on Climate Change [Stocker, T.F., D. Qin, G.-K. Plattner, M. Tignor, S.K. Allen, J. Boschung, A. Nauels, Y. Xia, V. Bex and P.M. Midgley (eds.)]. Cambridge University Press, Cambridge, United Kingdom and New York, NY, USA, p. 1535 pp.

Jayne, J.T., Leard, D.C., Zhang, X.F., Davidovits, P., Smith, K.A., Kolb, C.E., Worsnop, D.R., 2000. Development of an aerosol mass spectrometer for size and composition analysis of submicron particles. Aerosol Sci. Technol. 33, 49-70.

Karl, M., Dye, C., Schmidbauer, N., Wisthaler, A., Mikoviny, T., D'Anna, B., Muller, M., Borras, E., Clemente, E., Munoz, A., Porras, R., Rodenas, M., Vazquez, M., Brauers,

T., 2012. Study of OH-initiated degradation of 2-aminoethanol. Atmospheric Chemistry and Physics 12, 1881-1901.

Karl, M., Wright, R.F., Berglen, T.F., Denby, B., 2011. Worst case scenario study to assess the environmental impact of amine emissions from a CO2 capture plant. Int J Greenh Gas Con 5, 439-447.

Malloy, Q.G.J., Nakao, S., Qi, L., Austin, R., Stothers, C., Hagino, H., Cocker, D.R., 2009. Real-Time Aerosol Density Determination Utilizing a Modified Scanning Mobility Particle SizerAerosol Particle Mass Analyzer System. Aerosol Sci Tech 43, 673-678.

Mosier, A.R., Andre, C.E., Viets, F.G., Jr., 1973. Identification of Aliphatic Amines Volatilized from Cattle Feedyard. Environmental Science & Technology 7, 642-644.

Pope, C.A., Thun, M.J., Namboodiri, M.M., Dockery, D.W., Evans, J.S., Speizer, F.E., Heath, C.W., 1995. Particulate Air-Pollution as a Predictor of Mortality in a Prospective-Study of Us Adults. Am. J. Respir. Crit. Care Med. 151, 669-674.

Price, D.J., Clark, C.H., Tang, X.C., Cocker, D.R., Purvis-Roberts, K.L., Silva, P.J., 2014. Proposed chemical mechanisms leading to secondary organic aerosol in the reactions of aliphatic amines with hydroxyl and nitrate radicals. Atmos Environ 96, 135-144.

Reynolds, A.J., Verheyen, T.V., Adeloju, S.B., Meuleman, E., Feron, P., 2012. Towards Commercial Scale Postcombustion Capture of CO2 with Monoethanolamine Solvent: Key Considerations for Solvent Management and Environmental Impacts. Environmental Science & Technology 46, 3643-3654.

Silva, P.J., Erupe, M.E., Price, D.J., Elias, J., Malloy, Q.G.J., Li, Q., Warren, B., Cocker, D.R., III, 2008. Trimethylamine as precursor to secondary organic aerosol formation via nitrate radical reaction in the atmosphere. Environmental Science & Technology 42, 4689-4696.

Smith, J.N., Dunn, M.J., VanReken, T.M., Iida, K., Stolzenburg, M.R., McMurry, P.H., Huey, L.G., 2008. Chemical composition of atmospheric nanoparticles formed from nucleation in Tecamac, Mexico: Evidence for an important role for organic species in nanoparticle growth. Geophys Res Lett 35.

Tang, X.C., Price, D., Praske, E., Lee, S.A., Shattuck, M.A., Purvis-Roberts, K., Silva, P.J., Asa-Awuku, A., Cocker, D.R., 2013. NO3 radical, OH radical and O-3-initiated secondary aerosol formation from aliphatic amines. Atmospheric Environment 72, 105-112.

Veltman, K., Singh, B., Hertwich, E.G., 2010. Human and Environmental Impact Assessment of Postcombustion CO2 Capture Focusing on Emissions from Amine-Based Scrubbing Solvents to Air. Environmental Science & Technology 44, 1496-1502.

Watson, J.G., 2002. Visibility: Science and regulation. J Air Waste Manage 52, 628-713.

Westerholm, R., Li, H., Almen, J., 1993. Estimation of Aliphatic Amine Emissions in Automobile Exhausts. Chemosphere 27, 1381-1384.

5.6 Tables

Table 5.1. Initial conditions of the environmental chamber experiments.

Amine	Structure	Humidity	[Amine] ppb	Oxidant	[Oxidant] ppb
AE	$NH_2(C_2H_4)OH$	<0.001%	100	H_2O_2 (OH)	415
AE	$NH_2(C_2H_4)OH$	30%	100	H_2O_2 (OH)	415
AE	$NH_2(C_2H_4)OH$	<0.001%	100	N_2O_5 (NO_3)	310
AE	$NH_2(C_2H_4)OH$	30%	100	N_2O_5 (NO_3)	310
MAE	$CH_3NH(C_2H_4)OH$	<0.001%	200	H_2O_2 (OH)	415
MAE	$CH_3NH(C_2H_4)OH$	30%	100	H_2O_2 (OH)	415
MAE	$CH_3NH(C_2H_4)OH$	<0.001%	100	N_2O_5 (NO_3)	310
MAE	$CH_3NH(C_2H_4)OH$	30%	100	N_2O_5 (NO_3)	310
DMAE	$(CH_3)_2N(C_2H_4)OH$	<0.001%	100	H_2O_2 (OH)	415
DMAE	$(CH_3)_2N(C_2H_4)OH$	30%	100	H_2O_2 (OH)	415
DMAE	$(CH_3)_2N(C_2H_4)OH$	<0.001%	100	N_2O_5 (NO_3)	310
DMAE	$(CH_3)_2N(C_2H_4)OH$	30%	100	N_2O_5 (NO_3)	310

Table 5.2. Mass-based aerosol yield values and HR-ToF-AMS organic to nitrate ratios.

Amine	Oxidant	Humidity	Y_{max} (%)[a,b]	Y_{wlc} (%)[c]	Y_{nwlc} (%)[c]	Org/NO_3
AE	OH	dry	178.7	0.5	0.4	5.3
AE	OH	humid	178.7	26.3	18.1	3.9
AE	NO_3	dry	203.3	262.6	138.8	1.3
AE	NO_3	humid	403.2[d]	617.4	276.0	2.1
MAE	OH	dry	164.0	28.6	20.8	5.3
MAE	OH	humid	164.0	19.2	13.9	6.4
MAE	NO_3	dry	184.0	185.4	86.6	1.6
MAE	NO_3	humid	184.0	339.7	134.6	2.5
DMAE	OH	dry	153.9	5.5	4.9	6.9
DMAE	OH	humid	153.9	26.7	20.5	12.5
DMAE	NO_3	dry	170.8	202.6	96.3	5.7
DMAE	NO_3	humid	170.8	333.2	136.8	2.5

a) Maximum possible yield assuming the addition of three oxygen atoms. (OH experiments)
b) Maximum possible yield assuming the formation of amine nitrate salt. (NO_3 experiments)
c) Assuming complete conversion of the precursor amine.
d) Maximum possible yield assuming the formation of oligomer nitrate salt. (3-amine:HNO_3)

5.7 Figures

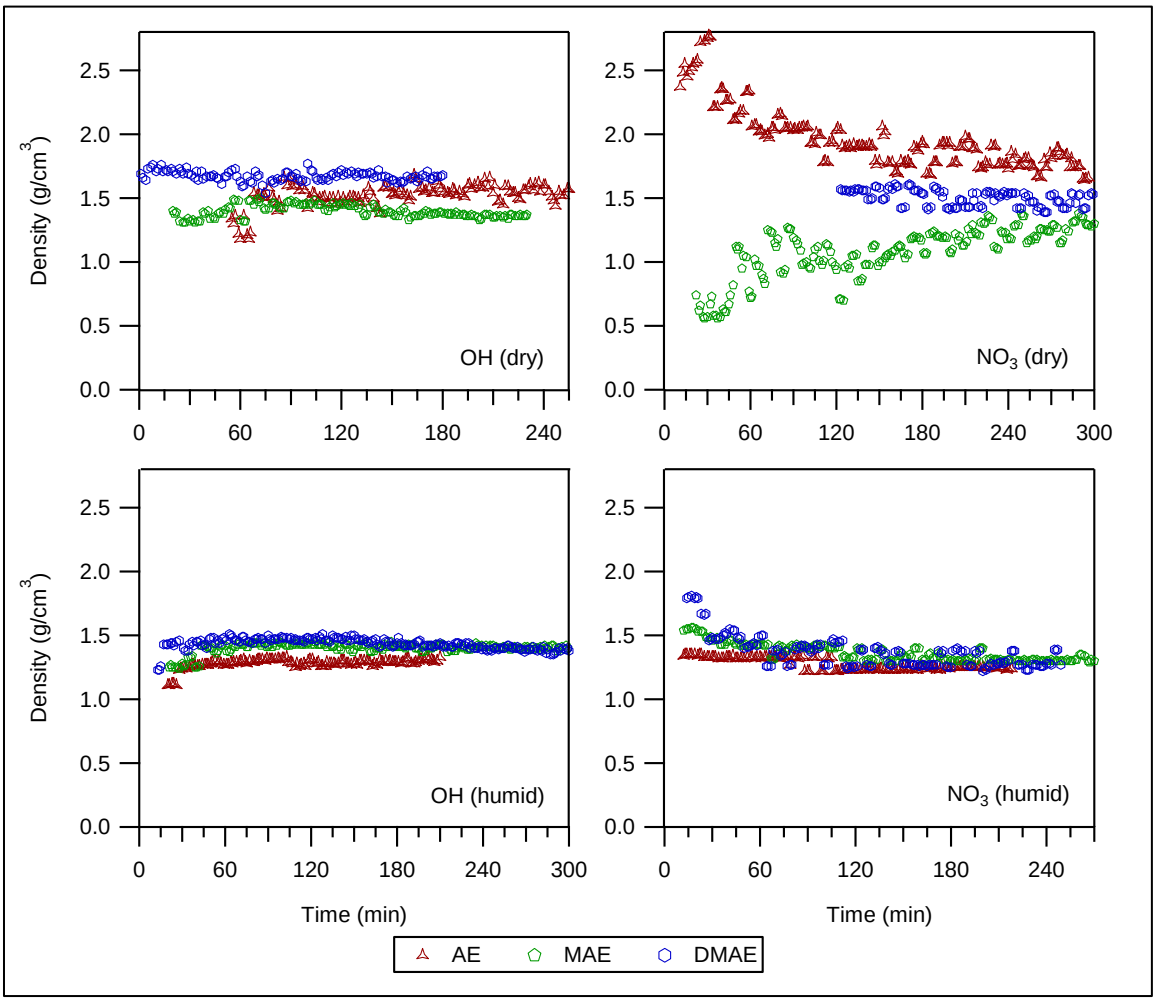

Figure 5.1. Density profiles for the aerosol produced in the amino alcohol oxidation experiments.

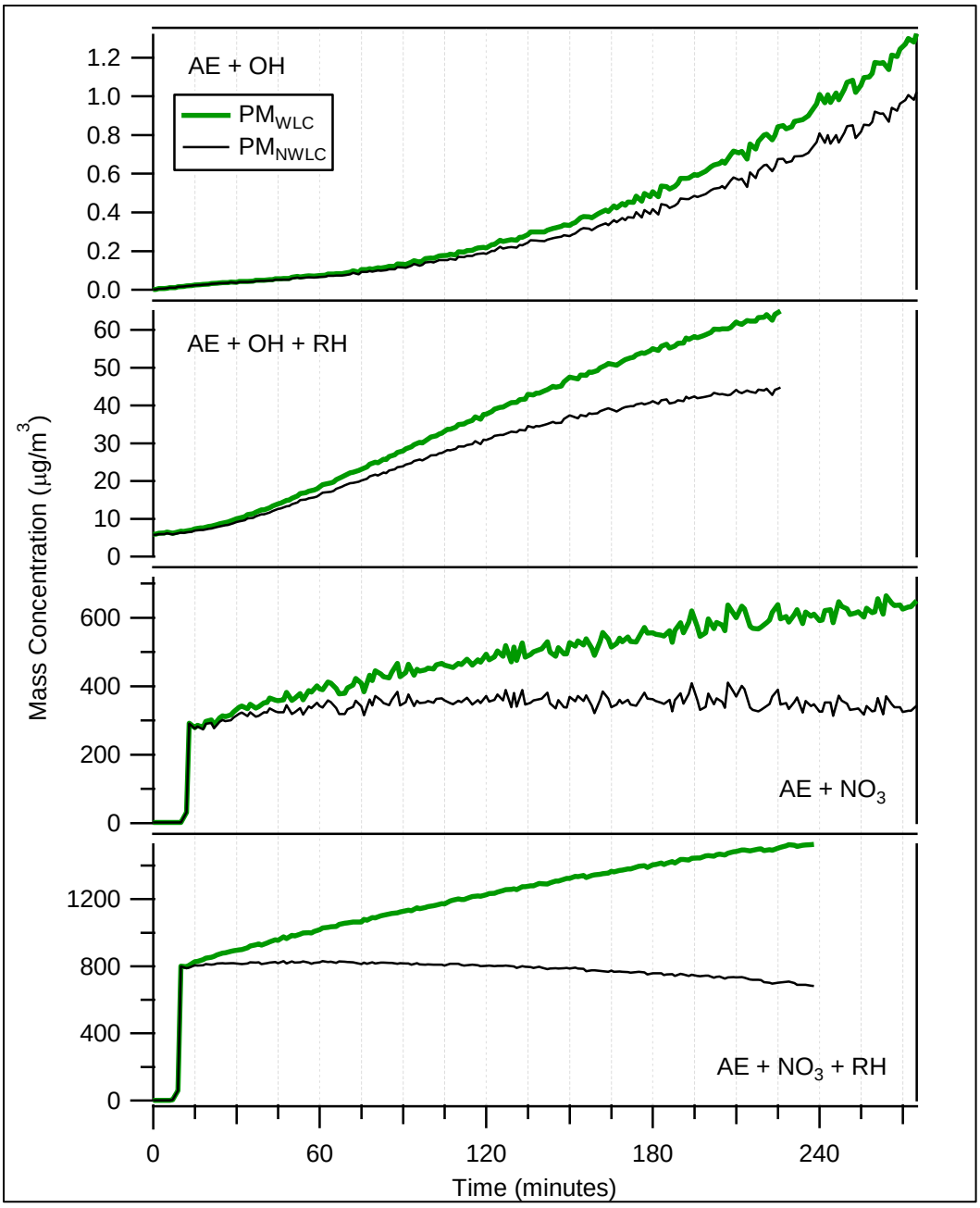

Figure 5.2. Particulate matter (PM) profiles for the 2-aminoethanol oxidation experiments. (WLC = wall loss correction, NWLC = non-wall loss corrected)

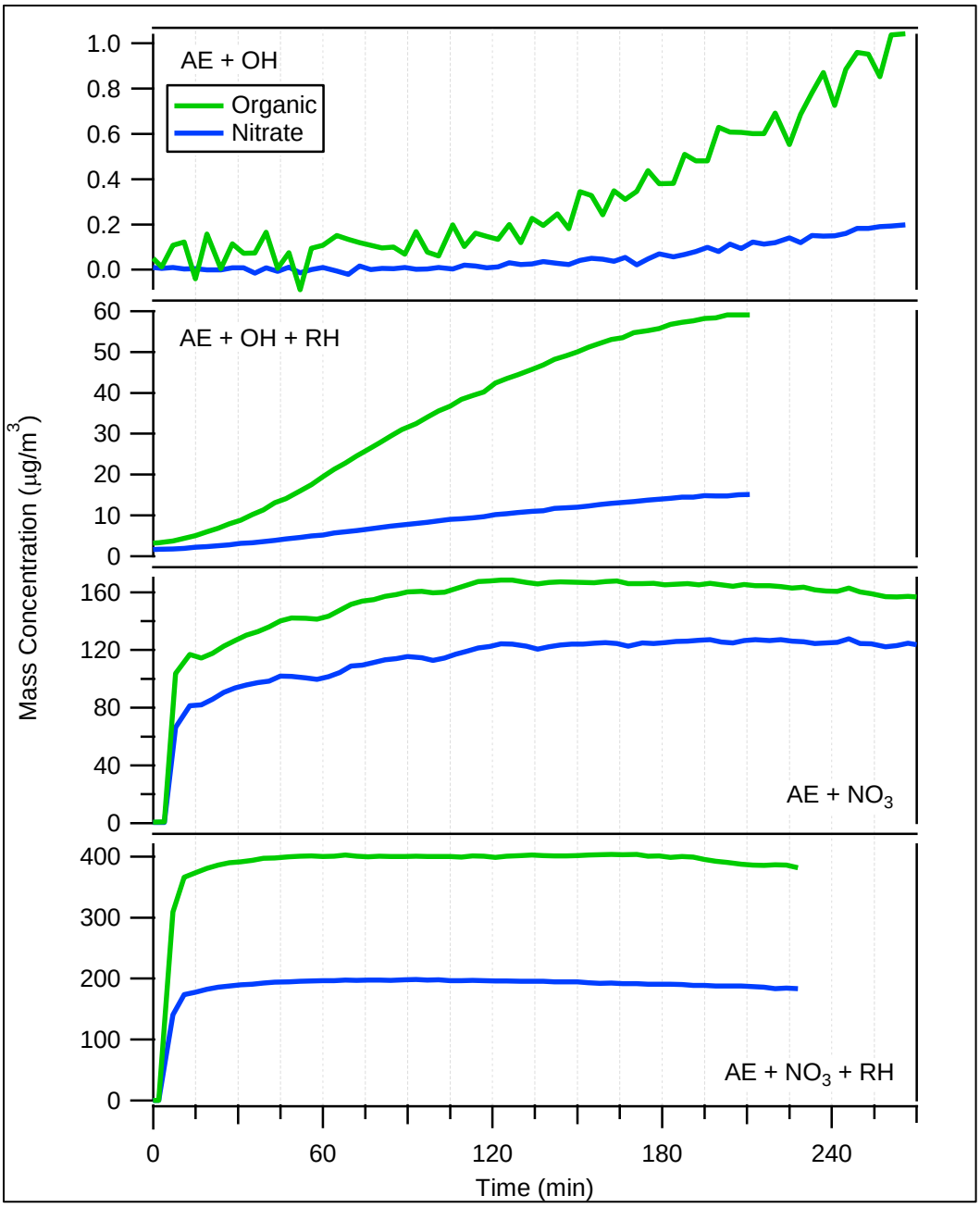

Figure 5.3. HR-ToF-AMS organic and nitrate concentration profiles for the 2-aminoethanol oxidation experiments.

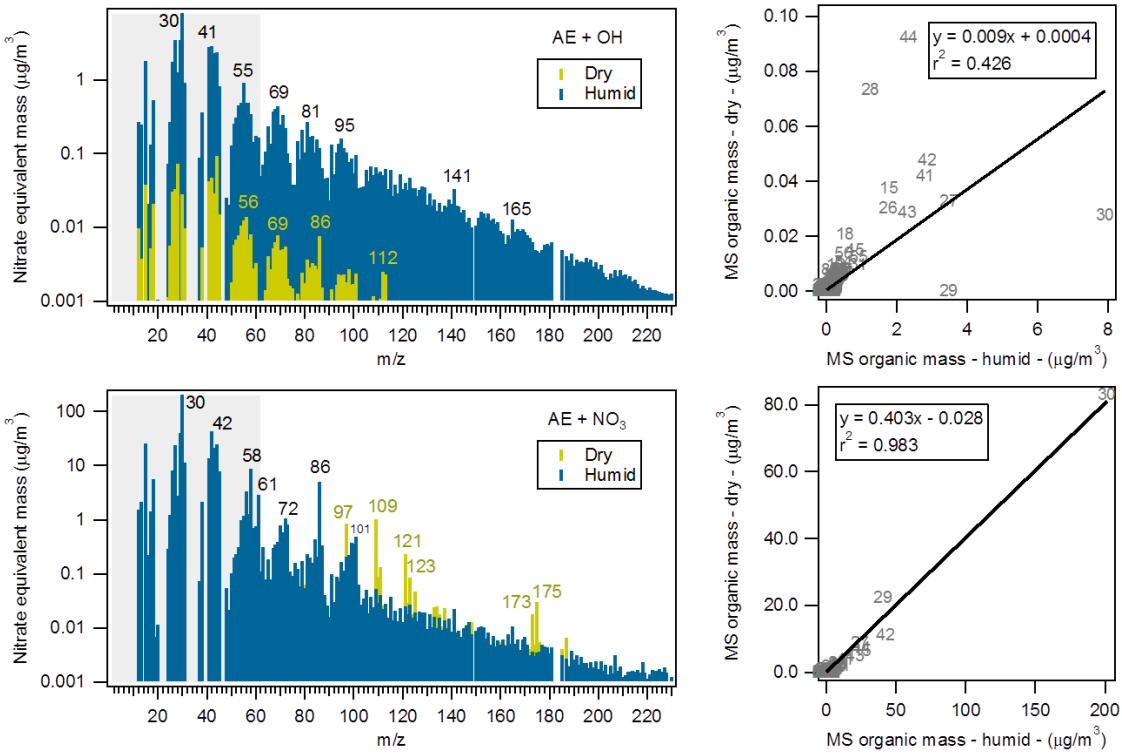

Figure 5.4. HR-ToF-AMS mass spectra and correlation plots for the dry and humid 2-aminoethanol oxidation experiments. The shaded area represents the precursor amine *m/z* range.

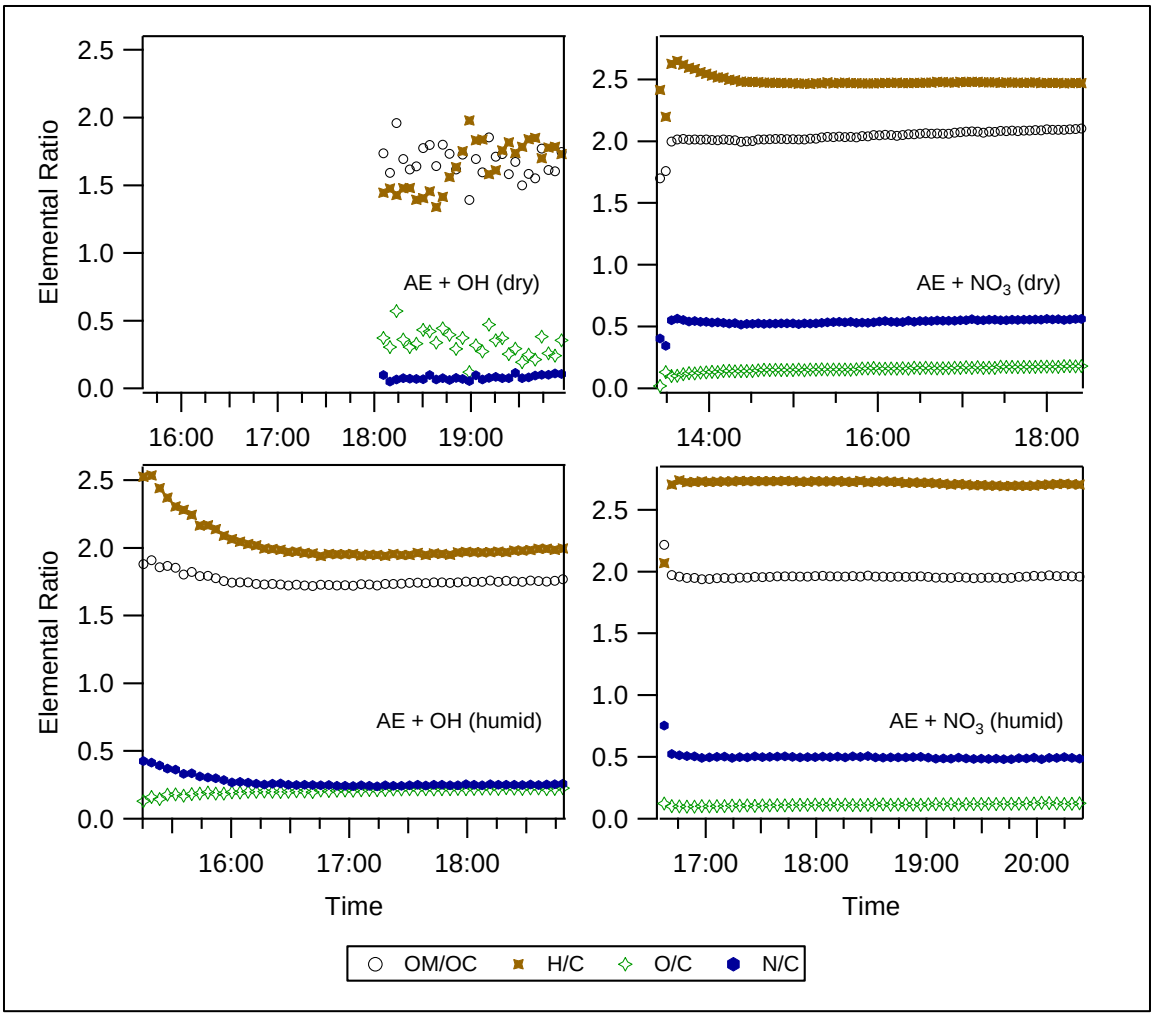

Figure 5.5. The elemental analyses for the aerosol formed in the 2-aminoethanol oxidation experiments.

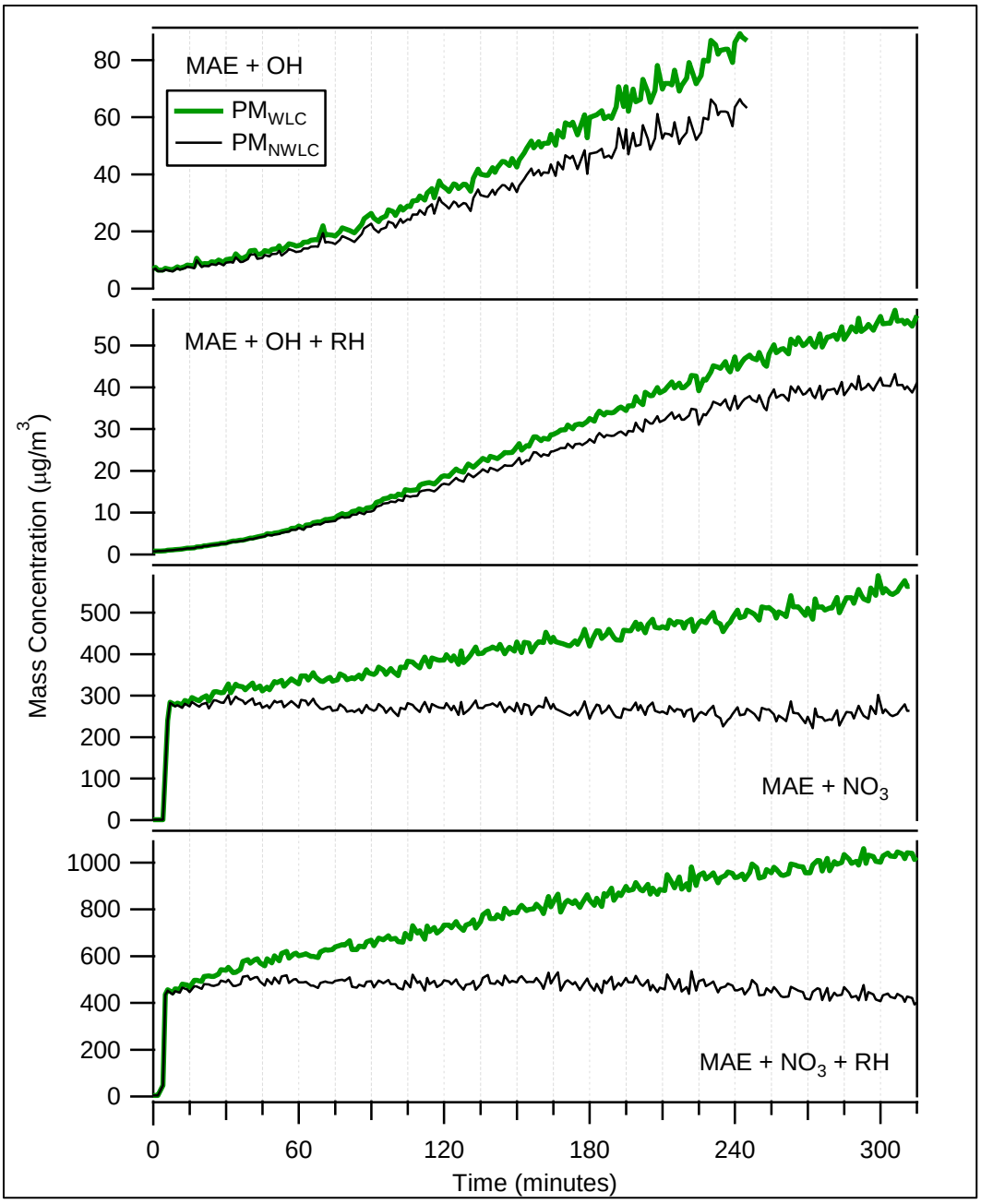

Figure 5.6. Particulate matter (PM) profiles for the 2-methylaminoethanol oxidation experiments. (WLC = wall loss correction, NWLC = non-wall loss corrected)

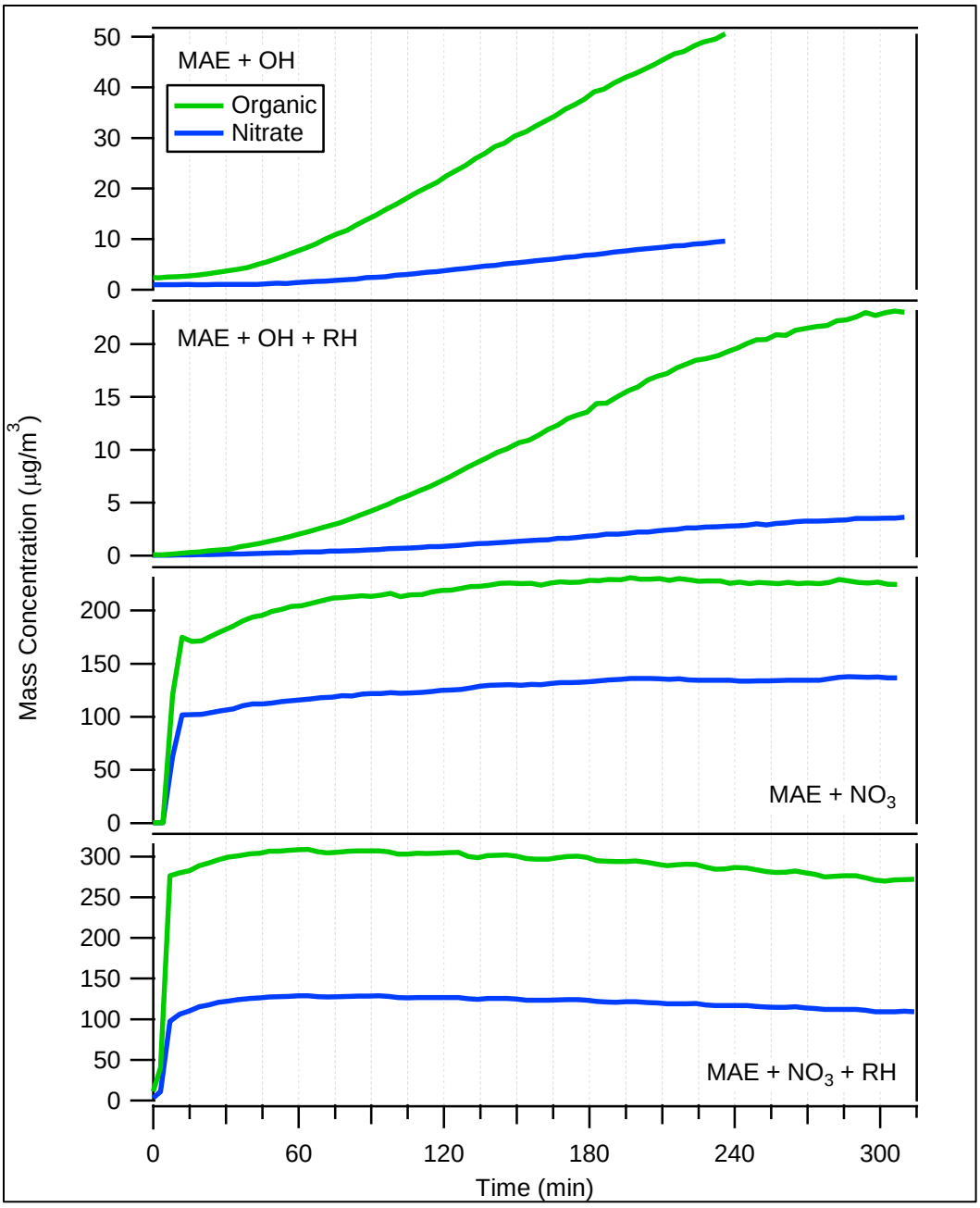

Figure 5.7. HR-ToF-AMS organic and nitrate concentration profiles for the 2-methylaminoethanol oxidation experiments.

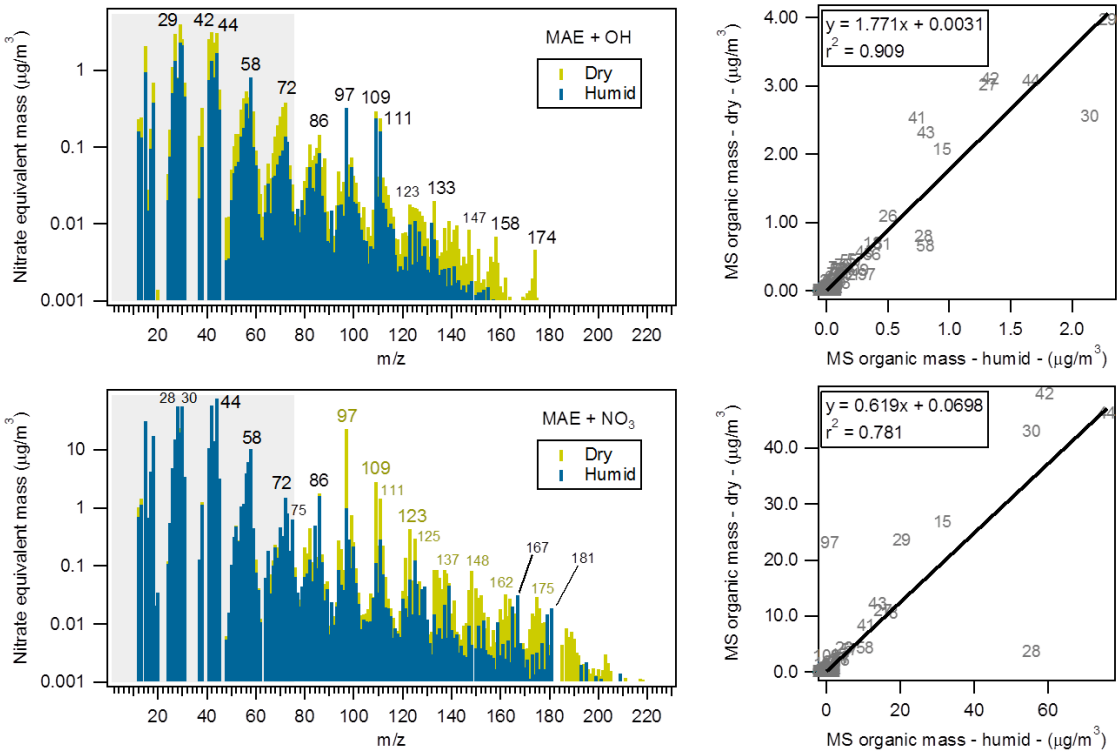

Figure 5.8. HR-ToF-AMS mass spectra and correlation plots for the dry and humid 2-methylaminoethanol oxidation experiments. The shaded area represents the precursor amine *m/z* range.

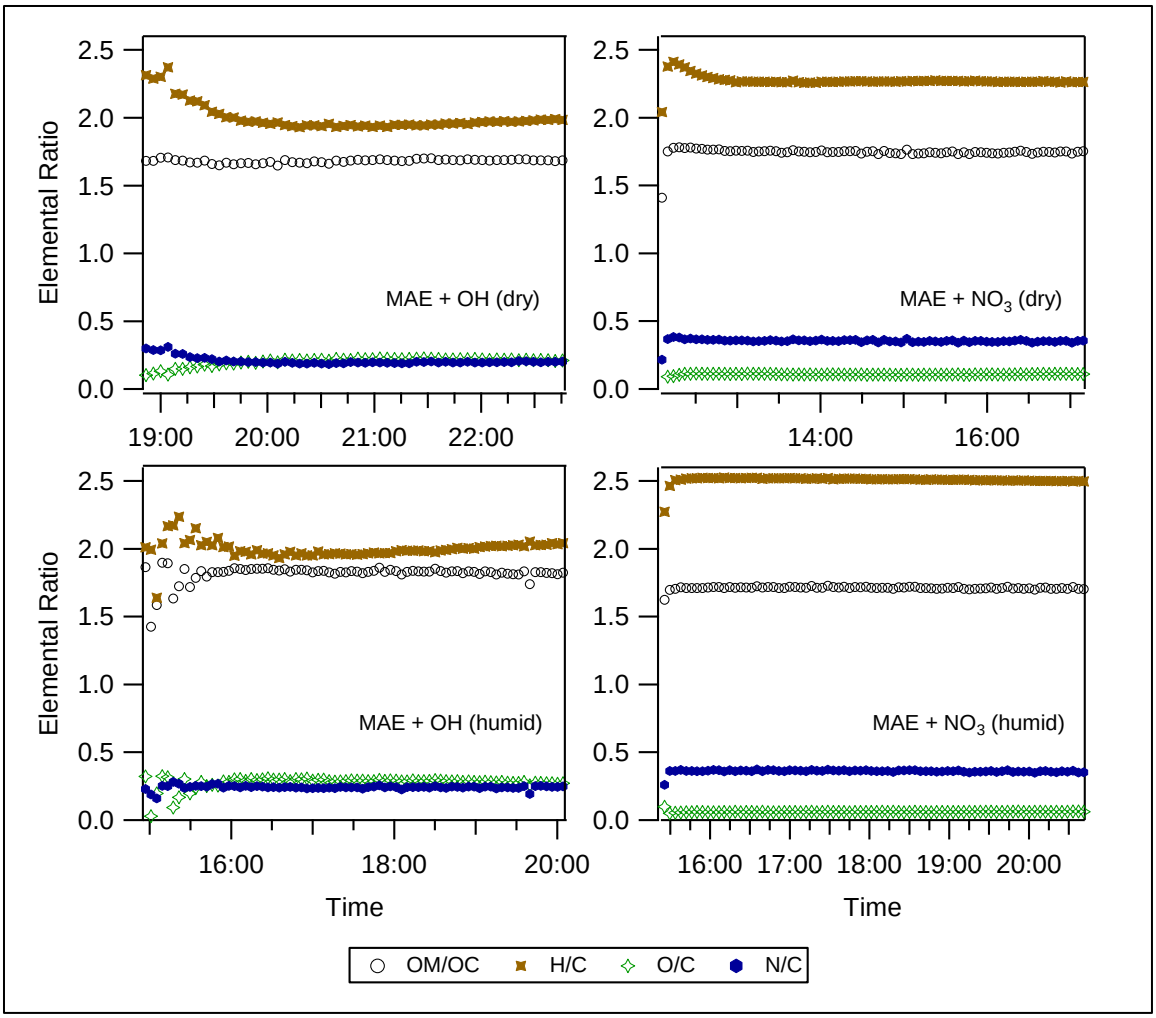

Figure 5.9. The elemental analyses for the aerosol formed in the 2-methylaminoethanol oxidation experiments.

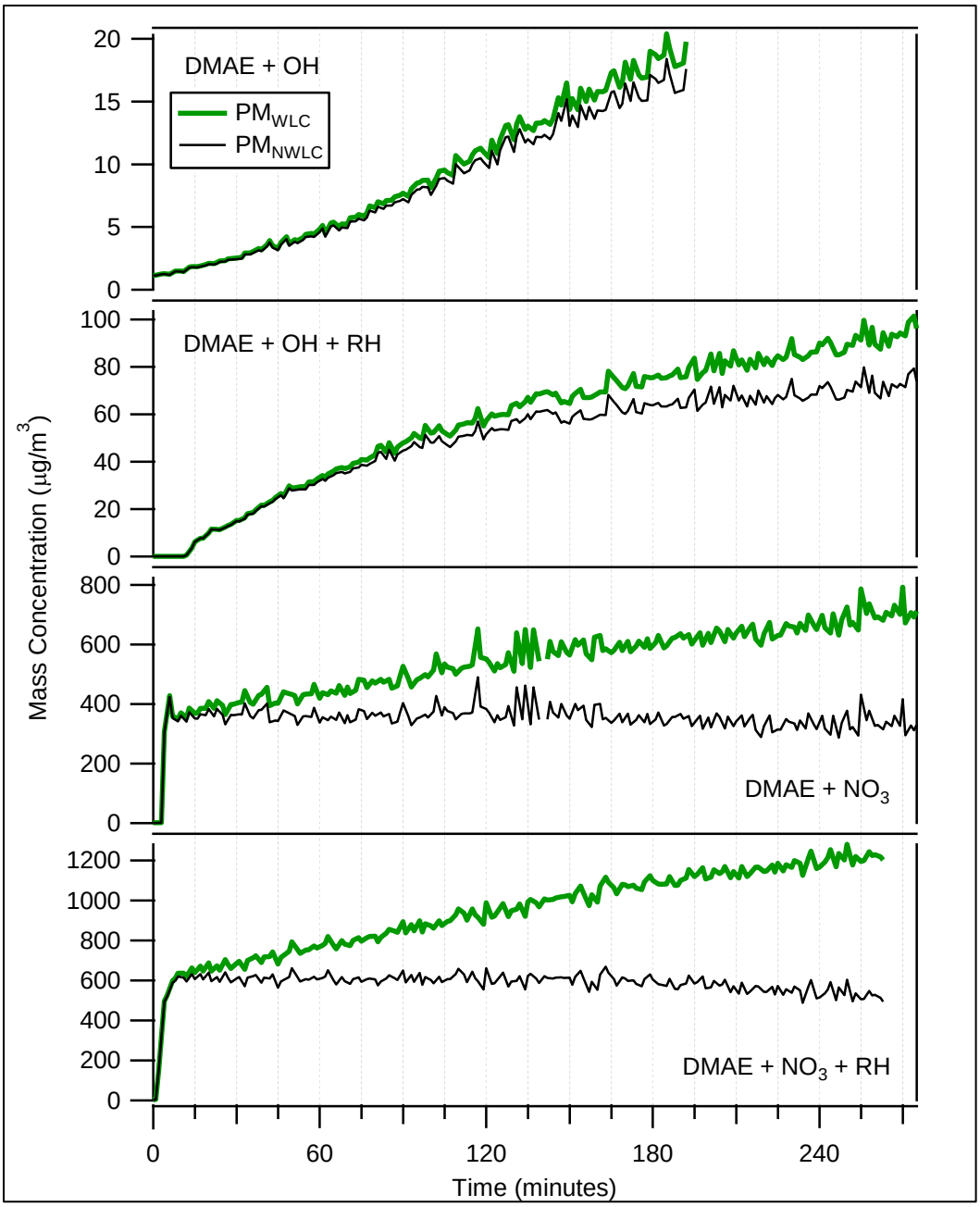

Figure 5.10. Particulate matter (PM) profiles for the 2-dimethylaminoethanol oxidation experiments. (WLC = wall loss correction, NWLC = non-wall loss corrected)

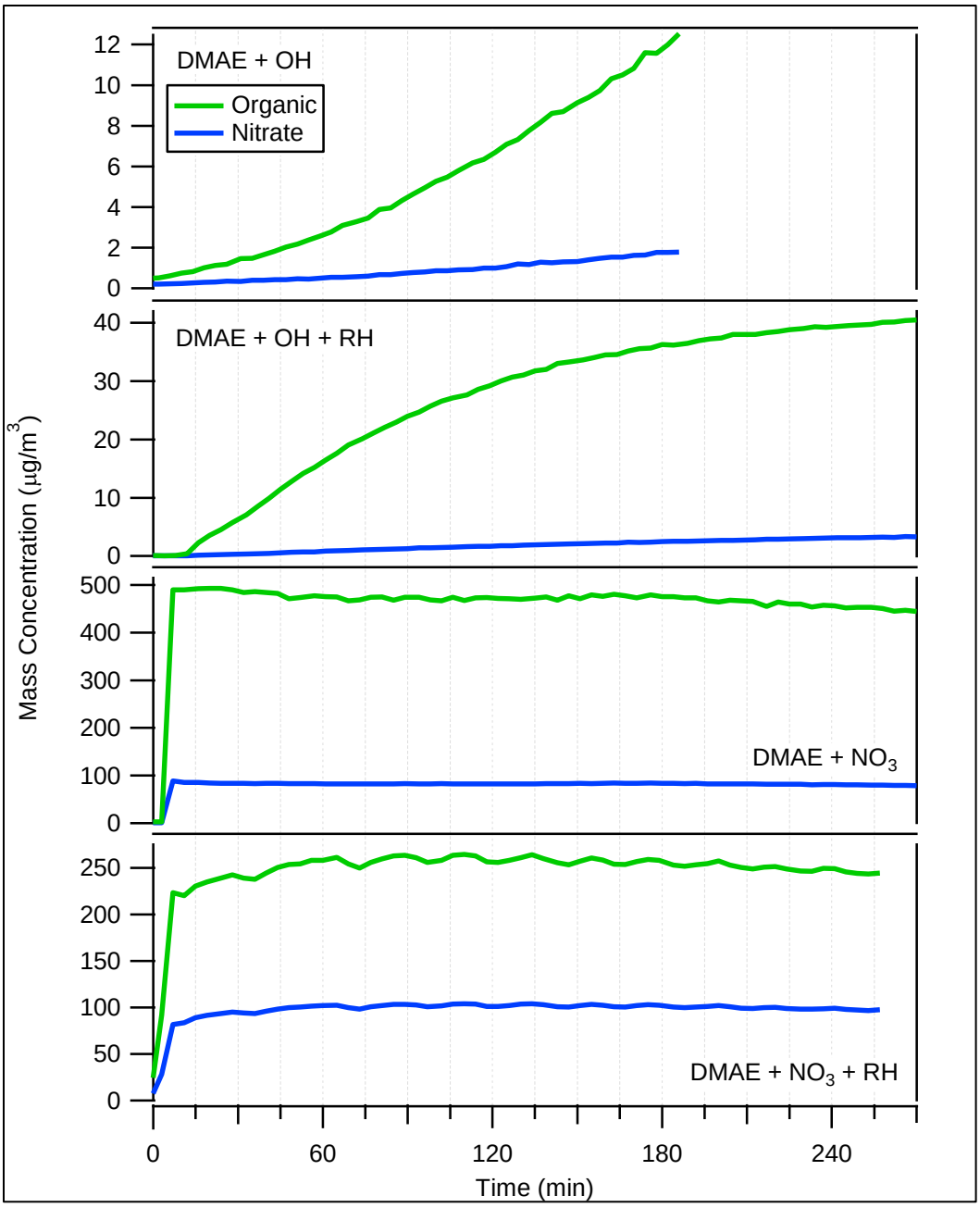

Figure 5.11. HR-ToF-AMS organic and nitrate concentration profiles for the 2-dimethylaminoethanol oxidation experiments.

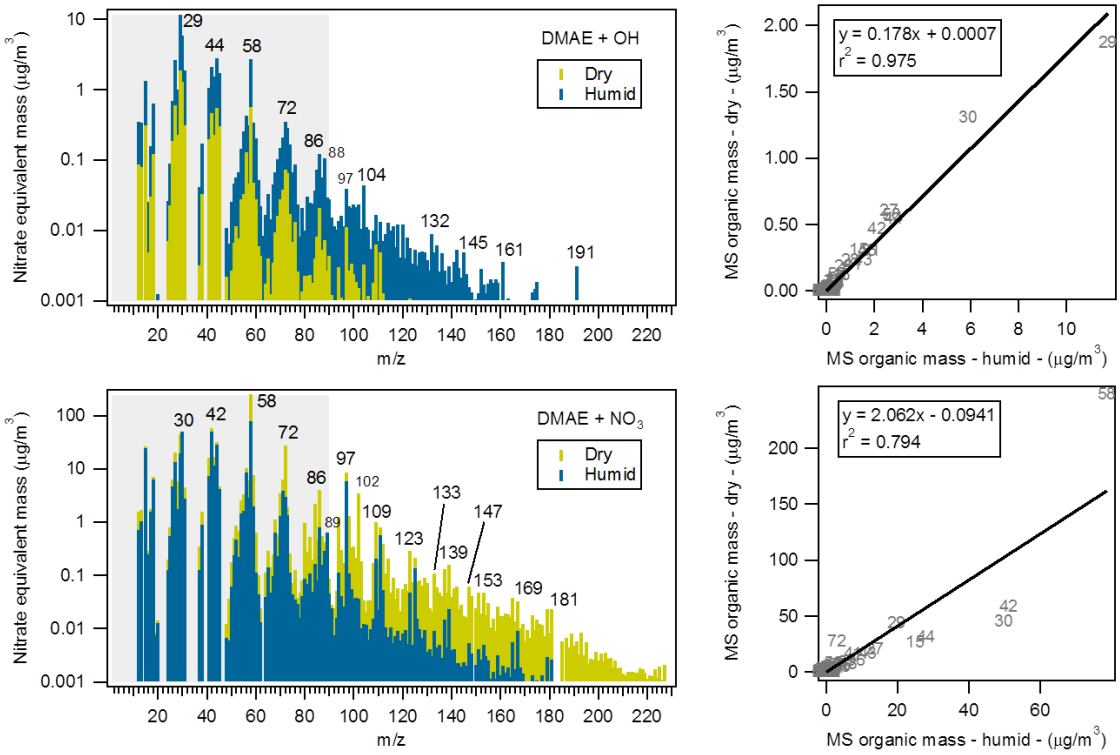

Figure 5.12. HR-ToF-AMS mass spectra and correlation plots for the dry and humid 2-dimethylaminoethanol oxidation experiments. The shaded area represents the precursor amine *m/z* range.

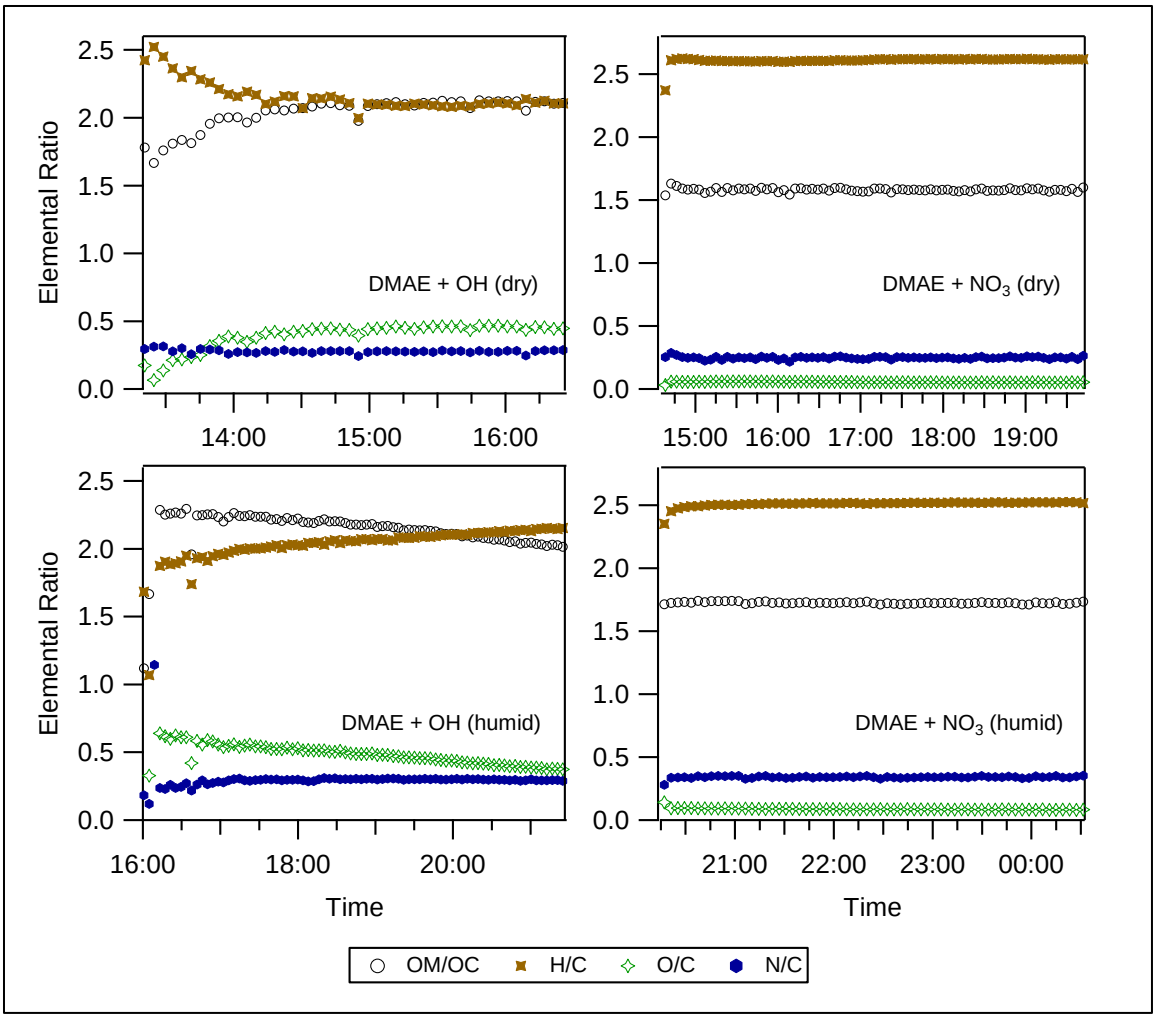

Figure 5.13. The elemental analyses for the aerosol formed in the 2-dimethylaminoethanol oxidation experiments.

Chapter 6: Summary

In chapter 2, the reaction mechanisms occurring with hydroxyl (OH) and nitrate (NO_3) radical oxidation of aliphatic amines, including trimethylamine, triethylamine, dimethylamine, and diethylamine were investigated. The assembly and fragmentation of molecules were predictable based on an understanding of known chemical behaviors. Alkyl peroxy chemistry was observed as an important pathway to the formation of secondary organic aerosol from amine precursors. This chemistry is initiated via hydrogen abstraction from the amine precursor by hydroxyl or nitrate radical. Two alkyl peroxy radicals can react to form amides, amino alcohols, or amine/amide peroxides. Additionally, oligomer formation was observed as a potential significant contributor to secondary organic aerosol from trimethylamine oxidation. This is atmospherically relevant in areas with high amine emissions, where $RO_2 + RO_2$ reactions are more likely to compete with $RO_2 + HO_2$ chemistry. It appears that alkyl peroxy chemistry via radical hydrogen abstraction is fundamental for oligomer growth. In the oligomer mechanism, alkyl peroxy "monomers" continue to add to the base molecule through peroxide linkages. The oligomer mechanism is observed in the trimethylamine experiment, but not the triethylamine or diethylamine experiments. This suggests that the ketone-amide functionality produced in the ethyl-amine reactions inhibits oligomer formation. The availability of N-H bonds in the secondary amines allowed for the formation of nitramines and imines. The formation of carcinogenic nitramines from secondary amines has negative human health implications in areas with high concentrations of secondary amines.

In chapter 3, the formation of secondary organic aerosol (SOA) from the OH and NO_3 radical oxidation of secondary aliphatic amines, including dimethylamine, diethylamine, dipropylamine, and dibutylamine was investigated. The availability of the N-H bonds in the secondary alkyl amines allowed for the formation of nitramines and imines. The formation of carcinogenic nitramines from the oxidation secondary alkyl amines has negative human health implications in areas with high concentrations of secondary amines. The addition of humidity to the system allows for the uptake of reaction products (amine products, HNO_3, etc.) into water, thereby introducing additional aqueous phase reactions leading to SOA formation under humid conditions.

In general, more aerosol was produced in the humid oxidation experiments than in the dry oxidation experiments. Also, the reactions with NO_3 produced far more aerosol than the OH reactions. The addition of humidity in the NO_3 oxidation experiments had the effect of inhibiting particle coagulation and loss to the walls. This is possibly due to the formation of amine nitrate salts that are unstable on surfaces and partition between the gas and particle phases.

Oligomer mechanisms are observed in the dimethylamine oxidation experiments, which is not seen in experiments with the other secondary amines. A highly reduced aerosol containing nitrogen and oxygen was observed in the DMA and DEA oxidation experiments. In general, the OH reactions produced highly oxidized organic aerosol while the NO_3 reactions produced reduced amine nitrate salt aerosol. The Org/NO_3 ratio increases with increasing carbon number. Humidity lowers the Org/NO_3 ratio in most of

the secondary amine experiments. Humidity enhances the amine nitrate salt mechanism, which leads to increased aerosol concentration while limiting the time for oxidation of the precursor amine.

In Chapter 4, the effects of temperature on the formation of SOA from aliphatic amine precursors, including trimethylamine, diethylamine, and butylamine were investigated. Temperature had a significant effect on aerosol formed from aliphatic amine precursors. The nucleation temperature is an important factor influencing the overall chemical composition of the aged aerosol, especially as the aerosol experiences temperature gradients. In general, more aerosol is formed at colder temperatures. This has important implications for locations influenced by amine emissions during the winter months.

The aerosol formed in the TMA + OH oxidation experiments supports the oligomer mechanism discussed in chapter 2. The formation of highly temperature dependent hydroperoxide amine compounds at cold temperatures confirms that $RO_2\cdot$ + $HO_2\cdot$ chemistry occurs significantly in addition to the $RO_2\cdot$ + $RO_2\cdot$ chemistry that leads to oligomer aerosol. Peroxy radical chemistry is an important contributor to aerosol formation during the daylight hours. The aerosol formed in the NO_3 oxidation experiments consists mainly of amine nitrate salts. These amine salts are highly dependent on temperature. Amine nitrate salts are an important contributor to aerosol formation during the nighttime hours, when temperatures tend to be cooler.

In chapter 5, the formation of SOA from the OH and NO_3 radical oxidation of amino alcohols, including 2-aminoethanol, 2-methylaminoethanol and 2-dimethylaminoethanol was investigated. Significant aerosol formation was observed in the amino alcohol experiments. In general, more aerosol was produced in the humid oxidation experiments than in the dry oxidation experiments. The addition of humidity to the system allows for the uptake of reaction products (amine products, HNO_3, etc.) into water, thereby introducing additional aqueous phase reactions leading to SOA formation under humid conditions. Also, the reactions with NO_3 produced far more aerosol than the OH reactions. There was little to no loss of particles to the chamber walls in the NO_3 oxidation experiments. This is possibly due to the formation of amine nitrate salts that are not stable on surfaces and partition between the gas and particle phases.

Different oligomer pathways were observed in the amino alcohol experiments. A highly reduced oligomer mechanism was observed in the 2-aminoethanol with OH oxidation experiments. Humidity enhanced this mechanism. It is proposed that these oligomer compounds are produced through nucleophilic addition-elimination reactions of the primary amine functionality of 2-aminoethanol with the alcohol functionality of another 2-aminoethanol. An oxidized oligomer pathway was observed in the dry amino alcohol experiments. A highly oxidized peroxide oligomer mechanism was observed in the humid 2-dimethylaminoethanol with OH oxidation experiment. A highly reduced aerosol containing nitrogen and oxygen was observed in the NO_3 oxidation experiments. In general, the OH oxidation reactions produced highly oxidized organic aerosol while

the NO_3 oxidation reactions produced reduced amine nitrate salt aerosol. Humidity enhanced the reduced-amine nitrate salt mechanism in the NO_3 oxidation reactions.

As the use of amino alcohols becomes increasingly prevalent in carbon capture sequestration and control technologies, it is imperative to understand the atmospheric reactivity of these compounds. The significant aerosol yields observed in the NO_3 oxidation of amino alcohols has important implications for the use of these compounds in carbon capture control devices. Measures to reduce or prevent the release of amino alcohols from the system should be implemented.